

ISSN 2074-272X

науково-практичний
журнал 2019/3

ЕІЕ Електротехніка і ЕІЕ Електромеханіка

Electrical Engineering

& Electromechanics

**Електротехніка. Визначні події. Славетні імена
Електричні машини та апарати**

Електротехнічні комплекси та системи.

Силова електроніка

Теоретична електротехніка та електрофізика

Техніка сильних електричних та магнітних полів.

Кабельна техніка

Електричні станції, мережі і системи

Ювілеї

**З 2015 р. журнал індексується у міжнародній
наукометричній базі Web of Science
Core Collection: Emerging Sources
Citation Index**



«ELECTRICAL ENGINEERING & ELECTROMECHANICS»

SCIENTIFIC & PRACTICAL JOURNAL

Journal was founded in 2002

Founders:

National Technical University «Kharkiv Polytechnic Institute» (Kharkiv, Ukraine)

State Institution «Institute of Technical Problems of Magnetism of the NAS of Ukraine» (Kharkiv, Ukraine)

INTERNATIONAL EDITORIAL BOARD

Klymenko B.V.	Editor-in-Chief , Professor, National Technical University "Kharkiv Polytechnic Institute" (NTU "KhPI"), Ukraine
Sokol Ye.I.	Deputy Editor , Professor, Corresponding member of NAS of Ukraine, Rector of NTU "KhPI", Ukraine
Rozov V.Yu.	Deputy Editor , Professor, Corresponding member of NAS of Ukraine, Director of State Institution "Institute of Technical Problems of Magnetism of the NAS of Ukraine"(SI "ITPM NASU"), Kharkiv, Ukraine
Batygin Yu.V.	Professor, Kharkiv National Automobile and Highway University, Ukraine
Biró O.	Professor, Institute for Fundamentals and Theory in Electrical Engineering, Graz, Austria
Bolyukh V.F.	Professor, NTU "KhPI", Ukraine
Colak I.	Professor, Nisantasi University, Istanbul, Turkey
Doležel I.	Professor, University of West Bohemia, Pilsen, Czech Republic
Féliachi M.	Professor, Technological Institute of Saint-Nazaire, University of Nantes, France
Gurevich V.I.	Ph.D., Honorable Professor, Central Electrical Laboratory of Israel Electric Corporation, Haifa, Israel
Ida N.	Professor, The University of Akron, Ohio, USA
Kildishev A.V.	Associate Research Professor, Purdue University, USA
Kuznetsov B.I.	Professor, SI "ITPM NASU", Ukraine
Kyrylenko O.V.	Professor, Member of NAS of Ukraine, Institute of Electrodynamics of NAS of Ukraine (IED of NASU), Kyiv, Ukraine
Nacke B.	Professor, Gottfried Wilhelm Leibniz Universität, Institute of Electrotechnology, Hannover, Germany
Podoltsev A.D.	Professor, IED of NASU, Kyiv, Ukraine
Rainin V.E.	Professor, Moscow Power Engineering Institute, Russia
Rezynkina M.M.	Professor, NTU "KhPI", Ukraine
Shkolnik A.A.	Ph.D., Central Electrical Laboratory of Israel Electric Corporation, member of CIGRE (SC A2 - Transformers), Haifa, Israel
Trichet D.	Professor, Institut de Recherche en Energie Electrique de Nantes Atlantique, Nantes, France
Yatchev I.	Professor, Technical University of Sofia, Sofia, Bulgaria
Yuferov V.B.	Professor, National Science Center "Kharkiv Institute of Physics and Technology", Ukraine
Zagirnyak M.V.	Professor, Member of NAES of Ukraine, rector of Kremenchuk M.Ostrohradskyi National University, Ukraine
Zgraja J.	Professor, Institute of Applied Computer Science, Lodz University of Technology, Poland

ISSUE 3/2019

TABLE OF CONTENTS

Electrical Engineering. Great Events. Famous Names

Baranov M.I. An anthology of the distinguished achievements in science and technique. Part 49: Aircraft designer Oleg Antonov and his accomplishments in airplane design 3

Electrical Machines and Apparatus

Bolyukh V.F., Kashanskij Yu.V., Schukin I.S. Influence of geometrical parameters of the inductor and armature on the indicators of a linear pulse electromechanical converter of an electrodynamic type 11

Baida Ye.I., Clemens M., Klymenko B.V., Korol O.G., Pustovoitov P.Ye. Application of the computing environment Maple to the calculation of the dynamics of the electromagnets in the complicated systems of forced control..... 18

Electrotechnical Complexes and Systems. Power Electronics

Andrienko P.D., Nemykina O.V., Andrienko A.A. High current harmonics influence on the choice of conductors of crane power supply systems 24

Theoretical Electrical Engineering and Electrophysics

Vasetsky Yu.M., Mazurenko I.L., Bondarevskiy S.L. Parametric analysis and stray fields of toroidal superconducting magnetic energy storage 30

High Electric and Magnetic Field Engineering. Cable Engineering

Baranov M.I. Refined selection of allowable cross-sections of electrical conductors and cables in the power circuits of industrial electrical equipment taking into account emergency operating modes. 37

Bezprozvannykh G.V., Mirchuk I.A., Kyessayev A.G. Technological parameters of the cooling mode of polymer insulation of power cables 44

Boyko M.I., Makogon A.V. The micro- and nanosecond discharges in gas bubbles for water disinfection and purification 50

Power Stations, Grids and Systems

Koliushko D.G., Rudenko S.S., Plichko A.V., Shcherbinin V.I. Modernization of the complex type IK-1U for measuring the impedance of the grounding device of a lightning arrester and supports of transmission lines..... 55

Lazurenko O.P., Moroz O.M., Tymchuk S.O., Miroshnyk O.O., Savchenko O.A. Optimization of design parameters of autotransformers in ice melting scheme with non-inductive circuit on 6-10 kV overhead power lines..... 59

Nizhevskiy I.V., Nizhevskiy V.I. Calculation estimation of overvoltage on insulation of the equipment of a substation at the lightning strike in its lightning arrester 67

Editorial office address: Dept. of Electrical Apparatus, NTU «KhPI», Kyrpychova Str., 2, Kharkiv, 61002, Ukraine
phones: +380 57 7076281, +380 67 3594696, e-mail: a.m.grechko@gmail.com (**Grechko O.M.**)

ISSN (print) 2074-272X

ISSN (online) 2309-3404

© National Technical University «Kharkiv Polytechnic Institute», 2019

© State Institution «Institute of Technical Problems of Magnetism of the NAS of Ukraine», 2019

Printed 20 June 2019. Format 60 x 90 1/8. Paper – offset. Laser printing. Edition 200 copies.
Printed by Printing house «Madrid Ltd» (11, Maksymilianivska Str., Kharkiv, 61024, Ukraine)

M.I. Baranov

AN ANTHOLOGY OF THE DISTINGUISHED ACHIEVEMENTS IN SCIENCE AND TECHNIQUE. PART 49: AIRCRAFT DESIGNER OLEG ANTONOV AND HIS ACCOMPLISHMENTS IN AIRPLANE DESIGN

Purpose. Preparation of short scientifically-historical essay about one of founders of domestic aircraft design, prominent Ukrainian aircraft designer O.K. Antonov. Methodology. Known scientific methods of collection, analysis and analytical treatment of scientific and technical information, touching becoming and development of Soviet aviation and resulted in scientific monographs, journals and internet reports. Results. A short scientifically-historical essay is resulted about the prominent Ukrainian aircraft designer Oleg Konstantinovich Antonov, becoming one of founders of Soviet military cargo and civil aviation. Basic scientific and technical achievements of the glorified aircraft designer O.K. Antonov are indicated and team of headed them in the period of 1952-1984 of legendary Design Bureau 473 (Kyiv) in area of aircraft design, bringing a domestic aviation around to world heights. Basic tactical and technical descriptions are described created under his scientific and technical guidance of such types of passenger airplanes known in the world as An-2, An-10 and An-24, and also troop-carriers of type An-12, An-22 «Antaeus», An-26, An-30, An-32, An-72 and An-124 «Ruslan». Short information is resulted about tactical and technical descriptions of the largest in the world of heavy distant turbo-jet military cargo airplane type An-225 «Mriya», created in 1980-th years in Design Bureau named after O.K. Antonov. It is marked that under scientific and technical guidance of aircraft designer O.K. Antonov in the former USSR about 100 types of aircrafts of the military and civil aircrafts were developed and created. It is pointed out that Doctor of Technical Sciences, Academician of the Academy of Sciences of the Ukrainian SSR and of the Academy of Sciences of the USSR became a founder acknowledged in the world of Ukrainian aviation scientific school. Information, touching common to all mankind qualities of this great aircraft designer, is resulted, and also handed O.K. Antonov for merits before Homeland of governmental rewards, bonuses and other insignia, underlining his prominent contribution to development of domestic aircraft construction. Originality. Certain systematization is executed known from scientific journals and other mass of scientific and technical materials media, touching becoming and development in the period of 20-21-th centuries of Soviet aviation and ponderable scientific and technical contribution to the military and civil aircraft design of the prominent Ukrainian aircraft designer O.K. Antonov. Practical value. Scientific popularization and deepening for the students of higher school, engineering, technical and scientific workers of scientific and technical knowledge in area of history of becoming and development of Soviet aircraft design, extending their scientific and technical range of interests and further development of scientific and technical progress in society. References 13, figures 17.

Key words: aviation technique, prominent Ukrainian aircraft designer Oleg Antonov, basic achievements in airplane design, scientifically-historical essay.

Наведено короткий науково-історичний нарис про видатного українського авіаконструктора Олега Костянтинівича Антонова, що став одним з основоположників вітчизняного літакобудування. Описані основні науково-технічні досягнення О.К. Антонова в галузі літакобудування, що принесли славу радянської військової і цивільної авіації і нашій Вітчизні. Показано, що авіаконструктор О.К. Антонов заснував в м. Києві відому в світі українську авіаційну наукову школу. Під керівництвом авіаконструктора О.К. Антонова в його ОКБ було розроблено близько 100 типів літальних апаратів військового і цивільного призначення. Бібл. 13, рис. 17.

Ключові слова: авіаційна техніка, видатний український авіаконструктор Олег Антонов, основні досягнення в літакобудуванні, науково-історичний нарис.

Приведен краткий научно-исторический очерк о выдающемся украинском авиаконструкторе Олеге Константиновиче Антонове, ставшем одним из основоположников отечественного самолетостроения. Описаны основные научно-технические достижения О.К. Антонова в области самолетостроения, принесшие славу советской военной и гражданской авиации и нашему Отечеству. Показано, что авиаконструктор О.К. Антонов основал в г. Киеве известную в мире украинскую авиационную научную школу. Под руководством авиаконструктора О.К. Антонова в его ОКБ было разработано около 100 типов летательных аппаратов военного и гражданского назначения. Библ. 13, рис. 17.

Ключевые слова: авиационная техника, выдающийся украинский авиаконструктор Олег Антонов, основные достижения в самолетостроении, научно-исторический очерк.

Introduction. As is well known, a modern aircraft, including an airplane, is a complex technical object containing various devices and systems based on the operation of which of electricity directly or indirectly. For operation of on-board equipment of any aircraft, constant and alternating electrical voltage generated by various powerful electrical sources (for example, batteries, motor converters, fuel cells, solar power plants, small nuclear generators, etc.) is necessary. Therefore, the world aircraft industry is inextricably linked with electrical engineering, penetrating all modern technology. Considering the

development of the aircraft industry, we simultaneously consider the development of the electrical industry in relation to the aircrafts. The history of the progressive development of technology on our planet is made by people. This is especially evident in the creative work of outstanding scientists in a particular area of scientific and technical knowledge. One of such outstanding personalities in the field of domestic aircraft design was the Ukrainian aircraft designer, Academician of the Academy of Sciences of the Ukrainian SSR (since 1968)

© M.I. Baranov

and the Academy of Sciences of the USSR (since 1981) Oleg Konstantinovich Antonov (Fig. 1) [1].

The goal of the paper is the preparation of a brief scientific and historical essay about one of the founders of the domestic aircraft industry, an outstanding Ukrainian aircraft designer O.K. Antonov.

1. The beginning of the life and career of O.K.

Antonov. He was born on February 7, 1906 in the village of Troitsa, Moscow Province of the Russian Empire, in the Russian noble family of Anna Efimovna (nee Bikoryukina) and Konstantin Konstantinovich Antonov [1]. Oleg's father was a civil engineer. In 1912 his family moved to the city of Saratov, located on the banks of the great river Volga. In the period 1915-1922 he first studied at the Saratov Real School (he graduated from two classes), and then in high school (now it is school No. 23 [1]). From a young age O.K. Antonov was interested in aircraft engineering and was enthusiastically engaged in the aviation amateur school club. In 1924, while studying at the University of Saratov at the Railway Department, he built his first glider, the «Dove» [1]. In 1925, Oleg Antonov entered the Engineering Department of the Leningrad Polytechnic Institute (LPI), which he graduated in 1930 and became a mechanical engineer.



Fig. 1. Outstanding Ukrainian aircraft designer, Hero of Labor, Doctor of Technical Sciences, Academician of the Academy of Sciences of the Ukrainian SSR and the Academy of Sciences of the USSR
Oleg Konstantinovich Antonov
(07.02.1906 – 04.04.1984) [1]

In 1933, O.K. Antonov, working as a chief designer at the Osoaviakhim glider bureau (Leningrad), was appointed chief designer at the design bureau of the first glider plant in the former USSR built in Moscow (Tushino district) [2]. The decision-makers of the country ordered to this design bureau to develop new light-wing machines, which would be massively manufactured at this plant. For five years of work in the city of Moscow, O.K. Antonov designed more than 20 types of gliders produced at the plant in Moscow Region [3]. In 1938, this plant was closed and O.K. Antonov was out of work. In this situation, he had to turn to his comrade on the All-Union gliders rally in the Crimea (Koktebel), the Head of the aircraft-building experimental Design Bureau Alexander

Sergeyevich Yakovlev, who later became an outstanding Russian aircraft designer and three times Hero of Labor [2]. So O.K. Antonov became only the lead engineer (after the position of chief designer of the glider design bureau occupied by him in Moscow) in the Design Bureau of A.S. Yakovlev. In the spring of 1940, O.K. Antonov was again appointed chief designer of a small design bureau at an aircraft plant in Leningrad, and in the first half of 1941 he was transferred to the aircraft plant No. 465 (Kaunas, Lithuanian SSR) in his previous position. And here he was when the Great Patriotic War (WWII) began. Upon his arrival in Moscow, the Commissariat of the Aviation Industry of the USSR entrusted him with the combat mission – the urgent creation of a landing glider [2]. And here the new order was to evacuate beyond the Urals in Tyumen city and create such a glider there. So in military conditions for a couple of months, O.K. Antonov and his colleagues developed an A-7 type airborne glider, which greatly assisted the partisan movement during the Second World War. Therefore, it is no coincidence that O.K. Antonov in 1944 was awarded the medal «Partisan of the Patriotic War». In February 1943 he was again transferred to the Design Bureau of Major General A.S. Yakovlev, where he becomes his deputy and is engaged in the modernization of the famous military fighter aircrafts during the Second World War, ranging from the Yak-3 and ending with Yak-9 [3].

2. The main achievements of the aircraft designer

O.K. Antonov in aircraft construction. In the autumn of 1945, O.K. Antonov was offered to head the Siberian branch of the Design Bureau of A.S. Yakovlev at the aircraft plant named after V.P. Chkalov (Novosibirsk city). He agreed without hesitation. He had to independently create not military aircraft, but agricultural and passenger planes. By the Resolution of the Council of Ministers of the USSR of May 31, 1946, this branch was transformed into a new aircraft-building Design Bureau No. 153 and O.K. Antonov became his chief designer [2]. The first-born aircraft of this design bureau took off on August 31, 1947. It turned out to be the multi-purpose aircraft of the An-2 type known in the aviation world, affectionately named by the people as «Annushka» (Fig. 2). Note that this airplane was the only aircraft in the world that has been mass-produced for over 50 years [3]. He won the fame of an exceptionally reliable flying machine. In 1952, O.K. Antonov and his associates for the creation of this aircraft were awarded the Stalin (State) Prize of the second degree. In the same 1952, O.K. Antonov and his leading specialists moved to the city of Kyiv and began to organize a new Design Bureau No. 473 from scratch [2]. In this connection, it is worth citing the words of O.K. Antonov [2]: «... *The collective is not created by orders, although they are needed. It is not created only by picking and rearranging people. The team does not unite by the building in which it works. The main thing without which the team can not exist, it is the unity of purpose. Creating a friendly, workable team is a special work, work of a higher order.*»



Fig. 2. The Soviet single-engine piston passenger biplane of the An-2 type «Annushka» (known to many as the «Kukuruznik») developed by the aircraft designer O.K. Antonov and his Design Bureau No. 153 (1947, Novosibirsk, USSR) [2]

The first contribution of the new design bureau to the development of the Soviet military transport aviation was a twin-engine gas turbine aircraft of the An-8 type (Fig. 3) [2].



Fig. 3. Soviet twin-engine gas turbine military transport aircraft of the An-8 type developed by the aircraft designer O.K. Antonov and his Design Bureau No. 473 (the lead designer of the project is A.Ya. Belolipetsky, 1958, Kyiv, Ukrainian SSR) [2]

In accordance with the Resolution of the Council of Ministers of the USSR of November 30, 1955, the Kyiv Design Bureau was entrusted with the creation of the country's first four-engine turboprop passenger aircraft for medium-range air lines and relatively short landing lanes. It turned out to be the An-10 type aircraft (Fig. 4), launched into mass production in 1957 [2].



Fig. 4. The first Soviet medium-haul four-engine turboprop passenger aircraft of the An-10 type developed by the Chief Aircraft Designer O.K. Antonov and his Design Bureau No. 473 (1957, Kyiv, Ukrainian SSR) [2]

An-10 aircraft carried more than one million passengers throughout the vast Soviet country [2, 3].

New government order for O.K. Antonov and his design bureau became the development of a four-engine turboprop military transport aircraft of the An-12 type (Fig. 5) [2]. The capacity of this aircraft was increased to 20 tons. He could fly to the Arctic at the drifting stations of the USSR «North Pole» and to the Antarctic at the station «Mirny» [2, 3].



Fig. 5. Soviet four-engine turboprop military transport aircraft of the An-12 type developed by the Chief Aircraft Designer O.K. Antonov and his Design Bureau No. 473 (1959, Kyiv, Ukrainian SSR) [2]

Since 1959 this aircraft with a take-off mass of 61 tons has been supplied to the country's Air Forces. In terms of its tactical and technical characteristics, it significantly exceeded foreign analogues [2]. For the creation of the An-12 aircraft, members of the group of authors from the Kyiv Design Bureau in 1962 were awarded the USSR Lenin Prize. After the creation of the An-10 and An-12 aircrafts, the Design Bureau No. 473 led by the talented Ukrainian aircraft designer O.K. Antonov took a deserved place among the leading aircraft-building firms of the Soviet country [2, 3].

In 1960, the twin-engine turboprop aircraft of the An-24 type (Fig. 6) developed in the Kyiv Design Bureau under the guidance of O.K. Antonov «came out» onto the passenger lines of our country, and later of many foreign countries [2]. The serial production of the An-24 type aircraft continued until 1979. During this time, about 1,200 machines were manufactured with 1000 of them produced at the «Aviant» Aviation Plant in Kyiv [2]. It served 450 air lines in the USSR. This flying machine was successfully exported to 25 countries of the planet [2, 3].



Fig. 6. Short-haul twin-engine turboprop passenger aircraft of the An-24 type developed by aircraft designer O.K. Antonov (1960, Kyiv, Ukrainian SSR) [2]

On the basis of the design of the An-24 passenger aircraft with the wide use of glued-welded joints of many elements of this aircraft in the future, the Kiev Design Bureau created An-26 military transport aircraft (Fig. 7) and An-30 aerial photography aircraft (Fig 8) [2, 3].



Fig. 7. Soviet twin-engine turboprop military transport aircraft of the An-26 type developed by aircraft designer O.K. Antonov (1962, Kyiv, Ukrainian SSR) [2]



Fig. 8. Soviet twin-engine turboprop aerial photography aircraft of the An-30 type developed by aircraft designer O.K. Antonov and his Design Bureau No. 473 (1963, Kyiv, Ukrainian SSR) [2]

The next flying «brainchild» of the Design Bureau's team, headed by O.K. Antonov, became the world's first wide-body military transport aircraft type An-22 «Antaeus» (Fig. 9) [2]. The creation of this domestic airplane marked the onset of a new stage in the global aircraft industry. In terms of its tactical and technical characteristics, it surpassed everything that was created in world aviation before it.



Fig. 9. The first Soviet military transport four-engine turboprop giant aircraft of the An-22 «Antaeus» type (60 tons payload; it set 12 world records) developed by General Designer O.K. Antonov and his Kyiv Design Bureau No. 473 (1965, Kyiv, Ukrainian SSR) [2]

The creation of the An-22 «Antaeus» type aircraft required a comprehensive solution of many scientific design and technological problems, as well as a huge amount of experimental work [2]. At the 26th International Aviation and Space Salon at Le Bourget (1965, Le Bourget, Paris), this domestic aircraft was in the center of the general attention of viewers and specialists and produced a real scientific and technical sensation. The English newspaper *The Times* wrote on this occasion [2]: «... Thanks to this plane, the Soviet Union was ahead of all other countries in the aircraft industry». Delivery of large cargoes (for example, gas

turbine stations, rotor excavators and trucks) to the Far North of the USSR with the help of the An-22 «Antaeus» type aircrafts confirmed that thanks to this unique aircraft transport aviation made a new progressive step forward.

In the 1960s, the Kyiv Design Bureau under the leadership of its General Designer O.K. Antonov (this high rank was conferred on him in 1962) continued work on the modernization of the An-26 aircraft and, as a result, developed a new design of the domestic high-altitude turboprop record airplane of the An-32 type (Fig. 10).



Fig. 10. Lightweight twin-engine turboprop transport aircraft of the An-32 type developed by General Designer O.K. Antonov (1964, Kyiv, Ukrainian SSR) [2]

In 1976, the next Resolution of the Council of Ministers of the USSR on the development and creation instead of the An-26 type aircraft by the Kyiv Design Bureau of a new twin-engine turbojet military transport aircraft, necessary for the uninhabited regions of the country with no concrete airfields, was adopted [2]. On August 31, 1977, such an aircraft, called the An-72 (Fig. 11), successfully completed its first flight. In 1978, the An-72 was launched into pilot production at the Kyiv aircraft plant, and in 1985 into serial production at the Kharkiv aircraft plant [3].



Fig. 11. Soviet twin-engine turbojet military transport aircraft of the An-72 type (affectionately called «Cheburashka» by pilots and aviation specialists) developed by General Designer O.K. Antonov and his legendary Design Bureau (1978, Kyiv, Ukrainian SSR) [2]

The An-72 type aircraft also had a civil modification. The power plant of this aircraft included two powerful turbojet engines of the Д-36 type mounted above the wing for use during its flight of the Coanda effect – the growth of lift due to the «sticking» of the exhaust jet to the wing [2]. The airframe design of the An-72 type aircraft, in which composite materials were widely used [4], was made all-metal. The main tactical and technical characteristics of the An-72 type aircraft

[5]: maximum flight speed 705 km/h (its cruising speed 550 km/h); flight range 2700 km; ceiling (lifting height) 10100 m; maximum take-off weight 32 tons; empty aircraft mass 19.5 tons; hull length 28 m; runway length 800 m, and the run 450 m. Note that over time, a modification of this aircraft appeared in the USSR, called An-74 [2, 5].

Under the scientific and technical guidance of the Ukrainian aircraft designer O.K. Antonov the extremely difficult task of developing and building in the USSR a new heavy long-range military transport aircraft of the An-124 «Ruslan» type (Fig. 12) successfully was solved (Fig. 12) [2, 6]. For this, General Designer O.K. Antonov went on very bold technical solutions for that time. In particular, the swept wing of a supercritical profile was used for the first time in the world on a plane of this class [6].



Fig. 12. Soviet heavy long-range four-engine turbojet military transport giant of the An-124 «Ruslan» type – a «swan song» by the General Designer O.K. Antonov (1982, Kyiv, Ukrainian SSR) [2]

One of the technological methods that made it possible to achieve a high weight index for the An-124 «Ruslan» type aircraft was the wide use of composite materials in it [4, 6]. Today, this aircraft is the largest mass-produced transport aircraft. We point out that the An-124 «Ruslan» military transport aircraft is currently used in cooperation with NATO countries in the transport of large-sized military cargoes (Fig. 13) [2].



Fig. 13. Loading a German military helicopter into the An-124 «Ruslan» military transport aircraft of the Volga-Dnepr international air transport company [2]

We emphasize the fact that for any design bureau in the world there are special projects, in the work on which its specialists reached the «top» of their professional skills. For the Kyiv Design Bureau, under the leadership of twice Academician (of the Republican and Union

Academies of Sciences) O.K. Antonov such a project was the aircraft of the type An-124 «Ruslan». Describing the features of this aircraft, which set 30 world records (as of 2006, there were 483 world records at the O.K. Antonov Design Bureau, 378 of which have not been beaten yet), experts often use the words «unique», «not having analogues in world aviation» and others [2, 6]. Kiev aircraft manufacturers have developed and created a lot of excellent airplanes. But even in this domestic aviation series, the An-124 «Ruslan» type of aircraft is a monumental technical object [6]. This aircraft was the last one created under the direct scientific and technical guidance of the great Ukrainian aircraft designer O.K. Antonov.

Let us give the basic tactical and technical characteristics of the An-124 «Ruslan» type aircraft [6]: wingspan 73.3 m; body length 69.1 m; height 20.8 m; empty aircraft mass 173 tons; maximum take-off weight 405 tons; normal take-off weight 392 tons; power plant is four turbofan engines Д-18Т; maximum flight speed 865 km/h; cruising flight speed (750-800) km/h; flight range 4500 km; ceiling (lifting height) 9500 m; useful flight load (120-150) t; crew is 6 people.

Orienting the team of the Kyiv Design Bureau to the solution of new problems, O.K. Antonov in one of his last speeches said [2]: «... Then you can only go in a revolutionary way, mastering new ideas. And, as you know, there are no limits to the new technology». After the death of General Designer O.K. Antonov his aviation plans embodied in the «life» of his talented followers.

In December 1988, at the Design Bureau named after O.K. Antonov, under the leadership of General Designer Peter Vasilyevich Balabuev, a new Soviet heavy long-range military transport turbojet aircraft of the An-225 «Mriya» type was created (Fig. 14) [2, 7].



Fig. 14. World's largest Soviet six-engine turbojet military transport giant of the An-225 «Mriya» type developed by the Design Bureau named after O.K. Antonov (1989, the photo was taken during the transportation of the «Buran» space shuttle by this plane) [2]

The An-225 «Mriya» type aircraft of extra-large carrying capacity, created on the basis of the design of the An-124 «Ruslan» type aircraft, is the largest aircraft in the world. It is designed to transport bulky goods weighing up to 250 tons inside the fuselage or on an external suspension to anywhere in the world. This aircraft can also be used as a launch complex for military space forces or launch vehicles of a new generation [2, 7]. Initially, it was created to transport a number of components of super-power launch vehicles of the «Energia» type and the Soviet «Buran» shuttle spacecraft from the

manufacturers of the USSR to the southern Baikonur cosmodrome. Its first test flight took place on December 21, 1988, which was a huge victory for Soviet aviation. On March 22, 1989, the An-225 «Mriya» made its flight with a payload of 156.3 tons on board. During this flight of the An-225 «Mriya» type aircraft, 109 world aviation records were set at once.

Let us indicate the main tactical and technical characteristics of the An-225 «Mriya» type aircraft [7]: wingspan 88.4 m; body length 84 m; height 18.2 m; empty aircraft mass 250 tons; maximum take-off weight 600 tons; fuel weight 300 tons; power plant S six turbofan engines Д-18Т; cruising flight speed 850 km/h; practical flight range 15600 km; practical ceiling 11000 m; useful flight load up to 250 tons; crew is 6 people.

It should be noted that in 2001, the relevant aviation services of Ukraine were issued certificates for the An-225 «Mriya» aircraft of its compliance with the standards of civil aviation aircraft. Currently, the only flying specimen of the An-225 «Mriya» type aircraft performs commercial cargo transportation as a part of the air transport division of the State Enterprise «Antonov» – Ukrainian «Antonov Airlines» Company [7]. From May 10 to 15, 2016, the An-225 «Mriya» type airplane made a flight along the Ukraine-Australia route, making four intermediate landings along the way with refueling [7]. Here, the full range of the flight with bulky cargo on board (generator of the «Brush SEM» Company weighing 117 tons) was 15.5 thousand km. Today, the An-225 «Mriya» is the owner of 250 world aviation records. The aircraft of the type An-225 «Mriya» is listed in the Guinness Book of Records [7].

In conclusion of this section, we point out that the Scientific-&-Research Planning-&-Design Institute «Molniya» of the Kharkov Polytechnic Institute (KhPI), now called the National Technical University (NTU) KhPI, has a certain relation to the development and creation at the Design Bureau, headed by O.K. Antonov, a number of transport aircraft. Here, the participation of specialists from the KhPI consisted in the joint solution of important tasks to ensure electromagnetic compatibility (EMC) and lightning protection of electronic equipment of such aircrafts (in particular, the An-124 «Ruslan» type aircraft) with designers of the Design Bureau. For the performance of these works, a number of employees of the Scientific-&-Research Planning-&-Design Institute «Molniya» of the NTU «KhPI» twice (in 2004 and 2014) were members of authors' teams whose were awarded the high title of Laureate of the State Prize of Ukraine in the field of science and technology. At present, such scientific and technical cooperation on the basis of contractual work between the Scientific-&-Research Planning-&-Design Institute «Molniya» of the NTU «KhPI» and the «Antonov» State Enterprise continues successfully. Its main tasks are the issues of providing EMC and durability of onboard devices and structural elements (for example, fuel tanks) of «Antonov» aircraft to the damaging effect of such a natural source of powerful pulsed electromagnetic interference (fields, currents and voltages) as linear lightning. The Scientific-&-Research Planning-&-Design Institute «Molniya» of the NTU «KhPI» to simulate the effects of lightning on the aircrafts

has the necessary high-voltage high-current electrophysical equipment of its own manufacture [8].

3. The universal human qualities of the aircraft designer O.K. Antonov. What kind of person in the life people remembered this outstanding Ukrainian aircraft designer? Externally, Oleg Konstantinovich looked much younger than his years (Fig. 15). He remained young in spirit, too. He is remembered by a man of athletic build, well dressed, elegant, emphatically intelligent and helpful in communication. He was distinguished by a rare spirituality. Perhaps this helped him to become not just famous, but the legendary aircraft designer [9]. Its distinguishing feature as an aircraft designer is that he did not create any combat «strike» aircraft – attack aircraft or bomber (of course, for this, in the former USSR there were other special design bureaus). All of his planes were produced as both passenger and transport. In each of his flying machine, O.K. Antonov provided an opportunity for its peaceful application. He impressed everyone who came across him with his highest inner culture, extraordinary erudition and range of his interests and hobbies [10]. It would be naive to assume that the creation and implementation into practice of the aircrafts, developed under the guidance of O.K. Antonov, as well as the solution of many problems in a large team of the Kyiv Design Bureau, passed without various contradictions and conflicts.

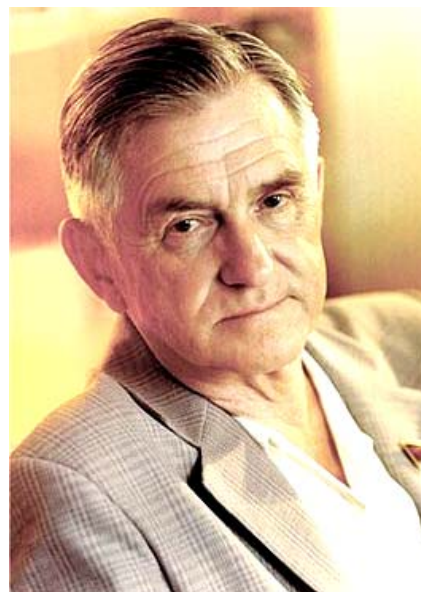


Fig. 15. Outstanding aircraft designer of our time, Academician O.K. Antonov in a quiet homely atmosphere in the period of successful conquest of his life and creative «heights» (1970s, Kyiv, Ukrainian SSR) [1]

A characteristic feature of the Soviet era in which O.K. Antonov worked, there was bureaucracy. Often the only way out of the situation at the design bureau and outside it was the struggle, which took away the aircraft designer infinitely many strength and health, undermined by a serious illness (tuberculosis) in the prewar period [2]. Oleg Konstantinovich married three times. In 1936, Lydia Sergeevna Kochetkova gave birth to his son Rolland. Elizaveta Avetovna Shakhmatuni (an aircraft designer who

has worked with him for several decades) gave birth to his daughter Anna. And the third young wife Elvira Pavlovna gave birth to his son Andrei and the daughter Elena. The most surprising thing here is that the aircraft designer with all his spouses until his death (he died of a stroke and was buried in the Baikovo cemetery, Kyiv) communicated cordially and in a friendly way [8]. By the way, after the third marriage of the General Designer of the Design Bureau, his superiors scolded him for «old-time pranks» (there was no trial, but the corresponding «treatment» was) [2]. We can only mentally imagine what kind of nerves for Oleg Konstantinovich all this «cost» and what he had to «pay» for his production and family victories.

At the work O.K. Antonov has always been strongly opposed to administrative-command methods of management. He almost never ordered. In his inherent intelligent form, he advised the employee or asked him about the execution of a particular task. Having become a world-famous aircraft designer, Oleg Konstantinovich amazed his subordinates with his very easy accessibility [9]. He had an amazing ability to recognize talented people. In all possible ways and forces he supported their undertakings and aspirations. He tried to invite them to work with him. This support for gifted people O.K. Antonov also transferred to students, having been successfully engaged in teaching since 1977 (he had the academic title of Professor) at the Kharkiv Aviation Institute (KhAI) named after N.E. Zhukovsky (in this high school he for many years headed the Department for Aircraft Design) and preparing for Ukraine's aircraft industry a new worthy shift [2, 9]. Under his «wing» there was the formation of many aircraft designers in Ukraine and abroad. At the Kyiv Design Bureau headed by Academician O.K. Antonov the Ukrainian aviation Scientific school recognized in the world has been established [9, 10].

From the memories of E.A. Shakhmatuni (a close associate of O.K. Antonov and the LAureate of the Lenin Prize of the USSR) [2]: «... *The main thing that characterizes Oleg Konstantinovich is his unconditional talent, exceptional love for his work, and, of course, intelligence. These qualities in the first place determined his relationship with the team. Everyone who came to work with Oleg Konstantinovich was immediately infected with his obsession. He was able to arrange people in such a way so as not to push them in their work. Employees themselves became carriers of his aspirations and his ideas*».

In the capital of Ukraine, city of Kyiv, on May 31, 2012, on the territory of the legendary Design Bureau No. 473 in honor of its former scientific and technical leader, an outstanding Ukrainian aircraft designer, Academician O.K. Antonov bronze monument was opened (Fig. 16) [11].

In the first capital of Ukraine, city of Kharkiv, on May 26, 2012, on one of the walls of the main educational building of the KhAI named after N.E. Zhukovsky, currently called the National Aerospace University named after N.E. Zhukovsky, in honor of his teacher, Professor, Academician O.K. Antonov bronze plaque was opened (Fig. 17) [12].



Fig. 16. Bronze monument to the Head of the legendary Design Bureau No. 473 Oleg Konstantinovich Antonov installed in the territory of the Aviation Scientific-Technical Complex named after O.K. Antonov (sculptor A. Shatalov; Kyiv, Academic Tupolev Str. 3, Ukraine) [11]



Fig. 17. A plaque in honor of the General Designer of the legendary Design Bureau No. 473 O.K. Antonov mounted on the wall of the educational building of the KhAI named after N.E. Zhukovsky (now National Aerospace University named after N.E. Zhukovsky, Kharkiv, Chkalov Str. 17, Ukraine) [12]

4. Awards and honors of O.K. Antonov. For outstanding merits of Oleg Konstantinovich Antonov in the field of domestic aircraft design, since November 19, 1984, the Kyiv Design Bureau was called the Design Bureau named after O.K. Antonov whose historical successor is the «Antonov» State Enterprise which is now apart of the State Concern «Ukroboronprom» [13].

For great success in the design of new aviation technology and in connection with the 60th anniversary of the birth, O.K. Antonov in 1966 was awarded the title of Hero of Labor 1966 and he was awarded the «Hammer and Sickle» gold medal. He became a holder of six orders (1944, 1945, 1957, 1966, 1971, 1975) of the Soviet country. For valiant work during the Second World War he was awarded a number of combat medals. He became the Laureate of the State (1952) and Lenin (1962) Prizes of the USSR, as well as the Honored Worker of Science and Technology of the Ukrainian SSR. In 1976, the creative work of an outstanding aircraft designer was

awarded the State Prize of the country in the field of science and technology for the creation and introduction of the An-24 passenger turboprop aircraft. He was awarded the A.N. Tupolev Gold Medal of the Academy of Sciences of the USSR (1979). He became an honorary citizen of the city of Saratov (1981). The streets in Kyiv, Saratov, Vinnitsa and Ulan-Ude as well as avenue in Ulyanovsk were named after him. In 2006, postage stamps of Ukraine and Russia dedicated to O.K. Antonov and the most famous aircrafts of his design were issued.

Conclusions. Outstanding Ukrainian aircraft designer, Academician of the Academy of Sciences of the Ukrainian SSR and the Academy of Sciences of the USSR Oleg Konstantinovich Antonov who was in the period 1952-1984 an authoritative scientific and technical leader of the world famous legendary Soviet aircraft Design Bureau No. 473, Kyiv made an enormous personal contribution to the development of domestic military transport and civil aviation. Under his direct design guidance, about 100 types of aircrafts were developed and built including the fascinating hobby of his youth – light-wing gliders. The unique four-engine turbojet military transport giant of type An-124 «Ruslan» possessing a payload up to 150 tons and performing commercial flights around the globe and today reliably transporting heavy expensive large-sized equipment to long-distance distances is a triumph of his aviation talent. At present, his aviation work in Ukraine is continued by the creatively inspired colleagues and followers of this talented scientist and designer.

REFERENCES

1. Available at: [https://en.wikipedia.org/wiki/Oleg_Antonov_\(aircraft_designer\)](https://en.wikipedia.org/wiki/Oleg_Antonov_(aircraft_designer)) (accessed 15 June 2017).
2. Available at: <http://nk.org.ua/tekhnologii/okantonov-okrylennyiy-mechtoy-106820> (accessed 08 May 2018). (Rus).
3. Available at: <http://to-name.ru/biography/oleg-antonov.htm> (accessed 12 April 2017). (Rus).
4. Baranov M.I. An anthology of the distinguished achievements in science and technique. Part 41: Composite materials: their classification, technologies of making, properties and application domains in modern technique. *Electrical engineering & electromechanics*, 2017, no.6, pp. 3-13. doi: **10.20998/2074-272X.2017.6.01**.
5. Available at: https://en.wikipedia.org/wiki/Antonov_An-72 (accessed 25 October 2017).
6. Available at: <https://militaryarms.ru/voennaya-texnika/aviaciya/an-124-ruslan> (accessed 22 May 2017). (Rus).
7. Available at: <https://ruspekhn.ru/events/item/ispytatelnyj-polet-samoljota-an-225-mriya> (accessed 10 July 2017). (Rus).
8. Baranov M.I., Buriakovskiy S.G., Rudakov S.V. The tooling in Ukraine of model tests of objects of energy, aviation and space-rocket engineering on resistibility to action of pulsed current of artificial lightning. *Electrical engineering & electromechanics*, 2018, no.4, pp. 45-53. doi: **10.20998/2074-272X.2018.4.08**.
9. Available at: http://www.stoletie.ru/sozidateli/legendarnyj_aviakonstruktor_686.htm (accessed 10 January 2018). (Rus).
10. Bondar' O.I. *O.K. Antonov – mnogogrannost' talanta* [O.K. Antonov is many-sided nature of talent]. Kyiv, AeroHobby Publ., 2012. 192 p. (Rus).
11. Available at: <http://www.warheroes.ru/hero/hero.asp?id=21788> (accessed 12 September 2017). (Rus).
12. Available at: <http://www.warheroes.ru/hero/hero.asp?id=18548> (accessed 28 November 2017). (Rus).
13. Available at: <https://en.wikipedia.org/wiki/Antonov> (accessed 23 July 2017).

Received 25.10.2018

M.I. Baranov, Doctor of Technical Science, Professor, Scientific-&-Research Planning-&-Design Institute «Molniya», National Technical University «Kharkiv Polytechnic Institute», 47, Shevchenko Str., Kharkiv, 61013, Ukraine, phone +380 57 7076841, e-mail: baranovmi@kpi.kharkov.ua

How to cite this article:

Baranov M.I. An anthology of the distinguished achievements in science and technique. Part 49: Aircraft designer Oleg Antonov and his accomplishments in airplane design. *Electrical engineering & electromechanics*, 2019, no.3, pp. 3-10. doi: **10.20998/2074-272X.2019.3.01**.

V.F. Bolyukh, Yu.V. Kashanskij, I.S. Schukin

INFLUENCE OF GEOMETRICAL PARAMETERS OF THE INDUCTOR AND ARMATURE ON THE INDICATORS OF A LINEAR PULSE ELECTROMECHANICAL CONVERTER OF AN ELECTRODYNAMIC TYPE

Purpose. The aim of the paper is to study the influence of geometrical parameters, namely, the number of layers and the cross section of the copper tire of the inductor and the armature coils on the power and speed indicators of a linear pulse electromechanical converter (LPEC) of an electrodynamic type. Methodology. On the basis of the developed chain mathematical model, recurrent relations are obtained for the calculation of interconnected electromagnetic, mechanical and thermal processes of LPEC of an electrodynamic type. The effect of the thickness of a square copper tire and the number of its layers in the inductor and armature coils on the characteristics and characteristics of electrodynamic LPEC is investigated. It is these parameters that determine the number of turns and the axial height of the coils with limited radial dimensions. Results. The influence of the geometrical parameters of the inductor and the armature coils with limited radial dimensions on the electrical and mechanical characteristics of LPEC of an electrodynamic type is established. It has been established that with an increase in the thickness of a rectangular cross-section of copper tire from 1 to 2.5 mm, an increase in the amplitude and pulse of electrodynamic forces (EF) occurs. However, the maximum speed of the armature is the highest at LPEC wound with a 1.5 mm thick tire. The highest efficiency value is demonstrated by LPEC, in which the inductor and armature coils are wound with a 2 mm thick tire. With an increase in the number of layers of the inductor coil tire, the amplitude of the EF decreases significantly, and the magnitude of the EF pulse decreases slightly. As a result, the maximum armature speed, efficiency and temperature rise of the coils are reduced. Originality. It is established that the largest amplitude of the EF is realized in LPEC with the minimum number of layers of tires of the inductor and armature coils. The largest value of the pulse EF occurs when the maximum number of layers of the inductor and the armature. In this case, the largest values of the amplitude and pulse of the EF occur under the condition that the number of tire layers of the inductor and the armature coils are the same. Practical value. It has been established that the greatest efficiency 21.82 % is realized in LPEC, in which the number of tire layers is 2 mm thick with inductor and armature coils are 4. A catapult model for launching an unmanned aerial vehicle was made and tested on the basis of LPEC of an electrodynamic type. References 12, figures 6.

Key words: linear pulse electromechanical converter of electrodynamic type, chain mathematical model, recurrent relations, geometrical parameters of inductor and armature coils, electrodynamic forces, efficiency.

Розроблена ланцюгова математична модель лінійного імпульсного електромеханічного перетворювача (ЛІЕП) електродинамічного типу. Отримано рекурентні співвідношення для розрахунку взаємопов'язаних електромагнітних, механічних і теплових процесів. Встановлено, що при збільшенні товщини квадратної мідної шини котушок індуктора і якоря від 1,0 до 2,5 мм збільшуються амплітуда і величина імпульсу електродинамічних зусиль (ЕДЗ). Максимальна швидкість якоря найбільша у ЛІЕП, котушки індуктора і якоря якого намотані шиною товщиною 1,5 мм. Найбільше значення ККД у ЛІЕП, котушки якого намотані шиною товщиною 2,0 мм. При збільшенні кількості шарів шини котушки індуктора амплітуда ЕДЗ знижується істотно, а величина імпульсу ЕДЗ – незначно. Внаслідок цього знижуються максимальна швидкість якоря, ККД і перевищення температури котушок. Найбільша амплітуда ЕДЗ реалізується в ЛІЕП при мінімальній кількості шарів шин котушок індуктора і якоря, а найбільша величина імпульсу ЕДЗ виникає при максимальній їх кількості. При цьому найбільші значення амплітуди і імпульсу ЕДЗ виникають за умови, коли число шарів шини котушок однакові. Найбільший ККД (21,82 %) реалізується в ЛІЕП, у якого котушки індуктора і якоря намотані в чотири шари квадратної шини товщиною 2,0 мм. На базі ЛІЕП електродинамічного типу була виготовлена і випробувана модель катапульты для запуску безпілотного літального апарату. Бібл. 12, рис. 6.

Ключові слова: лінійний імпульсний електромеханічний перетворювач електродинамічного типу, ланцюгова математична модель, рекурентні співвідношення, геометричні параметри котушок індуктора і якоря, електродинамічні зусилля, ККД.

Разработана цепная математическая модель линейного импульсного электромеханического преобразователя (ЛИЭП) электродинамического типа. Получены рекуррентные соотношения для расчета взаимосвязанных электромагнитных, механических и тепловых процессов. Установлено, что при увеличении толщины квадратной медной шины катушек индуктора и якоря от 1,0 до 2,5 мм увеличиваются амплитуда и величина импульса электродинамических усилий (ЭДУ). Максимальная скорость якоря наибольшая у ЛИЭП, катушки индуктора и якоря которого намотаны шиной толщиной 1,5 мм. Наибольшее значение КПД у ЛИЭП, катушки которого намотаны шиной толщиной 2,0 мм. При увеличении количества слоев шины катушки индуктора амплитуда ЭДУ уменьшается существенно, а величина импульса ЭДУ – незначительно. Вследствие этого снижаются максимальная скорость якоря, КПД и превышения температуры катушек. Наибольшая амплитуда ЭДУ реализуется в ЛИЭП при минимальном количестве слоев шин катушек индуктора и якоря, а наибольшая величина импульса ЭДУ возникает при максимальном их количестве. При этом наибольшие значения амплитуды и импульса ЭДУ возникают при условии, когда количество слоев шин катушек одинаковы. Наибольший КПД (21,82 %) реализуется в ЛИЭП, у которого катушки индуктора и якоря намотаны в четыре слоя квадратной шини толщиной 2,0 мм. На базе ЛИЭП электродинамического типа была изготовлена и испытана модель катапульты для запуска беспилотного летательного аппарата. Библ. 12, рис. 6.

Ключевые слова: линейный импульсный электромеханический преобразователь электродинамического типа, цепная математическая модель, рекуррентные соотношения, геометрические параметры катушек индуктора и якоря, электродинамические усилия, КПД.

Introduction. Linear pulse electromechanical converters (LPEC) allow to provide a high speed of the actuator (A) in the short active area and/or to create powerful force pulses at its slight displacement [1-3]. Such converters are used in many branches of science and technology as electromechanical accelerators and shock-power devices [4, 5]. One of the most promising is LPEC of electrodynamic type [6, 7]. In this converter, which has a coaxial configuration, the fixed inductor and accelerated armature are made in the form of monolithic disk coils, which are impregnated with epoxy resin. Serially connected the inductor and the armature are tightly wound with the same copper tire. The current from a pulsed power source containing a capacitive energy storage (CES) is excited in them [4, 8]. The armature is connected to the inductor and to the power source using movable (flexible or sliding) current leads. The inductor and the armature are connected in opposite directions by the magnetic field, as a result of which electrodynamic forces (EFs) of repulsion act between it. These EFs cause axial displacement of the armature relative to the fixed inductor (Fig. 1,a).

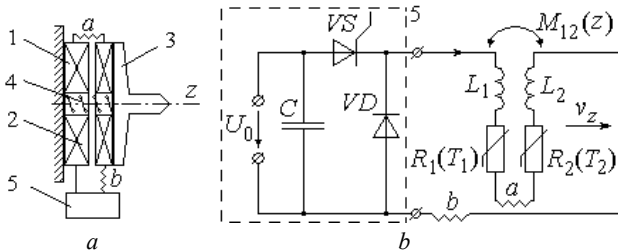


Fig. 1. Constructive (a) and electric (b) circuits of LPEC of electrodynamic type: 1 – inductor; 2 – armature; 3 – actuator; 4 – return spring; 5 – power supply; a, b – flexible current leads

In the process of LPEC operation, a change in the magnetic coupling between the armature and the inductor occurs. In addition, their resistances increase due to heating with high-density pulsed current. These features of the operating process must be taken into account in the mathematical model of LPEC of electrodynamic type [9]. When operating in a dynamic mode with a rapid change of electromagnetic, mechanical and thermal parameters, the efficiency of LPEC is not high enough, which is due, in particular, to the lack of justification for choosing the geometric parameters of active elements – inductor and armature coils.

The goal of the paper is the study of the influence of geometrical parameters, namely, the number of layers and the cross section of the copper tire of the inductor and the armature coils on the power and speed indicators of LPEC of electrodynamic type.

Mathematical model. Consider a mathematical model of LPEC of electrodynamic type, which uses the concentrated parameters of the inductor and the armature. We will assume that the fixed inductor and the accelerated armature are made in the form of coaxially mounted circular multi-turn disk coils that are tightly wound with the same square-section copper tire.

To take into account the interconnected electrical, magnetic, mechanical and thermal processes, as well as a

number of nonlinear dependencies, the solutions of the equations describing the indicated processes will be presented in recurrent form [10].

When a starting pulse is applied to the thyristor *VS*, the inductor and the armature are excited by an aperiodic polar pulse from the CES *C*, shunted by a reverse diode *VD* (Fig. 1,b). We believe that in a pulsed power supply the resistance of the diode *VD* and thyristor *VS* in the forward direction is negligible, and in the opposite direction their conductivity is just as small.

Electrical processes in LPEC of an electrodynamic type on the time interval $\{0, t_1\}$, where t_1 is the time at which the CES voltage is $u_C = 0$, can be described by the equation:

$$[R_1(T_1) + R_2(T_2)] \cdot i + \frac{d\psi}{dt} + \frac{1}{C} \int_0^t idt = 0, \quad u_C(0) = U_0, \quad (1)$$

where $n = 1, 2$ are the inductor and armature indexes, respectively; R_n, T_n, L_n are the active resistance, temperature and inductance of the n -th element; M_{12} is the mutual inductance between the inductor and the armature, moving along the z axis with speed v_z ;

$$\frac{d\psi}{dt} = [L_1 - 2M_{12}(z) + L_2] \frac{di}{dt} - 2iv_z(t) \frac{dM_{12}}{dz}. \quad (2)$$

Substituting equation (2) into (1) we obtain:

$$\left(R_1(T_1) + R_2(T_2) - 2v_z(t) \frac{dM_{12}}{dz} \right) \cdot i + [L_1 - 2M_{12}(z) + L_2] \frac{di}{dt} + \frac{1}{C} \int_0^t idt = 0. \quad (3)$$

The solution of equation (3) can be represented as:

$$i = A_1 \exp(\alpha_1 t) + A_2 \exp(\alpha_2 t), \quad (4)$$

where A_1, A_2 are the arbitrary constants,

$$\alpha_{1,2} = -0,5 \frac{\Theta}{\Xi} \pm \left[0,25 \left(\frac{\Theta}{\Xi} \right)^2 - \frac{1}{\Xi C} \right]^{0,5}$$

are the roots of the characteristic equation; $\Xi = L_1 - 2M_{12}(z) + L_2$;
 $\Theta = R_1(T_1) + R_2(T_2) - 2v_z(t) \frac{dM_{12}}{dz}$.

To represent the solution in a recurrent form, we define the values of arbitrary constants at the time t_k .

If $\Theta > 2\sqrt{\Xi C^{-1}}$, then after a series of transformations we get:

$$A_{1,2} = \frac{u_C(t_k) + \Theta \cdot i(t_k) + \alpha_{2,1} \Xi \cdot i(t_k)}{\Xi \exp(\alpha_{1,2} t_k) (\alpha_{2,1} - \alpha_{1,2})}. \quad (5)$$

Substituting expressions (5) into equation (4), we obtain the expression for the current:

$$i(t_{k+1}) = \frac{u_C(t_k) + \Theta \cdot i(t_k)}{\Xi(\alpha_2 - \alpha_1)} [\exp(\alpha_1 \Delta t) - \exp(\alpha_2 \Delta t)] + \frac{i(t_k)}{\alpha_2 - \alpha_1} [\alpha_2 \exp(\alpha_1 \Delta t) - \alpha_1 \exp(\alpha_2 \Delta t)], \quad (6)$$

where $\Delta t = t_{k+1} - t_k$.

Voltage on the CES:

$$u_C(t_{k+1}) = \frac{u_C(t_k) + \Theta \cdot i(t_k)}{\alpha_2 - \alpha_1} [\alpha_2 \exp(\alpha_1 \Delta t) - \alpha_1 \exp(\alpha_2 \Delta t)] + \varepsilon \frac{i(t_k)}{\alpha_2 - \alpha_1} [\alpha_2^2 \exp(\alpha_1 \Delta t) - \alpha_1^2 \exp(\alpha_2 \Delta t)] \quad (7)$$

If $\Theta < 2\sqrt{\varepsilon C^{-1}}$, then the roots of the characteristic equation can be represented as:

$$\alpha_{1,2} = -\delta \pm j\omega_1 = \omega_0 \exp(j(\pi \pm \theta)), \quad (8)$$

where $\delta = 0,5\Theta\varepsilon^{-1}$; $\theta = \arctg(4\varepsilon\Theta^{-2}C^{-1} - 1)^{0,5}$;

$$\omega_0 = (\varepsilon C)^{-0,5}; \quad \omega_1 = (\varepsilon^{-1}C^{-1} - 0,25\Theta^2\varepsilon^{-2})^{0,5}.$$

Substituting the values of the roots (8) into equations (6), (7) and taking into account that

$$2j\sin(\omega_1 \Delta t) = \exp(j\omega_1 \Delta t) - \exp(-j\omega_1 \Delta t),$$

we get:

$$i(t_{k+1}) = -\omega_1^{-1} \exp(-\delta \Delta t) \left\{ \varepsilon^{-1} [u_C(t_k) + \Theta \cdot i(t_k)] \sin(\omega_1 \Delta t) + \omega_0 i(t_k) \sin(\omega_1 \Delta t - \theta) \right\} \quad (9)$$

Voltage on the CES:

$$u_C(t_{k+1}) = -\omega_0 \omega_1^{-1} \exp(-\delta \Delta t) \left\{ [u_C(t_k) + \Theta \cdot i(t_k)] \times \sin(\omega_1 \Delta t - \theta) + i(t_k) \omega_0 \varepsilon \sin(\omega_1 \Delta t - 2\theta) \right\} \quad (10)$$

If $\Theta = 2\sqrt{\varepsilon C^{-1}}$, then $\delta = \omega_0$ and current is:

$$i(t_{k+1}) = \exp(-\delta \Delta t) \Delta t \left\{ i(t_k) \delta - \varepsilon^{-1} [u_C(t_k) + \Theta \cdot i(t_k)] \right\} \quad (11)$$

Voltage on the CES:

$$u_C(t_{k+1}) = [u_C(t_k) - i(t_k) \varepsilon \delta + \Theta \cdot i(t_k)] (\delta \Delta t + 1) \times \exp(-\delta \Delta t) + i(t_k) (\varepsilon \delta - \Theta) \quad (12)$$

Current in LPEC in the time interval $\{t_1, \infty\}$ varies according to the law:

$$i(t_{k+1}) = i(t_k) \exp(-\Theta \varepsilon^{-1} \Delta t) \quad (13)$$

Mechanical processes in LIEP can be described by the equation:

$$i^2(t) \frac{dM}{dz} = (m_a + m_2) \frac{dv_z}{dt} + K_P \Delta z(t) + K_T v_z(t) + 0,125\pi\gamma_a \beta_a D_{2m}^2 v_z^2(t), \quad (14)$$

where m_2, m_a are the mass of the armature and A, respectively; K_P is the value of elasticity of the return spring; $\Delta z(t)$ is the value of the displacement of the armature with A; K_T is the coefficient of dynamic friction; γ_a is the density of the medium of displacement; β_a is the aerodynamic resistance coefficient; D_{2m} is the outer diameter of the A.

The effectiveness of the axial force action on the armature will be estimated by the value of the impulse of EF [11]:

$$P_1 = \int F(z, t) dt, \quad (15)$$

where $F(z, t)$ is the instantaneous value of axial EF acting on the armature.

Based on equation (14), the value of the displacement of the armature with A can be represented as a recurrent relation:

$$s(t_{k+1}) = s(t_k) + v_z(t_k) \Delta t + g \Delta t^2 / (m_a + m_2), \quad (16)$$

where $v_z(t_{k+1}) = v_z(t_k) + g \Delta t / (m_a + m_2)$ is the speed of the armature with A along the z axis;

$$g = i^2(t_k) \frac{dM}{dz}(z) - K_P \Delta z(t_k) - K_T v_z(t_k) - 0,125\pi\gamma_a \beta_a D_{2m}^2 v_z^2(t_k).$$

Thermal processes. In the absence of displacement of the armature, which occurs either before the start of the forward stroke, or after the return stroke, there is a thermal contact between the inductor and armature coils through the insulation gasket. The temperatures of the n -th active elements of the LPEC of electrodynamic type can be described by the recurrent relation [12]:

$$T_n(t_{k+1}) = T_n(t_k) \xi + (1 - \xi) \left\{ \pi^{-1} i_n(t_k) R_n(T_n) (D_{en}^2 - D_{in}^2)^{-1} + 0,25\pi T_0 D_{en} H_n \alpha_{Tn} + T_m(t_k) \lambda_a(T) d_a^{-1} \right\} \left\{ 0,25\pi \alpha_{Tn} D_{en} H_n + \lambda_a(T) d_a^{-1} \right\}^{-1}, \quad (17)$$

$$\text{where } \xi = \exp \left\{ -\frac{\Delta t}{C_n(T_n) \gamma_n} \left(0,25 D_{en} \alpha_{Tn} + \frac{\lambda_a(T)}{d_a H_n} \right) \right\};$$

$\lambda_a(T)$ is the thermal conductivity of the insulation gasket; d_a is the gasket thickness; D_{en}, D_{in} are the outer and inner diameters of the active elements, respectively; α_{Tn} is the heat transfer coefficient of the n -th active element; C_n is the heat capacity of the n -th active element.

Temperatures of the n -th active elements when the armature is moved and there is no thermal contact between the armature and the inductor can be described by the recurrence relation:

$$T_n(t_{k+1}) = T_n(t_k) \chi + (1 - \chi) \left\{ T_0 + 4\pi^{-2} i_n(t_k) R_n(T_n) \alpha_{Tn}^{-1} \times D_{en}^{-1} H_n^{-1} (D_{en}^2 - D_{in}^2)^{-1} \right\}, \quad (18)$$

$$\text{where } \chi = \exp \left\{ -0,25 \Delta t D_{en} \alpha_{Tn} C_n^{-1} (T_n) \gamma_n^{-1} \right\}.$$

The initial conditions of the mathematical model of LPEC are as follows:

$T_n(0) = T_0$ – the temperature of the n -th active element;

$i_n(0) = 0$ – the current of the n -th active element;

$s(0) = s_0$ – the initial axial distance between the coils of the armature and the inductor;

$u_c(0) = U_0$ – the CES voltage;

$v_z(0) = 0$ – the armature speed along the z axis.

The efficiency of the LPEC of electrodynamic type will be estimated by the relation:

$$\eta = 100 \frac{(m_2 + m_a) v_z^2 + K_P s^2}{CU_0^2} \%. \quad (19)$$

Main parameters of LPEC of electrodynamic type. Consider LPEC, whose movable armature and fixed inductor are made in the form of flat coaxially mounted disk coils. At the armature, one end side faces the inductor, and the second one interacts with A. The inductor ($n=1$) and the armature ($n=2$) are tightly wound with K_{pn} layers of a square-section copper tire with thickness a . The outer diameter of the n -th element is $D_{en}=100$ mm, the inner diameter is $D_{in}=10$ mm. The CES has the following parameters: capacitance $C = 3$ mF, voltage $U_0 = 0,4$ kV. The initial distance between the inductor and the armature is $s_0=1$ mm. The coefficient of elasticity of the return spring $K_P=25$ kN/m. Mass of A is $m_a=0,25$ kg.

We investigate the influence of the thickness a of a copper square tire and the number K_{pn} of its layers in the

inductor and armature coils on the characteristics and indicators of the LPEC of electrodynamic type. These parameters determine the number of turns

$$N_n = Ent \left(0,5 \frac{D_{en} - D_{in}}{a + 2\delta} \right) K_{pn}$$

and the axial height

$$H_n = (a + 2\delta) K_{pn}$$

of the n -th coils with limited radial dimensions, where $Ent(f)$ is the largest integer not exceeding f ; δ is the insulation thickness of the copper tire.

Investigation of operation processes in LPEC.

Consider the electrical and mechanical characteristics of the LPEC of electrodynamic type, in which both the inductor and armature coils are tightly wound in four layers $K_{pn}=4$ with a square tire of different thickness (Fig. 2). As the thickness of the copper tire a increases from 1 to 2,5 mm, the number of turns of each coil N_n decreases from 160 to 68, and the axial height H_n increases from 4,4 to 10,4 mm. In this case, the amplitude of the current i_m increases significantly – from 0,30 to 1,56 kA, and the amplitude of the current density j_m decreases slightly from 304,3 to 250,4 A/mm².

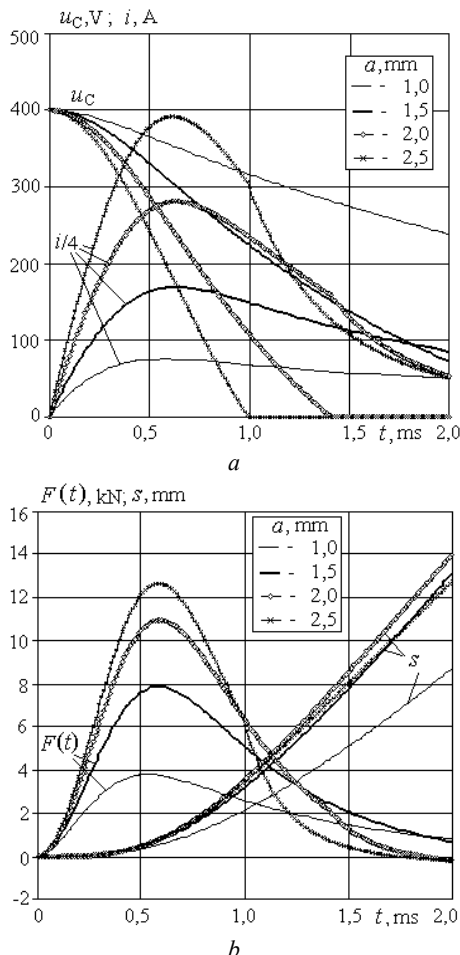


Fig. 2. Electrical (a) and mechanical (b) characteristics of LPEC, the coils of which are wound with a copper tire of different thickness a

An increase in the thickness of the copper tire a changes the regularities of the flow of electrical processes: the CES voltage u_C decreases to zero value

faster, and the current takes the form of a clear pulse with a significant increase in the leading front and falling of the falling front. With an increase in the thickness of the copper tire a from 1 to 2,5 mm, the power indicators of LPEC increase. The amplitude of the EF F_m increases from 3,78 to 12,65 kN, and the impulse of the EF P_1 increases from 4,52 to 9,16 N·s. However, speed indicators depending on the thickness of the tire do not have an unequivocal pattern.

The maximum speed of the armature V_m is the greatest at LPEC, whose coils are wound with a tire of thickness $a = 1,5$ mm, and is 11,24 m/s. If the tire has a smaller or greater thickness, then the speed decreases: at $a = 1$ mm – $V_m = 8,16$ m/s, and at $a = 2,5$ mm – $V_m = 9,44$ m/s.

An ambiguous dependence on tire thickness is also demonstrated by the efficiency of the LPEC of electrodynamic type. The highest efficiency value $\eta = 21,8$ % has LPEC, in which the inductor and armature coils are wound with a tire of thickness of $a = 2$ mm. If the coils are wound with thinner or thicker tires, the efficiency decreases: at $a = 1,5$ mm $\eta = 20$ %, at $a = 2,5$ mm $\eta = 18,8$ %. Note that if the coils are wound with an even thinner tire $a = 1$ mm, then the efficiency takes an even lower value $\eta = 8,5$ %.

With increasing thickness of copper tire a from 1 to 2,5 mm, the temperature rise of the inductor and armature coils θ_n decreases from 0,6 to 0,23 °C.

On the basis of the analysis performed, it can be concluded that the most effective is the LPEC of electrodynamic type, in which the inductor and armature coils are wound with a copper tire with a thickness of $a = 2$ mm. The number of turns of each coil is $N_n = 84$, and their axial height is $H_n = 8,4$ mm.

Investigate the effect of the number of layers of the tire of the inductor coil K_{p1} on the indicators of the LPEC of electrodynamic type. Obviously, as K_{p1} increases, the number of turns N_1 and the axial height H_1 of the inductor coil increase. We will consider LPEC, in which the inductor and armature coils are wound with a copper tire with thickness of $a = 2$ mm. The armature coil is wound in two layers, contains the number of turns $N_2 = 22$ and has the axial height $H_2 = 4,2$ mm. Consider the electrical and mechanical characteristics of LPEC, in which the inductor coil is wound with several layers K_{p1} (Fig. 3).

With an increase in the number of tire layers of the inductor coil K_{p1} three times (from 2 to 6), the amplitude of the current i_m decreases almost in the same proportion (from 2,57 to 0,86 kA), and the current pulse itself becomes more stretched due to an increase in the front and rear fronts. When the parameter K_{p1} is increased, the voltage of the CES u_C decreases to zero value more slowly.

With an increase in the number of tire layers of the inductor coil K_{p1} 3 times the amplitude of the EF F_m decreases 4.1 times (from 18,72 to 4,57 kN), while the impulse of the EF P_1 decreases slightly (from 6,79 to 5,69 N·s). As a result, the maximum speed of the armature with A V_m (from 12,54 to 10,53 m/s), efficiency η (from 18,08 to 13,57%) and temperature rise of the coils θ_n (from 0,73 to 0,3 °C) are reduced. These patterns of change in the maximum speeds V_m depending on the number of layers

of the tire of the inductor coil K_{p1} manifest themselves in a change in the nature of the displacement of the armature with A s (see Fig. 3,b).

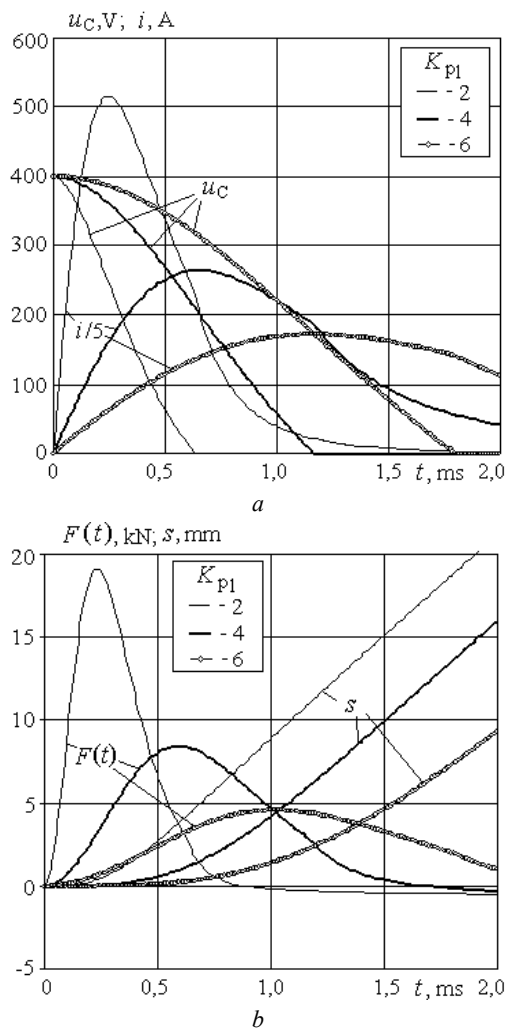


Fig. 3. Electrical (a) and mechanical (b) characteristics of LPEC, the coils of which are wound with tire thickness $a = 2$ mm with a different number of layers of the inductor coil tire K_{p1}

Influence of the number of layers of the tire of inductor and armature coils on the indicators of LPEC. Consider the effect of the mutual ratio of the number of layers of the tire of inductor K_{p1} and armature K_{p2} coils of thickness $a = 2$ mm on operation indicators of LPEC of electrodynamic type. We assume that the maximum number of layers of the tire coils $K_{p1} = K_{p2} = 6$.

With an increase in the number of tire layers of the inductor coil K_{p1} and/or of the armature coil K_{p2} , the amplitude of the current i_m decreases, but in different degrees. So, if the number of tire layers of both coils is minimal $K_{p1} = K_{p2} = 1$, then $i_m = 5,8$ kA. If the number of tire layers of one of the coils is minimal and of the second one is maximum, then the following pattern is observed: at $K_{p1} = 1, K_{p2} = 6$ the current amplitude decreases to $i_m = 0,865$ kA, and at $K_{p1} = 6, K_{p2} = 1$ the current amplitude decreases to $i_m = 0,846$ kA. If the number of tire layers of both coils is maximum $K_{p1} = K_{p2} = 6$, then the current amplitude decreases to the greatest extent (to the value $i_m = 0.7$ kA).

Similar dependencies on the number of tire layers of the inductor K_{p1} and armature K_{p2} coils are observed at the coil temperature rises. The maximum temperature rise ($\theta_{1,2} = 1,5$ °C) occurs at the minimum number of layers of the coil tire $K_{p1} = K_{p2} = 1$ and minimum ($\theta_{1,2} = 0,21$ °C) at the maximum number of layers of the tire $K_{p1} = K_{p2} = 6$. At $K_{p1} = 1$ and $K_{p2} = 6$ the temperature rises $\theta_{1,2} = 0,33$ °C, and at $K_{p1} = 6$ и $K_{p2} = 1$ the temperature rises $\theta_{1,2} = 0,31$ °C.

The ratio of the number of layers of tire of coils significantly affects the power indicators of the LPEC of electrodynamic type (Fig. 4).

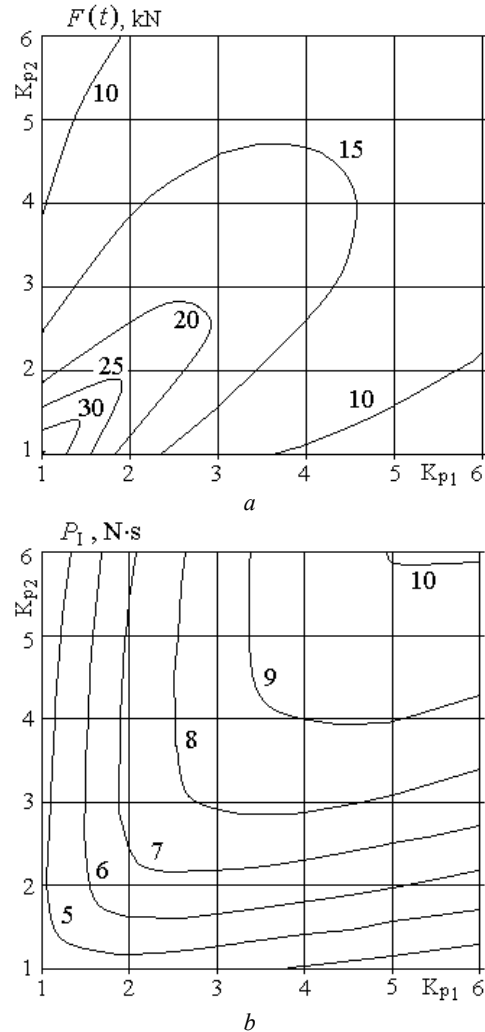


Fig. 4. Distributions of the maximum value (a) and impulse (b) of the EF depending on the ratio of the number of tire layers of the inductor and armature coils of the LIEP

The amplitude of the EF F_m is the greatest at the minimum number of layers of tires of inductor and armature coils. At $K_{p1} = K_{p2} = 1$, the value of $K_{p1} = K_{p2} = 1$ kN. With an increase in the number of layers of the tire of one of the coils, this value is significantly reduced. So, at $K_{p1} = 1$ and $K_{p2} = 6$ the amplitude of the EF is $F_m = 2,75$, and at $K_{p1} = 6$ and $K_{p2} = 1$ the amplitude of the EF is $F_m = 2,34$ kN. If the number of tire turns of the inductor and armature coils is maximum $K_{p1} = K_{p2} = 6$, then the amplitude of the EF increases to $F_m = 7,6$ kN. We can note the following pattern: the largest values of the amplitude of the EF F_m are observed under the condition that the numbers of tire layers of the inductor and armature coils are the same.

Impulse of EF P_1 has a different pattern on the ratio of the number of tire layers of the inductor and armature coils. The largest value of the impulse of EF occurs at the maximum number of layers of the tire of coils. At $K_{p1}=K_{p2}=6$ the value of $P_1=10,06$ N·s. If the number of layers of the inductor and the armature tire is minimal, then the value of the impulse of EF is reduced by more than two times. At $K_{p1}=K_{p2}=1$ the value of $P_1=4,49$ N·s. The highest impulse values of the EF P_1 are realized when the number of tire layers of the inductor and armature

coils is equal. If the number of tire layers of one of the coils is maximal, and in the second one is minimal, then the EF impulse decreases. At $K_{p1}=1$ and $K_{p2}=6$ the impulse of EF $P_1=4,06$ N·s, and at $K_{p1}=6$ and $K_{p2}=1$ $P_1=3,3$ N·s.

Let us consider the regularity of the distribution of the efficiency of LPEC of electrodynamic type as a function of the ratio of the number of tire layers of the inductor and the armature coils for its various thickness a (Fig. 5).

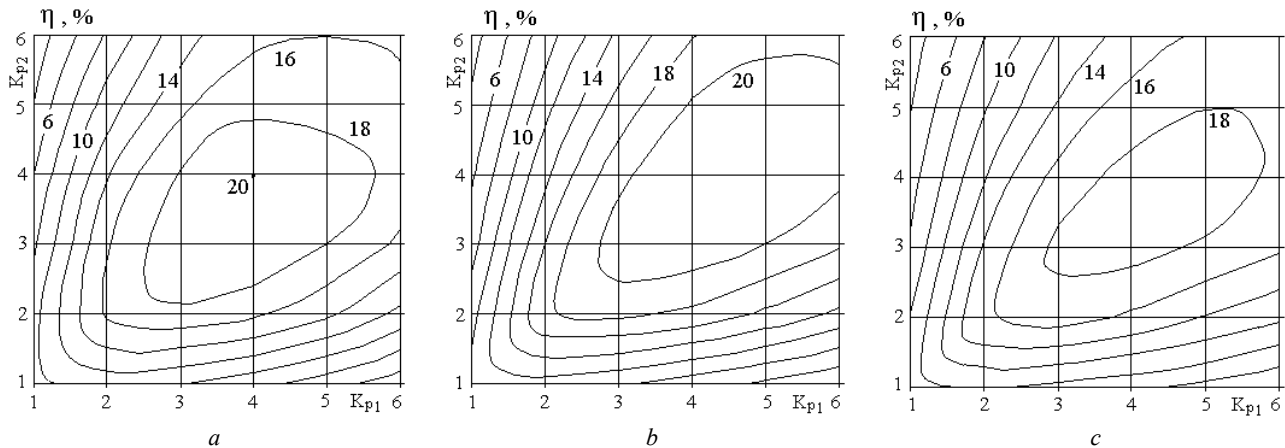


Fig. 5. The LPEC efficiency distributions depending on the ratios of the number of tire layers of the inductor and armature coils at the tire thickness a : 1,5 mm (a); 2 mm (b); 2,5 mm (c)

The highest values of efficiency are realized at a certain ratio of K_{p1} and K_{p2} . If the tire thickness a is equal to 1,5 mm or 2 mm, then the highest efficiency value is realized at $K_{p1}=K_{p2}=4$ and takes the values $\eta = 20,01$ % and $\eta = 21,82$ %, respectively. If the tire thickness is $a = 2,5$ mm, then the greatest efficiency value ($\eta = 18,91$ %) is realized at $K_{p1}=4$ and $K_{p2}=3$.

On the basis of the research carried out, it can be concluded that there is an optimal thickness of the copper tire $a = 2$ mm and the corresponding number of turns in each layer of the inductor and armature coils. From the point of view of power indicators, the number of layers of the tire of coils should be the maximum of the considered range ($K_{p1}=K_{p2}=6$). From the point of view of the efficiency of acceleration of A, coils should have fewer layers ($K_{p1}=K_{p2}=4$).

Taking into account the relationships obtained, on the basis of an LPEC of electrodynamic type a model of a catapult for launching an unmanned aerial vehicle (UAV) was made (Fig. 6).

In this model, both inductor and armature coils are wound with a copper tire and are compounded with epoxy resin in a rectangular insulating frame. The inductor coil is attached to the starting stop wall, and the armature coil is made with the possibility of axial movement along the central guide.

The electrical leads of the inductor and armature coils are located between the two dielectric guide plates and are connected by flexible wires to each other and to the power source. The armature coil is braked by means of an elastic damper attached to the brake stop wall. To the coil of the armature accelerating protrusion is attached that pushes the UAV.



Fig. 6. Model of a catapult for launching an UAV: 1 – guide plates for moving an UAV; 2 – UAV; 3 – guide plates for moving the current leads of the armature coil; 4 – brake stop wall; 5 – brake elastic damper; 6 – accelerating protrusion; 7 – armature coil; 8 – inductor coil; 9 – starting stop wall; 10 – current lead coils

The carried out tests of the model with the parameters set above confirmed the validity of the theoretical studies carried out on the LPEC of electrodynamic type.

Conclusions.

1. On the basis of the developed chain mathematical model, recurrent relations are obtained for the calculation of interconnected electromagnetic, mechanical and thermal processes in LPEC of electrodynamic type.

2. It is established that with an increase in the thickness of the square copper tire of the inductor and armature coils from 1 to 2,5 mm, the amplitude and impulse of the EF increase. However, the maximum speed of the armature is the highest at LPEC, the coils of which are wound with a tire 1,5 mm thick. The highest efficiency value is demonstrated by LPEC, in which the coils are wound with a tire 2 mm thick.

3. With an increase in the number of layers of the inductor coil tire, the amplitude of the EF decreases significantly, while the value of the EF impulse decreases slightly. This reduces the maximum speed of the armature, efficiency and temperature rise of the inductor and armature coils.

4. The greatest amplitude of the EF is implemented in LPEC at the minimum number of tire layers of the inductor and armature coils. The largest value of the impulse of the EF occurs at the maximum number of layers of the tire of coils. In this case, the largest values of the amplitude and impulse of the EF occur under the condition that the number of tire layers of both coils is the same.

5. The highest efficiency (21,82%) is realized in LPEC, in which the inductor and armature coils have four layers of square tire 2 mm thick.

6. A catapult model for launching an unmanned aerial vehicle was made and tested on the basis of the LPEC of electrodynamic type.

REFERENCES

1. Balikci A., Zabar Z., Birenbaum L., Czarkowski D. Improved performance of linear induction launchers. *IEEE Transactions on Magnetics*, 2005, vol.41, no.1, pp. 171-175. doi: **10.1109/tmag.2004.839283**.
2. Tomashevsky D.N., Koshkin A.N. Modeling of linear impulse electric motors. *Russian Electrical Engineering*, 2006, no.1, pp. 24-27. (Rus).
3. Bissal A., Magnusson J., Engdahl G. Electric to mechanical energy conversion of linear ultrafast electromechanical actuators based on stroke requirements. *IEEE Transactions on Industry Applications*, 2015, vol.51, no.4, pp. 3059-3067. doi: **10.1109/tia.2015.2411733**.
4. Bolyukh V.F., Shchukin I.S. *Lineinye induktsionno-dinamicheskie preobrazovateli* [Linear induction-dynamic converters]. Saarbrücken, Germany, LAP Lambert Academic Publ., 2014. 496 p. (Rus).
5. Bissal A., Eriksson A., Magnusson A., Engdahl G. Hybrid multi-physics modeling of an ultra-fast electro-mechanical actuator. *Actuators*, 2015, vol.4, no.4, pp. 314-335. doi: **10.3390/act4040314**.
6. Bolyukh V.F., Oleksenko S.V., Shchukin I.S. Comparative analysis of linear pulse electromechanical converters electromagnetic and induction types. *Technical Electrodynamics*, 2016, no.5, pp. 46-48. (Rus).
7. Bissal A., Magnusson J., Engdahl G. Comparison of two ultra-fast actuator concept. *IEEE Transactions on Magnetics*, 2012, vol.48, no.11, pp. 3315-3318. doi: **10.1109/tmag.2012.2198447**.
8. D.-K. Lim, D.-K. Woo, I.-W. Kim, D.-K. Shin, J.-S. Ro, T.-K. Chung, H.-K. Jung. Characteristic Analysis and Design of a Thomson Coil Actuator Using an Analytic Method and a Numerical Method. *IEEE Transactions on Magnetics*, 2013, vol.49, no.12, pp. 5749-5755. doi: **10.1109/tmag.2013.2272561**.
9. Li W., Koh C.S. Parametric analysis of Thomson-coil actuator using adaptive equivalent circuit method. *Digests of the 2010 14th Biennial IEEE Conference on Electromagnetic Field Computation*, May 2010, pp. 1-9. doi: **10.1109/cefc.2010.5481673**.
10. Bolyukh V.F., Kocherga A.I., Schukin I.S. Investigation of a linear pulse-induction electromechanical converter with different inductor power supply circuits. *Electrical engineering & electromechanics*, 2018, no.1, pp. 21-28. doi: **10.20998/2074-272X.2018.1.03**.
11. Bolyukh V.F., Oleksenko S.V., Schukin I.S. Efficiency of linear pulse electromechanical converters designed to create impact loads and high speeds. *Electrical engineering & electromechanics*, 2015, no.3, pp. 31-40. doi: **10.20998/2074-272X.2015.3.05**.
12. Bolyukh V.F., Schukin I.S. Investigation of thermal processes in a linear pulse-induction electromechanical converter of cyclic action. *Electrical engineering & electromechanics*, 2017, no.5, pp. 14-22. doi: **10.20998/2074-272X.2017.5.02**.

Received 05.03.2019

V.F. Bolyukh¹, Doctor of Technical Science, Professor,
Yu.V. Kashanskij¹, Postgraduate Student,

I.S. Schukin², Candidate of Technical Science, Associate
Professor,

¹National Technical University «Kharkiv Polytechnic Institute»,
2, Kyrpychova Str., Kharkiv, 61002, Ukraine,
phone +380 57 7076427, e-mail: vfbolyukh@gmail.com

²Firm Tetra, LTD,
2, Kyrpychova Str., Kharkiv, 61002, Ukraine,
phone +380 57 7076427, e-mail: tech@tetra.kharkiv.com.ua

How to cite this article:

Bolyukh V.F., Kashanskij Yu.V., Schukin I.S. Influence of geometrical parameters of the inductor and armature on the indicators of a linear pulse electromechanical converter of an electrodynamic type. *Electrical engineering & electromechanics*, 2019, no.3, pp. 11-17. doi: **10.20998/2074-272X.2019.3.02**.

Ye.I. Baida, M. Clemens, B.V. Klymenko, O.G. Korol, P.Ye. Pustovoitov

APPLICATION OF THE COMPUTING ENVIRONMENT MAPLE TO THE CALCULATION OF THE DYNAMICS OF THE ELECTROMAGNETS IN THE COMPLICATED SYSTEMS OF FORCED CONTROL

Загальний опис теми дослідження. Розглядається запропонована авторами методика розрахунку динаміки електромагнітів, що працюють у складних форсованих системах. Подібні форсовані електромагніти широко застосовуються в електромеханічних комутаційних апаратах, зокрема у вакуумних контакторах, для зменшення їх розмірів, споживання енергії та для підвищення швидкодії, що свідчить про актуальність даної теми. Математична модель динаміки форсованої електромагнітної системи, що враховує особливості поведінки у нестационарних процесах її окремих елементів – механічної системи, магнітного та електричного кіл з урахуванням взаємодії електромагніта з пристроєм керування під час спрацювання апарата, містить певні ознаки наукової новизни і є метою статті. Методика розрахунку динаміки форсованих електромагнітів застосовує математичний пакет Maple. В основу розрахунку покладено математичну модель, яка представляє собою систему нелінійних диференціальних рівнянь магнітного і електричного кіл, доповнених рівняннями руху елементів механічної системи. Застосування пакету Maple, який багато в чому бере на себе складнощі математичного опису різних процесів, автоматично здійснюючи дуже складні і громіздкі математичні перетворення, дозволяє, уникаючи складних процесів вибору способу чисельного інтегрування, програмування складних й громіздких рівнянь та процедур їх чисельного інтегрування, отримувати результати розрахунків у зручній табличній та/або графічній формі, що свідчить про практичну значущість даної роботи. Наведені у статті результати зіставлення розрахунків з опублікованими раніше експериментальними даними, свідчать про високу ефективність запропонованих моделей та методик. Бібл. 10, рис. 6.

Ключові слова: електромагніти, динаміка, форсоване керування, комутаційні апарати, вакуумні контактори, математичний пакет Maple.

Общее описание темы исследования. Рассматривается предложенная авторами методика расчета динамики электромагнитов, работающих в сложных форсированных системах. Подобные форсированные электромагниты широко применяются в электромеханических коммутационных аппаратах, в частности в вакуумных контакторах, для уменьшения их размеров, потребления энергии и для повышения быстродействия, что свидетельствует об актуальности данной темы. Математическая модель динамики форсированной электромагнитной системы, учитывающая особенности поведения в нестационарных процессах ее отдельных элементов – механической системы, магнитной и электрической цепей с учетом взаимодействия электромагнита с устройством управления при срабатывании аппарата, содержит определенные признаки научной новизны и является целью статьи. Методика расчета динамики форсированных электромагнитов применяет математический пакет Maple. В основу расчета положена математическая модель, которая представляет собой систему нелинейных дифференциальных уравнений магнитного и электрического кругов, дополненных уравнениями движения элементов механической системы. Применение пакета Maple, который во многом берет на себя сложности математического описания различных процессов, автоматически осуществляя очень сложные и громоздкие математические преобразования, позволяет, избегая сложных процессов выбора способа численного интегрирования, программирование сложных и громоздких уравнений и процедур их численного интегрирования, получать результаты расчетов в удобной табличной и/или графической форме, что свидетельствует о практической значимости данной работы. Приведенные в статье результаты сопоставления расчетов с опубликованными ранее экспериментальными данными, свидетельствуют о высокой эффективности предложенных моделей и методик. Библ. 10, рис. 6.

Ключевые слова: электромагниты, динамика, форсированное управление, коммутационные аппараты, вакуумные контакторы, математический пакет Maple.

Introduction. DC electromagnets are simpler in design than the AC electromagnets as they have higher reliability and durability. In terms of initial traction force, size and mass, however, they lose significantly in comparison to the the AC electromagnets (which are actually forced electromagnets), because during the operation of the electromagnet, the currents in their windings exceed (ten times or more) the values of currents that are in the windings after the operation of the electromagnet. Forced control of DC electromagnets essentially means that during operation a current flows through a winding, whose value significantly exceeds the current permissible under long-term heating, is used to increase the traction force during operation and to increase the speed of the apparatus. After operation, the current in the winding and, accordingly, its magnetomotive force (MMF) are reduced, but the armature of the electromagnet remains in the final (brought) state, since, at small gaps, the traction force is usually superfluous even at small values of MMF.

Forced electromagnetic systems (FEMS) [1] are widely used in drive systems of low and medium voltage electromechanical switching devices, in particular in contactors, which execute switching operations (switching on and off) the main circuits of powerful electric motors and some other objects.

The FEMS usually includes the electromagnetic mechanism (EMM) – the main contact module and the actuator, which provides the execution of switching operations by contacts (in contactors, the actuator's role is most often performed by a forced unpolarized electromagnet with a rotating spring) and a control device (CD) that performs changes in the windings' control circuit to provide the required values of currents both during operation and in the final state. Note, that in the AC electromagnet which is actually forced, since during the operation the current in the winding is much greater than the current in the final state, the values of the current change without any CD due to the difference in the values of the inductance in the released and final states).

When designing switching devices with FEMS, it is necessary to take into account the interaction of the electromagnet with the control device during the operation of the apparatus. Therefore, it is necessary to calculate the dynamics of the electromagnet taking into account the action of the CD. There is a large number of publications devoted to the methods of calculating the dynamics of electromagnets, some of which are listed in references [2 – 9]. Nonetheless, in our opinion, insufficient attention is given to the issue of the interaction of the forced electromagnet with a CD taking into account the large variety of existing CDs and some features of operation of forced electromagnets in switching devices.

The goal of the work is to describe the mathematical model of FEMS dynamics, which takes into account peculiarities of behavior in switching devices of individual elements of FEMS during transients, as well as to build a technique for calculating the dynamics of forced electromagnets using the computing environment Maple.

Mathematical model. The calculation of the FEMS dynamics, where the electromagnet is only a part of the control system that contains the power source, the mechanical system, the forced control device and the electromagnet itself, is reduced to a solution of coupled differential equations. These describe the transients in the circuits of the windings and in the circuits of the forced control device of these windings, transients in magnetic circuits of electromagnets taking into account the effect of eddy currents. They also describe the dynamics of the moving part of the switching device, namely, the armature of the electromagnet, the main contacts of the apparatus, mechanical parts that connect armature with moving contacts (levers, rods, springs, etc.). In many cases, forced control systems are designed so that, when the switching device is operated, the circuit diagrams of the windings are automatically changed if there are several windings or if there are certain changes in the circuits of the forced control device. In the process of performing the on and off operation of the device, also the mass (the moment of inertia) of the moving system can significantly change. If the switching of the main circuits uses vacuum interrupters, the process of movement is significantly affected by bellows and the actual vacuum, which “prevents” the opening of the contacts, pulling the moving contact to the fixed one. All of the above-mentioned factors must be taken into account by creating separate fragments of the mathematical model of the dynamics of the electromagnet in the composition of the forced control system, i.e., writing the equation for transients in the mechanical system, as well as in the magnetic and electric circuits of the forced electromagnetic system.

Transients in the mechanical system of the switching device. Kinematics of switching devices in many cases are built so that the part of moving elements carries translational motion, and the other part carries rotary motion (Fig. 1). Since the angles of rotation of moving parts in actual apparatus are relatively small and usually do not exceed 10–15°, a rotating motion with a slight error can be reduced to a translational motion relative to an element adopted as a basic one. Such

element may be, for example, an actuator whose armature moves progressively along the axis of the actuator, which is at a distance r_a from the axis of rotation O of the lever, to which other parts of the switching device are attached and which operate at different distances (shoulders) from the axis O. From the initial armature position the path s passed by the actuator is measured. In calculating the dynamics of motion reduced to the motion of the base element (in our case, to the actuator's armature), the masses of parts moving at different distances from the O axis must be replaced by reduced masses in accordance with the condition of maintaining the moment of inertia. For example, the reduced mass m'_d of the part with mass m_d acting at distance r_d from the O axis is given by the formula:

$$m'_d = m_d \cdot r_d^2 / r_a^2 . \quad (1)$$

If the moment of inertia J of some part, for example of the lever shown in Fig. 1, is known, then the calculation of its reduced mass is carried out according to the formula:

$$m'_j = J / r_a^2 . \quad (2)$$

Thus, the actuator's mass reduced to the axis of the actuator's motion for the fragment shown in Fig. 1 will be equal to:

$$m'_a = m_a + m_d \cdot r_d^2 / r_a^2 + J / r_a^2 . \quad (3)$$

The forces that counteract the movement of the actuator's armature must also be replaced by reduced forces, which are calculated in accordance with the condition of maintaining the moment of force. For example, the force F_s of a spring acting at a distance r_s from the O axis in the calculation of the dynamics of the actuator's armature motion should be replaced by the reduced force

$$F'_s = F_s \cdot r_s / r_a . \quad (4)$$

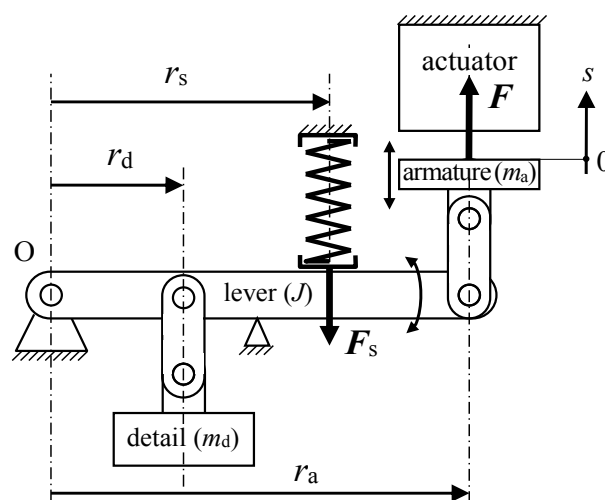


Fig. 1. A fragment of the mechanical system of the switching device

A characteristic feature of electromechanical switching devices is the gradual nature of the forces opposing the movement of the actuator's armature as well as the gradual nature of the change in the mass of moving parts due to the peculiarities of the kinematics of these devices (Fig. 2).

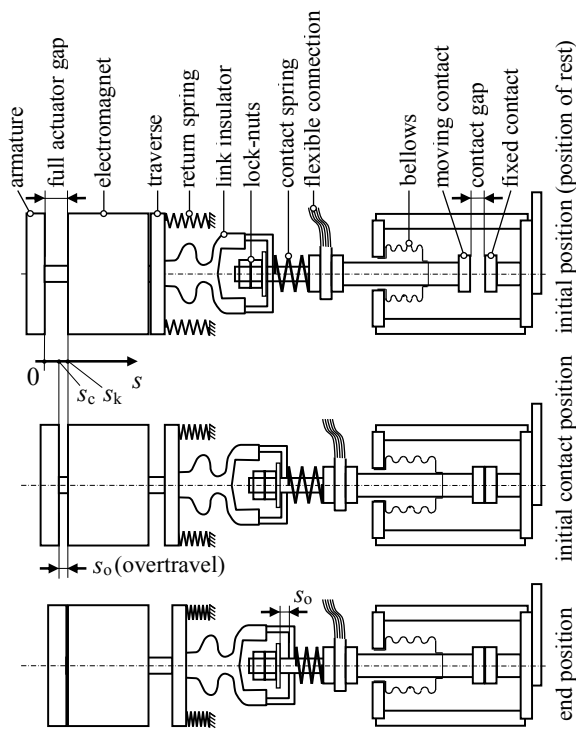


Fig. 2. Kinematic circuits of the switching device in three characteristic positions

During the operation of the switching device, two stages of the motion of its mechanical system can be observed: the first stage – from the initial position (position of rest) to the initial contact position ($0 < s < s_c$) and the second stage – from the of initial contact position to the end position ($s_c < s < s_k$). At the first stage, the reduced mass of moving parts is comprised of the reduced mass of the mechanical system m_v and a reduced mass of moving contacts m_c . At the second stage, the moving contacts stop – they are faced with fixed contacts, therefore the reduced mass of moving parts is almost abruptly reduced to the value m_v

$$m = \begin{cases} m_v + m_c & \text{at } s < s_c; \\ m_v & \text{at } s \geq s_c. \end{cases} \quad (5)$$

Thus, when the switching device operates, there is a motion with a variable mass, which is described by such a system of differential equations:

$$\frac{d}{dt}(m \cdot v) = F - F_r; \quad (6)$$

$$\frac{ds}{dt} = v, \quad (7)$$

where F is the electromagnetic force providing the actuator's movement, F_r is the reduced force that counteracts the movement of the actuator's armature, v is the speed of the actuator's armature, s is the path passed by the armature from the beginning of the movement, t is time.

After performing the differentiation operation in (6), we obtain:

$$m \cdot \frac{dv}{dt} + \frac{dm}{ds} \cdot v^2 = F - F_r; \quad (8)$$

Function (5) is discontinuous, at its differentiation there are pulsed functions which makes it practically impossible to carry out further calculations using (8),

therefore we have applied the approximation of this function with the use of hyperbolic tangent. As a result, the following expression is obtained:

$$m = m_v + m_c \cdot (1 - \text{th}(A \cdot (s - s_c))) / 2, \quad (9)$$

where A is a suitably chosen large constant number.

The function (9) is smooth, allowing for a differentiation operation, but the mathematical expression of the derivative is very cumbersome, but the Maple computing environment does not require the programmer to perform transformations related to bringing the equations to a canonical form: this code performs all the required complex algebraic transformations itself. In the Maple environment it is only necessary to write expressions (7), (8), (9) and write the command that provides the solution of the system of differential equations.

The force F_r , which counteracts the movement of the actuator's armature is formed due to the action of the rotary and contact springs, the action of forces of the deformation of the bellows, the action of vacuum and friction. This force has a step-by-step nature, but since it does not require differentiation, the corresponding expression in the code can be written as follows:

$$F_r = \begin{cases} F_1 + \frac{F_2 - F_1}{s_c} \cdot s & \text{at } s < s_c; \\ F_3 + \frac{F_4 - F_3}{s_k - s_c} \cdot (s - s_c) & \text{at } s \geq s_c, \end{cases} \quad (10)$$

where F_1, F_2 are the values of reduced countermeasures force, respectively, at the beginning and end of the first stage of the movement of the mechanical system of the apparatus; F_3, F_4 are the values of reduced countermeasure force, respectively, at the beginning and end of the second stage of the movement of the mechanical system of the apparatus.

The difference between F_3 and F_2 must be equal to the sum of the values of the initial contact forces at all poles of the apparatus.

Transients in the magnetic circuit. A mathematically rigorous calculation of transient magnetic field can be carried out by solving a system of nonlinear partial differential equations featuring the magnetic vector potential A . Similar problems are solved relatively simply for 2D plane-parallel or plane-meridian fields [9]. In such cases, where the total costs of simulating high-fidelity 3D models is inacceptably high and even 2D models are not applicable, alternative techniques may need to be used including those that have proven themselves well in the past. Such a technique for magnetic circuits is a method of electromagnetic analogies, complemented by new features provided by modern software products, in particular the Maple code.

Figure 3 shows a substitution circuit of the magnetic circuit of a double-rod electromagnet used in the vast majority of vacuum and low voltage contactors. In contrast to the well-known circuit, which is given in many sources, in particular in [1], in this circuit, on each section of the core, divided along the axis into n equal parts, the «eddy» MMFs that arise during transients are introduced:

$$\Delta F_{mej} = \Delta G_c \cdot \frac{d\Phi_j}{dt}, \quad j = 1, 2, \dots, n. \quad (11)$$

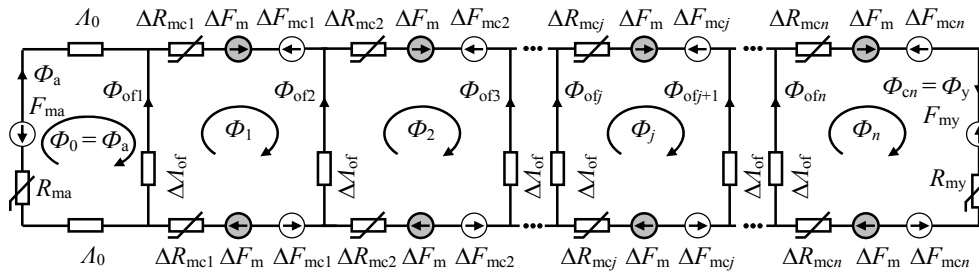


Fig. 3. Substitution circuit of the magnetic circuit of a double-rod electromagnet taking into account the effect of eddy currents in cores, armature and yoke

«Eddy» MMFs also appear in the branches of the substitution circuit corresponding to the sections of the armature and yoke:

$$F_{ma(y)} = G_{a(y)} \cdot \frac{d\Phi_{a(y)}}{dt}. \quad (12)$$

In (11), (12) and in Fig. 3 the following notation is used: ΔG_c is the electrical conductance of the equivalent short-circuited circuit in the eddy current path that arises in the area with the number j divided into n equal parts of the core of length l_c , $G_{a(y)}$ is the electrical conductance of the equivalent short-circuited circuit in the eddy current path generated in the armature, Φ_j is the magnetic flux through the area of the core with the number j . The variables Φ_a , Φ_y are magnetic fluxes through the armature and the yoke, respectively. The variable F_m denotes the MMF of one coil¹, ΔF_m is the MMF of one part of the coil, divided into n equal parts ($\Delta F_m = F_m/n$), R_{ma} , R_{my} are the magnetic resistance of the armature and yoke, respectively. The variable ΔR_{mcj} is the magnetic resistance of the core section with the number j , A_0 is the magnetic conductivity of the working gap, ΔA_{of} is the magnetic conductivity of outflow which falls on one area of the core. The variables F_{ma} , F_{my} describe the «eddy» MMFs arising respectively in the armature and yoke; F_{mcj} is the «eddy» MMF that occurs in the core section with the number j .

The calculation of the magnetic resistances ΔR_{mcj} , R_{ma} , R_{my} , the electrical conductances ΔG_c , G_a , G_y , as well as the magnetic conductance of outflow ΔA_{of} is carried out according to the formulas:

$$R_{mcj} = l_c / (n \cdot \mu(\Phi_j / S_c) \cdot S_c), \quad (13)$$

$$R_{ma(y)} = l_{a(y)} / (\mu(\Phi_{a(y)} / S_{a(y)}) \cdot S_{a(y)}), \quad (14)$$

$$\Delta G_c = l_c / (n \cdot 8 \cdot \pi \cdot \rho_s), \quad (15)$$

$$G_{a(y)} = l_{a(y)} / (16 \cdot \rho_s \cdot (c_{a(y)} / b_{a(y)} + b_{a(y)} / c_{a(y)})), \quad (16)$$

$$\Delta A_{of} = \lambda \cdot l_c / n, \quad (17)$$

where λ is the specific magnetic conductivity of outflow; in the case of two parallel circular cores we have:

$$\lambda = \mu_0 \cdot \frac{\pi}{\ln\left(l/d_c + \sqrt{(l/d_c)^2 - 1}\right)}. \quad (18)$$

The conductances of working gaps can be calculated by the method of enlarged field tubes:

$$A_0 = \frac{\mu_0}{2} \cdot \left(\frac{\pi \cdot d_p^2}{4 \cdot \delta} + 1.63 \cdot d_p + 1.232 \cdot \delta + l_p \cdot \left(\frac{4 \cdot d_p}{2 \cdot \delta + l_p} + 2 \right) \right). \quad (19)$$

In (13)-(19) we indicate: μ is the relative magnetic permeability, i.e., a nonlinear function (for a specific magnetic material; this function, depending on the magnetic flux density, is usually given in tabular form.), d_c , S_c are the diameter and cross-sectional area of the core, d_p , S_p , l_p are the diameter, cross-sectional area and thickness of the pole tip, l is the distance between the axes of the cores and δ is the working air gap between the pole tip and armature.

The calculation of the magnetic circuit makes it possible to determine the magnetic fluxes, and thus the traction force created by the electromagnet. On the other hand, the traction power determines the movement of the mechanical system, therefore, processes in the mechanical system and in the magnetic circuit are interrelated. These processes, however, are inextricably coupled with processes in electrical circuits, which we consider below.

Transients in the electric circuit. In this paper, choosing from a lot of existing systems of forced control, we consider a system, which is most often used in low and medium voltage contactors (Fig. 4).

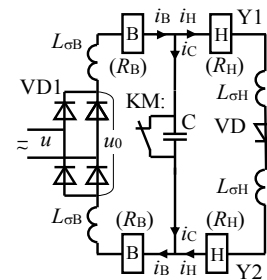


Fig. 4. Principle electrical circuit of a widespread system of forced control that is used in low and medium voltage vacuum contactors and in some SF6 medium voltage contactors [10]; u is the instantaneous value of the nominative voltage of the control circuit; u_0 is the voltage at the output of the diode bridge

This forced control system provides power supply from a DC or AC source:

$$u = \begin{cases} U & \text{for DC;} \\ U_m \cdot \sin(2 \cdot \pi \cdot f \cdot t + \alpha) & \text{for AC.} \end{cases} \quad (20)$$

where f is the frequency, α is the initial phase.

Thus, the voltage at the output of the diode bridge can be constant or rectified, but in any case, the voltage reduction due to its drop in the bridge diodes should be taken into account, which can be especially significant when powered from the network of ultra-low voltage:

$$u_0 = |u| - 2 \cdot u_d(i_B). \quad (21)$$

In this paper, the nonlinear characteristic of the diode is replaced by a piecewise linear dependence: a very large resistance to R_{rd} at negative (reverse) currents, at relatively large positive currents of the voltage drop on the diode is

¹ Electromagnet, the circuit of which is shown in Fig. 3, is double-rod, so it has two identical coils, each of which can have one or more windings. In the first case, the MMF of the coil is equal to the MMF of its winding, in the second case, the MMF of the coil is equal to the sum of MMFs of windings with different number of turns and different currents in them.

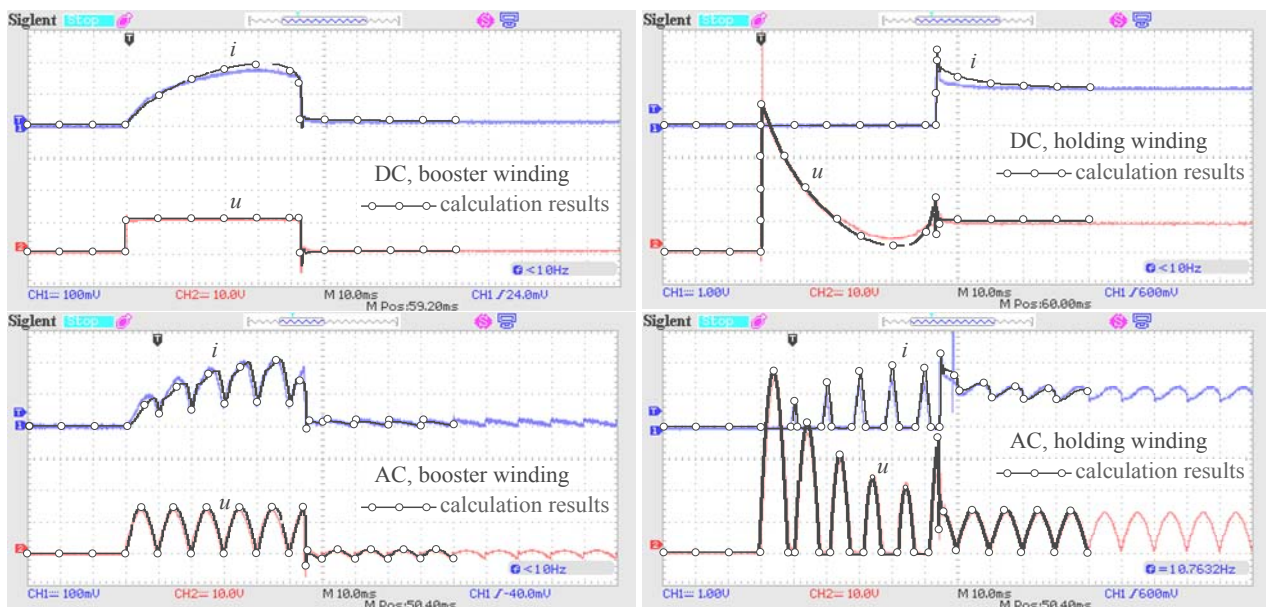


Fig. 6. Comparison of experimental data obtained on industrial samples of vacuum contactors with calculation results using a simplified model of the magnetic circuit, which is considered as a circuit with lumped parameters

REFERENCES

1. Klymenko B.V. *Forced electromagnetic systems*. Moscow, Energoatomizdat, 1989. 160 p. (Rus).
2. Koltermann P.I., Assumpção Bastos J.P., Arruda S.R. A Model for Dynamic Analysis of AC Contactor. *IEEE Transactions on Magnetics*, 1992, vol. 28, no. 2, pp. 1348-1350. doi: 10.1109/20.123941.
3. Nowak L., Demenko A. 3D coupled field-circuit simulation of electromechanical converter dynamics. *COMPEL - The international journal for computation and mathematics in electrical and electronic engineering*, 1998, vol. 17, no. 4, pp. 439-447. doi: 10.1108/03321649810210613.
4. Wada M., Yoshimoto H., Kitaide Y. Dynamic analysis and simulation of electromagnetic contactors with AC solenoids. *IEEE 2002 28th Annual Conference of the Industrial Electronics Society, IECON 02*, 5-8 Nov. 2002. doi: 10.1109/iecon.2002.1182829.
5. Ruiz J.-R. R., Espinosa A.G. A Novel Parametric Model for AC Contactors. *IEEE Transactions on Magnetics*, 2008, vol. 44, no. 9, pp. 2215-2218. doi: 10.1109/tmag.2008.2000544.
6. Li Y., Xia K., Liu W., Li D. Design and simulation analysis of electromagnetic repulsion mechanism. *2010 IEEE International Conference on Industrial Technology*, 2010. pp. 914-918. doi: 10.1109/ICIT.2010.5472562.
7. You Jiaxin, Liang Huimin, Ma Guangcheng, Chen Shuqing, Cai Zhaowen. Research on the dynamic calculation model for a DC solenoid electromagnetic contactor and its contact characteristics in break process. *2015 IEEE 61st Holm Conference on Electrical Contacts (Holm)*, San Diego, CA, 2015, pp. 191-194. doi: 10.1109/HOLM.2015.7355096.
8. Tatevosian A.S. *Dinamika elektromagnitov* [Dynamics of electromagnets]. Omsk, Omsk State Technical University Publ., 2016. 148 p. (Rus).
9. Bajda Ye.I., Klymenko B.V., Pantelyat M.G., Yelanskyi Yu.A., Trichet D., Wasselynck G. Peculiarities of calculating the dynamics of high-speed electromagnets using tunable elastic meshes. *Book of Abstracts of the 19th International Symposium on Electromagnetic Fields in Mechatronics, Electrical and Electronic Engineering (ISEF2019)*, Nancy, France, August 2019, 2 p., accepted.
10. Korol O.G., Klymenko B.V., Yeresko O.V. Investigations of transients in the forced control device for the monostable electromagnet of the vacuum contactor. *Bulletin of NTU «KhPI». Series: Problems of Improvement of Electrical Machines and Apparatus. Theory and Practice*, 2018, no. 32 (1308), pp. 34-40. doi: 10.20998/2079-3944.2018.32.06. (Ukr).

How to cite this article:

Bajda Ye.I., Clemens M., Klymenko B.V., Korol O.G., Pustovoitov P.Ye. Application of the computing environment Maple to the calculation of the dynamics of the electromagnets in the complicated systems of forced control. *Electrical engineering & electromechanics*, 2019, no.3, pp. 18-23. doi: 10.20998/2074-272X.2019.3.03.

Received 07.02.2019

Ye.I. Bajda¹, M. Clemens², B.V. Klymenko¹, O.G. Korol¹, P.Ye. Pustovoitov¹

¹National Technical University «Kharkiv Polytechnic Institute», 2, Kyrpychova Str., Kharkiv, 61002, Ukraine,

phone +380 57 7076281, e-mail: b.v.klymenko@gmail.com

²University of Wuppertal,

Rainer-Gruenter-Straße 21, 42119 Wuppertal, Germany,

phone +49 202 439-1924, e-mail: clemens@uni-wuppertal.de

Application of the computing environment Maple to the calculation of the dynamics of the electromagnets in the complicated systems of forced control.

General description of the research topic. The authors propose a technique for calculating the dynamics of electromagnets operating in complex forced systems. Such forced electromagnets are widely used in electromechanical switching devices, in particular in vacuum contactors, to reduce their size, energy consumption and to increase speed, which indicates the **relevance of this topic**. A mathematical model of the dynamics of a forced electromagnetic system, which takes into account the peculiarities of behavior in transients of its individual elements – the mechanical system, the magnetic and electrical circuits, taking into account the interaction of the electromagnet with a control device when the apparatus is activated, contains certain signs of **scientific novelty and is the purpose of the paper**. The technique of calculating the dynamics of forced electromagnets uses the **computing environment Maple**. The calculation is based on a mathematical model, which is a system of nonlinear differential equations of the magnetic and electric circuits, supplemented by the equations of motion of the elements of a mechanical system. The use of the **computing environment Maple**, applied here to automatically perform the mathematical transformations, allows avoiding the complicated processes of choosing the numerical integration method, programming of complex and cumbersome equations and numerical integration procedures, to obtain results of calculations in convenient tabular and/or graphic form. This specifically indicates the **practical significance** of this work. The results of the comparison of calculations with previously published experimental data presented in the paper indicate the **high efficiency** of the proposed models and techniques. References 10, figures 6.

Key words: electromagnets, dynamics, forced control, switching devices, vacuum contactors, computing environment Maple.

P.D. Andrienko, O.V. Nemykina, A.A. Andrienko

HIGH CURRENT HARMONICS INFLUENCE ON THE CHOICE OF CONDUCTORS OF CRANE POWER SUPPLY SYSTEMS

Purpose. To study the effect of high current harmonics on the power and voltage losses in the conductive lines of the crane power supply systems and the development of an account method for this influence in practical calculations. *Methodology.* For research analytical methods and methods of simulation are used. *Results.* Analytical calculations have been performed for power losses and voltage losses for the conductors of crane power supply systems in the conditions of high harmonic generation for frequency-controlled drives. *Originality.* For the first time, the authors have obtained the analytical expressions and graphical dependencies in relative units for practical calculations that allow determining the effect of high harmonics to the values of power losses and voltage losses for crane supply systems, while the parameters of steel conductors are nonlinear for load current and frequency. We have established that the values of power losses and voltage losses increase for crane power supply systems. It is shown that the power losses lead to a decrease the efficiency of crane supply systems up to 7 %, which must be taken into account when choosing electric drive systems and its payback period. *Practical value.* The obtained theoretical expressions can be used for calculations, design, optimization of crane power supply systems in terms of high harmonic generation. References 12, tables 2, figures 4.

Key words: high harmonics, voltage losses, power losses, conductors, steel materials, aluminum tires, crane power systems.

У статті проведено дослідження впливу вищих гармонік струму на втрати напруги і потужності в струмопроводах систем живлення кранів. Отримані необхідні розрахункові співвідношення для визначення параметрів струмопроводів при наявності вищих гармонік. На прикладі найбільш розповсюджених частотно-регульованих приводів показано, що в тролейних лініях зі сталевих матеріалів втрати напруги і потужності зростають до 4 разів і до 1,43 рази, відповідно. Показано, що наявність нелінійної залежності активного опору сталевих струмопроводів від струму навантаження і частоти призводить до збільшення розрахункової величини втрат потужності в порівнянні з розрахунком через коефіцієнт спотворення струму. Встановлено, що величина $\text{tg}\varphi_{\omega 1}$ може бути використана як конструктивний показник струмопроводу. Наявність втрат потужності призводить до зниження ККД систем живлення кранів до 7 %, що необхідно враховувати при виборі систем електроприводу і його терміну окупності. Бібл. 12, табл. 2, рис. 4.

Ключові слова: вищі гармоніки, втрати напруги, втрати потужності, струмопроводи, сталеві матеріали, алюмінієві шини, системи живлення кранів.

В статье проведено исследование влияние высших гармоник тока на потери напряжения и мощности в токопроводах систем питания кранов. Получены необходимые расчетные соотношения для определения параметров токопроводов при наличии высших гармоник. На примере наиболее часто встречающихся частотно-регулируемых приводов показано, что в тролейных линиях из стальных уголков потери напряжения и мощности возрастают до 4 раз и до 1,43 раза, соответственно. Показано, что наличие нелинейной зависимости активного сопротивления стальных токопроводов от тока нагрузки и частоты приводит к увеличению расчетной величины потерь мощности по сравнению с расчетом через коэффициент искажения тока. Установлено, что величина $\text{tg}\varphi_{\omega 1}$ может быть использована как конструктивный показатель токопровода. Наличие потерь мощности приводит к снижению КПД систем питания кранов до 7 %, что необходимо учитывать при выборе систем электропривода и его срока окупаемости. Библ. 12, табл. 2, рис. 4.

Ключевые слова: высшие гармоники, потери напряжения, потери мощности, токопроводы, стальные уголки, алюминиевые шины, системы питания кранов.

Introduction. The main number of cranes is powered by alternating current of power frequency, which is decisive when choosing the type of used electric drives of cranes. The modern state of crane production industry is characterized by the introduction of semiconductor converters, significantly changing the quality of the crane electric drive, providing uniformly accelerated start and stop of mechanisms, which contributes to the reliability and durability of their mechanical structures and moving parts with significant energy saving [1-3]. In most cases, the advantage is given to the use of a variable frequency drive (VFD). The presence of semiconductor converters leads to the emergence of higher harmonics currents in the power supply system of cranes (PSSC), which in turn negatively affects the quality of electric power, electromagnetic compatibility, leads to a drop in voltage and power losses. When choosing a type of adjustable drive, an economic assessment is made by comparing

their efficiency, cost, without taking into account losses in AC PSSC, which cause deterioration of the efficiency of the PSSC-VFD system [4-6].

The goal of the paper is to study the effect of higher current harmonics on the power losses and voltages in the conductors of the power supply systems of cranes and the development of methods for taking this influence into account in practical calculations.

Main materials of investigations.

1. Initial data. In existing practice, the AC power supply system is mainly used, and for the implementation of adjustable electric drives in crane installations, controlled rectifiers with DC motors or VFDs based on a two-stage frequency converter with an independent voltage inverter, having an uncontrolled, controlled or active bridge rectifier are used. The presence of bridge rectifiers leads to the appearance of higher harmonics of

$n=6k\pm 1$ order (k is the natural number $k = 1, 2, 3, 4, \dots$) in the AC network, which leads to an increase in the calculated current by an amount taken into account by the distortion coefficient ν or the harmonic factor THD_I in accordance with the requirements of International Standards IEEE 519-1992 or IEC 61000-3-12:2012 [5-7].

To assess the effect of higher harmonics in the AC PSSC using a two-stage frequency converter (FC), an equivalent circuit has been used (Fig. 1). The power source (G) in the equivalent circuit is a symmetric system of limited power voltages. The power supply network is simulated by successive $R_i L_i$ chains.

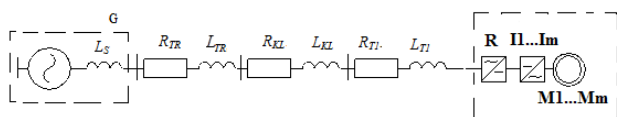


Fig. 1. Equivalent circuit of the AC PSSC

Each chain includes a corresponding inductance and a resistance: of a transformer – $R_{TR} L_{TR}$, of a cable line – $R_{KL} L_{KL}$, of a section of a conductor $R_{TI} L_{TI}$ – respectively to the first crane in the span.

When modernizing cranes, the VFD circuit with the common rectifier (R) which is located on the crane is most often used. Depending on the type of crane, conductors of profiled steel, aluminum tires, flexible cables are used.

The following assumptions were made during the analysis:

- the constancy of the amplitude, the sinusoidal shape and symmetry of the three phase voltages on the secondary winding of the power transformer;
- the inductive and active resistances of all network elements, except the main conductor, are considered constant and independent on current;
- taking into account the influence of higher harmonics of the current is carried out by the simulation results for the PSSC with a VFD or by analytical relations, while the parameters of the conductor depend on the frequency and load current.

The choice of conductor sections is made according to the heating condition and is checked for voltage losses at the most distant point [8, 9].

The rated current of the conductor at non-sinusoidal load is determined based on the value of the calculated power (P) by the relation [9]:

$$I = \frac{P}{\sqrt{3} \cdot \lambda \cdot U_{nom}} = \frac{P}{\sqrt{3} \cdot \cos \varphi_1 \cdot \nu \cdot U_{nom}}, \quad (1)$$

where U_{nom} is the nominal voltage, $U_{nom} = 380$ V; λ , $\cos \varphi_1$, ν are, respectively, the power factor for the non-sinusoidal circuit, the power factor of the main harmonic and the distortion factor.

For crane installations with controlled rectifiers and DC motors or two-stage frequency converters and VFD operating in intermittent mode, the input power factor is $\lambda = 0.5 \div 0.6$ [2]. Ensuring electromagnetic compatibility (EMC) of the frequency converter (FC) with the supply network is achieved by installing an input smoothing reactor and/or an active rectifier. In this case, the input power factor of the main harmonic increases and can

reach unity. Further studies were performed with $\cos \varphi_1 = 0.5 \div 1$ [4].

In the case of generation of higher harmonics, the calculated current of the conductor is determined by the relation [10]:

$$I = \sqrt{\sum_{i=1}^n I_n^2}, \quad (2)$$

where I_n is the value of the calculated current of the harmonic of the n -th order in conductors.

For a bridge rectifier, the relative values of the higher harmonics of the input current are determined from the relation:

$$I_n^* = k_n \cdot \frac{I_n}{I_1} = k_n \cdot \frac{1}{n} = k_n \cdot \frac{1}{f_n^*}, \quad (3)$$

where k_n is the coefficient taking into account the relative value of the amplitude of the n -th harmonic at different pulsations of the rectified current.

For the ideal rectifier $L_d = \infty$, $k_n = 1$ the input current distortion factor $\nu = 0.955$.

For a three-phase bridge rectifier in the input link of the FC and a capacitive filter, the values of higher harmonic currents were obtained by the simulation method [11], which was performed in the Matlab software package (Table 1).

The relation (2) in relative units with regard to (3) takes the form:

$$I^* = \sqrt{\sum_{i=1}^n \left(k_n \cdot \frac{1}{f_n^*} \right)^2}. \quad (4)$$

Table 1

Higher harmonic input current values							
$I_n/I_1, \%$	$n=5$	$n=7$	$n=11$	$n=13$	$n=17$	$n=19$	ν
$L_d = \infty, k_n = 1$	38.3 %	2.2 %	7 %	3 %	3 %	2 %	0.926
k_n	1.91	0.87	0.77	0.42	0.5	0.4	–

2. Determination of the parameters of conductors taking into account higher harmonics. A feature of conductors in terms of the generation of higher harmonics is the dependence of their active resistance on the magnetic permeability of the steel conductor and the frequency of the current.

The value of the active resistance of conductors made of corner steel is determined by the relations [9]:

$$\left. \begin{aligned} R_\omega &= K_\omega R_0 = K_\omega \cdot \rho_{50} \cdot \frac{l}{S_t} \\ K_\omega &= 1 + 0,84 \cdot \beta_w, \quad \text{at } \beta_w < 1 \\ K_\omega &= 0,758 + \sqrt{1,34 \cdot \beta_w - 0,83}, \quad \text{at } 1 < \beta_w < 3 \\ K_\omega &= 0,758 + 1,159 \beta_w, \quad \text{at } \beta_w \geq 3 \\ \beta_w &= 2 \cdot 10^{-2} \frac{S}{P} \cdot \sqrt{\frac{f}{\rho_{50} \mu}} \end{aligned} \right\}, \quad (5)$$

where S, P, l are, respectively, the section, cm^2 , perimeter, cm, length, m; R_0 is the ohmic resistance of steel conductor to direct current, Ω/km ; μ is the relative magnetic permeability of steel conductor, which is determined by the curves [10], depending on the magnetic field strength $H = 0.4 \cdot \pi \cdot I/P$, A/cm; ρ_{50} is the resistivity to

direct current, $\Omega \cdot \text{mm}^2/\text{m}$; I is the current in the conductor, A, S_i is the section, mm^2 .

For trolley lines made of corner steel $50 \times 50 \times 5$ and $75 \times 75 \times 10$, according to the condition of permissible heating, the magnetic field strength values H are within $6 \div 23.5$ A/cm, which corresponds to the value $\mu = 1500 \div 750$. According to relations (5), β_w for the frequency 50 Hz (the first harmonic) takes the values $\beta_{w1} = 3.6 \div 3.2$ and $\beta_{w1} = 6.5 \div 5.8$, respectively. The specified values of β_{w1} correspond to the coefficient $K_{\omega 1} = 5 \div 4.5$ and $K_{\omega 1} = 8.25 \div 7.6$. Active resistance to alternating current $R_{\omega 1} = 1.5 \div 1.4$ Ω/km and $R_{\omega 1} = 0.85 \div 0.78$ Ω/km for corner steel $50 \times 50 \times 5$ and

$75 \times 75 \times 10$, while the ohmic resistance of the corners to direct current is 5 and 8.25 times less, respectively (Table 2).

The value of the inductive resistance of trolley lines of corner steel for the first harmonic is determined by the relation [9]:

$$X_{\omega 1} = X^1 + X^{11} \approx X^1 + 0,56R_{\omega 1}, \quad (6)$$

where X^1 and X^{11} are the internal and external inductive resistances of trolley lines, respectively.

The values of active and internal inductive resistances of trolley lines made of corner steel $R_{\omega 1}$ and X^{11} , according to relations (5), (6), depend on the load current and frequency. The value of the internal inductive resistance X^1 does not depend on the load current.

Table 2

Parameters of the investigated conductors

	Dimensions, mm	Load current, A	R_0 , Ω/km	$R_{\omega 1}$, Ω/km	$X_{\omega 1}$, Ω/km		I_{max} , A	$\text{tg}\varphi_{\omega 1}$
					X^1 , Ω/km	X^{11} , Ω/km		
Trolleys	$50 \times 50 \times 5$	100/170	0.3	1.5/1.36	0.216	0.85/0.77	328	0.71/0.725
	$75 \times 75 \times 10$	200/360	0.103	0.85/0.78	0.18	0.49/0.44	542	0.788/0.795
Tires	40×4	–	0.192	0.222	0.214		475	0.96
	120×10	–	0.0255	0.0331	0.153		2070	4.6

The parameters of the most used conductors in the form of steel trolley lines and aluminum tires for the first harmonic are given in Table 2. Analysis of data of Table 2 shows that for trolley lines made of corner steel, $\text{tg}\varphi_{\omega 1}$ varies in the range of $0.71 \div 0.795$ and practically does not depend on their section; with a slight error, $\text{tg}\varphi_{\omega 1} \approx 0.75 = \text{const}$ can be taken, while for tires, $\text{tg}\varphi_{\omega 1}$ increases with increasing section of tires.

Internal inductive resistance for the corners of $50 \times 50 \times 5$ and $75 \times 75 \times 10$ is in the range of $0.216 \div 0.18$ Ω/km and with a slight error $X^1 \approx 0.195 = \text{const}$ can be taken.

When generating harmonic currents $n \geq 5$ in the steel conductor, the coefficient β_w , expression (5), therefore, with an accuracy of up to 10%, $K_{\omega n} \approx 1.159 \cdot \beta_{wn}$ can be taken.

The relative value of the active resistance of the conductor for the harmonics of the n -th order, taking into account expressions (5):

$$R_{\omega n}^* = \frac{R_{\omega n}}{R_{\omega 1}} = \frac{K_{\omega n}}{K_{\omega 1}} \approx \frac{\beta_{wn}}{\beta_{w1}} = \sqrt{f_n^*}, \quad (7)$$

where $f_n^* = f_n/f_1$ is the relative frequency of the harmonic of the n -th order; f_n, f_1 are the frequency of the harmonic of the n -th order and the fundamental frequency, respectively.

Active and inductive resistance of trolley lines for the harmonics of the n -th order:

$$R_{\omega n} = R_{\omega 1} \cdot \sqrt{f_n^*}, \quad (8)$$

$$X_{\omega n} = X_{\omega 1} \cdot f_n^* = \left(X^1 + 0,56R_{\omega 1} \cdot \sqrt{f_n^*} \right) \cdot f_n^*. \quad (9)$$

Using relations (8) and (9) we express the value:

$$\text{tg}\varphi_{\omega n} = \frac{X_{\omega n}}{R_{\omega n}} = \frac{\left(0,195 + 0,56 \cdot R_{\omega 1} \cdot \sqrt{f_n^*} \right) \cdot f_n^*}{R_{\omega 1} \cdot \sqrt{f_n^*}}. \quad (10)$$

At $f_n^* > 5$, the value of the internal inductive resistance of the trolley lines is small compared with the external inductive resistance, therefore, with enough accuracy for practice, it is possible to use the relation:

$$\text{tg}\varphi_{\omega n} = \text{tg}\varphi_{\omega 1} \cdot f_n^* \approx 0,56 \cdot f_n^*. \quad (11)$$

Note that for aluminum tires and copper conductors in the frequency range under study, the manifestation of the skin effect is insignificant, therefore the tires resistance is constant $R_{\omega n} = R_{\omega 1}$.

The $\text{tg}\varphi_{\omega n}$ value for harmonics of the n -th order of aluminum tires and copper conductors is determined by the relation $\text{tg}\varphi_{\omega n} = \text{tg}\varphi_{\omega 1} \cdot f_n^*$.

3. Determination of voltage losses in conductors taking into account higher harmonics. In the general case, the voltage losses are determined by the relation [10]:

$$\Delta U = \sqrt{\sum_{i=1}^n \Delta U_i^2}, \quad (12)$$

where ΔU_n are the voltage losses for harmonics of the n -th order in conductors:

$$\begin{aligned} \Delta U_n &= \frac{\sqrt{3} k_{\text{max}} \cdot I_n \cdot (R_{\omega n} \cdot l \cdot \cos \varphi_1 + X_{\omega n} \cdot l \cdot \sin \varphi_1)}{U_{\text{nom}}} \cdot 100 = \\ &= \frac{\sqrt{3} k_{\text{max}} \cdot I_n \cdot R_{\omega n} \cdot l (\cos \varphi_1 + \text{tg}\varphi_{\omega n} \cdot \sin \varphi_1)}{U_{\text{nom}}} \cdot 100, \end{aligned} \quad (13)$$

where I_n, φ_1 are the current value of the n -th harmonic and the shift angle of the main harmonic, respectively; l is the conductor length; k_{max} is the coefficient taking into account the increase in peak current relative to the calculated value of current.

The value of $\cos \varphi_1$ is determined by the switching angle γ for rectifiers installed in the input link of the FC.

Using the previously accepted assumptions, we transform the relation (12). For steel conductors, the relation takes the form:

$$\Delta U^* = \frac{\sqrt{\sum_{i=1}^n \Delta U^2_n}}{\Delta U_1} = \sqrt{1 + \sum_{k=1}^{n=6k\pm 1} (k_n)^2 \frac{1}{f_n^*} \left(\frac{\cos \varphi_1 + 0,56 \cdot f_n^* \cdot \sin \varphi_1}{\cos \varphi_1 + \operatorname{tg} \varphi_{\omega 1} \cdot \sin \varphi_1} \right)^2} \quad (15)$$

For aluminum tires the relation (15) takes the form:

$$\Delta U^* = \sqrt{1 + \sum_{k=1}^{n=6k\pm 1} (k_n)^2 \frac{1}{(f_n^*)^2} \left(\frac{\cos \varphi_1 + \operatorname{tg} \varphi_{\omega 1} \cdot f_n^* \cdot \sin \varphi_1}{\cos \varphi_1 + \operatorname{tg} \varphi_{\omega 1} \cdot \sin \varphi_1} \right)^2} \quad (16)$$

In the study of voltage losses in terms of the generation of higher harmonics, it was found that their value is determined mainly by the product $\operatorname{tg} \varphi_{\omega 1} \cdot f_n^* \cdot \sin \varphi_1$, which is part of the function $f(\varphi) = (\cos \varphi_1 + \operatorname{tg} \varphi_{\omega 1} \cdot f_n^* \cdot \sin \varphi_1)$.

The dependencies of the function $f(\varphi) = (\cos \varphi_1 + \operatorname{tg} \varphi_{\omega 1} \cdot \sin \varphi_1)$ for the main harmonic are shown in Fig. 2.

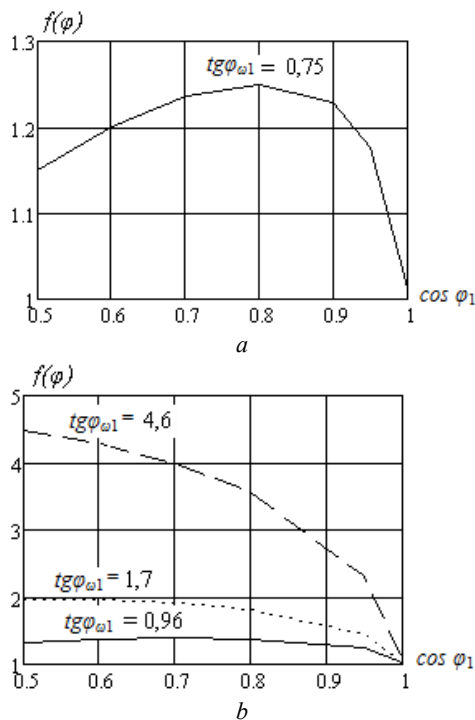


Fig. 2. Dependencies $f(\varphi) = (\cos \varphi_1 + \operatorname{tg} \varphi_{\omega 1} \cdot \sin \varphi_1)$ for conductors made by trolley lines (a) and tires (b)

For trolley lines ($\operatorname{tg} \varphi_{\omega 1} = 0,75$) at changes $0,6 < \cos \varphi_1 < 0,95$, the function $f(\varphi)$ can be approximated with enough accuracy for practice by the value $f(\varphi) \approx 1,2$, which greatly simplifies the calculations. The maximum value of the function $f(\varphi) \approx 1,25$ takes at $\cos \varphi_1 = 0,8$.

When using tires $\operatorname{tg} \varphi_{\omega 1}$ varies in the range of $0,96 \div 4,6$.

For $\operatorname{tg} \varphi_{\omega 1} = 0,96$, at $0,5 < \cos \varphi_1 < 0,95$, the values $f(\varphi) \approx 1,37$. For $\operatorname{tg} \varphi_{\omega 1} \geq 1,7$, which is typical for tires of 50×6 mm and more, the function monotonously increases with decreasing $\cos \varphi_1$. The minimum value the function $f(\varphi)$ takes at $\cos \varphi_1 = 1$.

The dependencies of the relative values of $\Delta U^* = f(\cos \varphi_1)$ for trolley lines and tires, calculated by

relations (15) and (16), are shown in Fig. 3. Analysis of dependencies shows that at the same harmonic composition of the current, the relative value of the voltage losses in conductors of the steel corner is much higher than in tires. This is explained by the fact that for trolley lines the component ΔU^*_n is inversely proportional to f_n^* , and for tires to $(f_n^*)^2$. When reducing the shift coefficient to $\cos \varphi_1 = 0,5$, which is typical for controlled rectifiers, voltage losses increase 4 times for steel corners, and 2.5 times for tires.

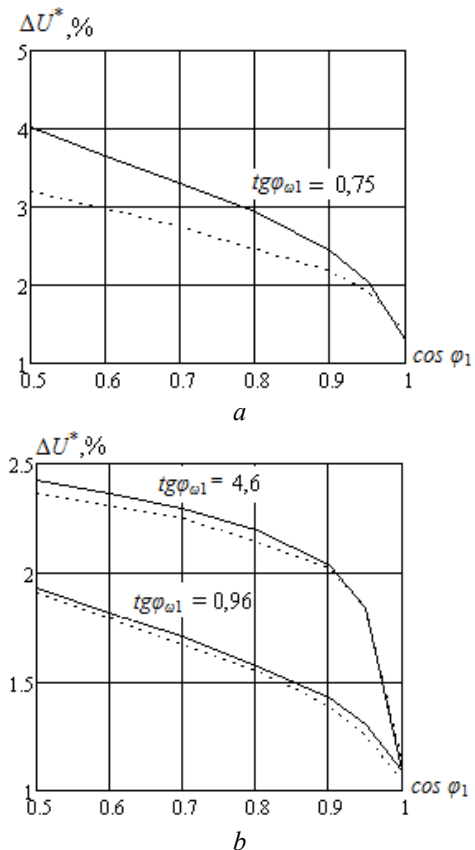


Fig. 3. Dependencies $\Delta U^* = f(\cos \varphi_1)$ for conductors at $v = 0,955$ (solid line) and $v = 0,926$ (dotted line), made by trolley lines (a) and tires (b)

This circumstance confirms the need to take into account the effect of higher harmonics when calculating the voltage losses.

The decrease in the distortion coefficient v from 0.955 to 0.926 leads to a decrease in the voltage losses in the conductors, which indicates a non-linear dependence of ΔU^* on the amplitudes of the harmonic components of the current curve.

Therefore, when designing PSSCs that have semiconductor converters (rectifiers, FCs, voltage regulators), it is necessary to determine the harmonic composition by simulation modeling. Dependencies of ΔU^* have a number of characteristic points.

For conductors of corner steel, the relation (15) takes the form:

- at $v \leq 0,95$ and $\cos \varphi_1 = 1$

$$\Delta U^* = \sqrt{1 + \sum_{k=1}^{n=6k\pm 1} (k_n)^2 \frac{1}{f_n^*}} \quad (17)$$

- at $\sin\varphi_1 = 1$ ($\cos\varphi_1 = 0$)

$$\Delta U^* = \sqrt{1 + \sum_{k=1}^{n=6k\pm 1} (k_n)^2}, \quad (18)$$

- at $k_n = 1$, $\Delta U^* \rightarrow \sqrt{2}$.

The absolute value of the voltage losses is proportional to the calculated value of I_n and the active resistance R_{on} according to (13). Since the tire resistance is less than steel corners one, at an equal value of the calculated current, the absolute value of the voltage drop in the tires is significantly less.

Note that the use of cable conductors for powering portal [12] and gantry cranes provides a significant reduction in voltage losses due to their relatively low $\text{tg}\varphi_{\omega 1}$.

4. Determination of power losses in conductors taking into account higher harmonics. The power losses in the AC conductors for the first harmonic is determined by the relation [9]:

$$\Delta P_1 = 3(I_1)^2 R_{\omega 1} = 3 \left(\frac{P}{\sqrt{3} \cdot \cos\varphi_1 \cdot U_{nom}} \right)^2 R_{\omega 1}, \quad (19)$$

where I_1 is the calculated value of the main harmonic current.

The relative value of the additional losses in the AC conductor in the conditions of generation of higher harmonics is determined from the relationship:

$$\Delta P_{\Sigma}^* = \frac{\sum_{k=1}^{n=6k\pm 1} \Delta P_n}{\Delta P_1} = \sum_{k=1}^{n=6k\pm 1} R_{\omega n}^* \cdot (I_n^*)^2, \quad (20)$$

where ΔP_1 are the power losses at the main harmonic in the AC conductor.

Taking into account expressions (3) and (7), the relative value of the additional losses in the conductor:

$$\Delta P_{\Sigma}^* = \sum_{k=1}^{n=6k\pm 1} k_n \cdot \frac{\sqrt{f_n^*}}{(f_n^*)^2}. \quad (21)$$

Relative total losses taking into account the first harmonic:

$$\Delta \Sigma P^* = (1 + \Delta P_{\Sigma}^*). \quad (22)$$

After summing up the series (21) for the conductor under consideration at $\nu = 0.955$, we obtain the value $\Delta P_{\Sigma}^* = 0.26$. The relative total losses $\Delta \Sigma P^* = 1.26$ according to (22).

When calculating using the distortion coefficient ν , the relative total losses:

$$\Delta \Sigma P^* = \Delta P_1 / \nu^2 = 1 / \nu^2 = 1 / 0.95 = 1.11.$$

The resulting value by the ratio (22) $1.26 / 1.11 = 1.135$ times more compared with the well-known conventional approach.

When the distortion coefficient $\nu = 0.926$ according to the data of Table 1 relative value of additional losses according to the expression (21) $\Delta P_{\Sigma}^* = 0.436$. Relative total losses taking into account the main harmonic $\Delta \Sigma P^* = 1.436$.

When calculating using the distortion factor: $\Delta \Sigma P^* = 1 / 0.93^2 = 1.15$.

The value of the relative total losses increase by $1.436 / 1.15 = 1.25$ times.

In conductors made of aluminum tires (for example, for powering portal cranes), the active resistance value is not significantly dependent on the presence of higher harmonics, therefore, with enough accuracy for practice, power losses can be determined using the standard technique: $\Delta \Sigma P^* = \Delta P_1 / \nu^2 = 1 / \nu^2$.

This circumstance confirms the need to take into account the effect of higher harmonics when calculating power losses in conductors.

5. Influence of power losses in conductors on the efficiency of power supply systems of cranes. Figure 4 shows the dependence of the relative value of the main harmonic power losses ($\Delta P_1^* = \Delta P_1 / P_1$) in conductors 100 m long at load currents and the parameters of the conductors given in Table 2 when changing the values of $\cos\varphi_1 = 0.5 \div 1$.

The dependency analysis (see Fig. 4) shows that at $\cos\varphi_1 = 1$ and $l = 100$ m, the relative power losses in the trolley lines are 5% and 6.1%, respectively for the corners $50 \times 50 \times 5$ and $75 \times 75 \times 10$, for aluminum tires 1.4 % and 1.03%, respectively, for sections 40×4 mm and 120×10 mm. At $\cos\varphi_1 = 0.5$, the relative losses in trolley lines are 20 % and 25 %, respectively for $50 \times 50 \times 5$ and $75 \times 75 \times 10$, the losses in tires are 4.1 % and 5.5 %, respectively for sections 120×10 mm and 40×4 mm.

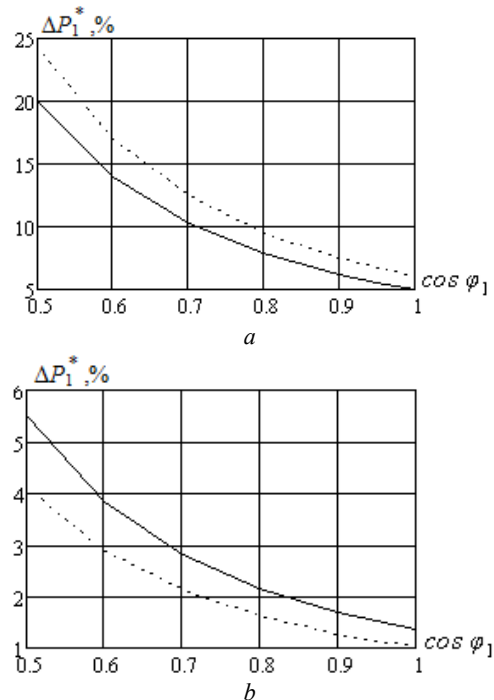


Fig. 4. Dependencies $\Delta P_1^* = f(\cos\varphi_1)$ for conductors made by trolley lines (a) $50 \times 50 \times 5$ mm at $P = 59$ kW (solid line) and $75 \times 75 \times 10$ mm at $P = 125$ kW (dotted line); as well as made by tires (b), 40×4 mm at $P = 100$ kW (solid line) and 120×10 mm at $P = 500$ kW (dotted line)

Thus, the relative losses in trolley lines increase by 3-3.5 times as compared with tires. At real lengths of 60-70 m and the location of the nodes for feeding trolley lines, the losses in them are 3-5 %, depending on the angle of the corner. Taking into account the additional losses from higher harmonics and real power factors, the power losses increase to 4.5-7 %.

At tire lengths up to 300 m, which is typical of gantry cranes, the losses amount to 4.2 %, taking into account the additional losses the power losses increase to 5 %.

This circumstance leads to a decrease in the efficiency of the PSSC with VFD, which must be taken into account when justifying the payback period of the electric drive system.

Conclusions.

1. The presence of higher harmonics in the conductors of power supply systems of cranes at changing values of $\cos\varphi_1 = 0.5 \div 0.95$ causes:

- an increase in voltage losses of 1.8-2.5 times as compared with sinusoidal current for tires $\operatorname{tg}\varphi_{\omega_1}$ and of 3.2-4 times for steel trolley lines;

- an increase in power losses of 1.26-1.43 times compared with sinusoidal current at using steel trolley lines.

2. It is shown that the decisive parameter affecting the voltage and power losses is the tangent of the conductor $\operatorname{tg}\varphi_{\omega_1}$, which can be used as a design parameter of the conductor. Conductors with minimal $\operatorname{tg}\varphi_{\omega_1}$ have minimal losses.

3. The presence of power losses in conductors made by trolley lines, taking into account the additional losses leads to a decrease in the efficiency of power supply systems of cranes to 4.5-7 % at using trolley lines and up to 5 % when using tires, which must be taken into account during the feasibility study of electric drive systems. The presence of additional losses from higher harmonics in the power systems of AC cranes leads to an increase in the cost of the implementation of conductors.

REFERENCES

1. Gerasimyak R.P., Busher V.V., Kalinin A.G. *Elektroprivody i sistemy upravleniia kranovykh mekhanizmov* [Electric drives and control systems of crane mechanisms]. Odessa, Science and Technology Publ., 2014. 202 p. (Rus).
2. Volkov I.V. The new concept of building power circuits of frequency-controlled asynchronous electric drives. *Technical electrodynamic*, 1999, no.4, pp. 21-26. (Rus).
3. Tishchenko V.N., Kolotilo V.I. The current state of electric lifting mechanisms. *Transactions of NTU «KhPI». Chapter «Problems of automated electric drive». Theory and practice*, 2005, no.45, pp. 303-306. (Rus).

How to cite this article:

Andrienko P.D., Nemykina O.V., Andrienko A.A. High current harmonics influence on the choice of conductors of crane power supply systems. *Electrical engineering & electromechanics*, 2019, no.3, pp. 24-29. doi: 10.20998/2074-272X.2019.3.04.

4. Nemykina O.V. The choice of the power supply system of cranes with variable frequency drive. *Electrotechnic and computer systems*, 2015, no.19, pp. 54-57. (Rus).

5. IEEE 519-1992. *IEEE Recommended Practices and Requirements for Harmonic Control in Electrical Power Systems*, USA, New York, 1993.

6. IEC 61000-3-12:2012. *Electromagnetic compatibility (EMC) of technical equipment*. International Standard, 2012.

7. IEC 61000-3-12:2004. *Limitation of emission of harmonic currents in low voltage power supply systems for equipment with rated current greater than 16 A per phase*. International Standard, 2004.

8. Rudnitskiy V.G. *Vnutrishnotsehave elektropostachannya*. [Innerly electric power supply]. Sumy, University Book Publ., 2007. 280 p. (Ukr).

9. *Spravochnik energetika promyishlennykh predpriyatiy. T.1. Elektrosnabzheniye*. [Reference energy industry enterprises. Vol.1. Power supply]. Moscow, Leningrad, Gosenergoizdat Publ., 1961. 840 p. (Rus).

10. Zhezhelhenko I.V., Saenko Yu.L. *Pokazateli kachestva i ih kontrol na promyishlennykh predpriyatiyah* [Quality indicators and their control at industrial enterprises]. Moscow, Energoatomizdat Publ., 2000. 252 p. (Rus).

11. Andrienko P.D., Nemykina O.V., Andrienko D.S. Electromagnetic compatibility of power supply systems of cranes with variable frequency drives. *Electrical Engineering and Electromechanics. Special edition of the XXII scientific-technical conference Power electronics and energy efficiency*, 2016/4(2), vol.2, pp. 109-112. (Rus).

12. Radimov S.N. Experimental determination of the actual electrical parameters of crane busbars – an informational basis for optimizing their operation. *Bulletin of the Odessa National Maritime University*, 2001, no.7, pp. 161-168. (Rus).

Received 07.01.2019

P.D. Andrienko¹, Doctor of Technical Science, Professor,
O.V. Nemykina¹, Candidate of Technical Science, Associate Professor,

A.A. Andrienko¹, Postgraduate Student,

¹Zaporozhye National Technical University,
64, Zhukovsky Str., Zaporozhye, 69063, Ukraine,
e-mail: andrpd@ukr.net, olganemikina@ukr.net

Yu.M. Vasetsky, I.L. Mazurenko, S.L. Bondarevskyi

PARAMETRIC ANALYSIS AND STRAY FIELDS OF TOROIDAL SUPERCONDUCTING MAGNETIC ENERGY STORAGE

Purpose. To carry out a parametric analysis of superconducting toroidal magnetic systems with a discrete winding, establishing the possibility of using an idealized model in the form of a toroidal current surface and an approximate method for determining the level of fields of scattering of a real magnetic system. *Methodology.* The calculation of the distribution of the magnetic flux density in the winding, the field of scattering and energy of the storage's field was carried out using asymptotic methods for solution of the problems of electrostatics in systems with massive curvilinear conductors with current. An iterative calculation procedure was used to determine the dimensionless characteristics. *Results.* The dimensionless characteristics of a toroidal magnetic system with a winding in the form of individual superconducting coils of circular shape are calculated. The results are obtained depending on the value of the storage's energy capacity for various values of the relative radial size of the torus. For a toroidal superconducting storage device with energy capacity of 450 MJ, enough to perform the function of damping irregular oscillations of power transmitted over the transmission line, magnetic fields of scattering are calculated for different numbers of coils and torus section sizes. *Originality.* Based on a comparison of the values of dimensionless characteristics calculated for a system with individual coils, and for an idealized mathematical model of a continuous current surface, it was established that the relative deviation of the dimensionless characteristics does not exceed 10 %. In contrast to the idealized model, the magnetic field of a toroidal system composed of individual coils spreads beyond the toroidal surface and decreases the faster, the smaller the relative radial sectional size of the torus, the greater the number of coils used and the closer they are to each other. *Practical value.* The results obtained for dimensionless characteristics allow to conclude that the idealized model can be used at the first stage of the development of a superconducting inductive storage. The estimation of the field of scattering can be made on the basis of a simple model of unidirectional current filaments. References 15, figures 7.

Key words: superconducting magnetic energy storage, parametric analysis, stray magnetic field.

Розглянуто надпровідну тороїдальну магнітну систему з котушками круглої форми. Досліджено можливість використання ідеалізованої математичної моделі у вигляді суцільної струмової поверхні для проведення параметричного аналізу магнітних систем з обмеженою кількістю окремих котушок. На основі порівняння величин безрозмірних характеристик, розрахованих для системи з окремими котушками і для ідеалізованої моделі, встановлено, що відносне відхилення не перевищує 10 %. Отримано залежності магнітного поля розсіювання для магнітної системи енергоємністю 450 МДж від відносного розміру перерізу тора і кількості котушок. Виконано оцінку характерної відстані від тороїдальної поверхні, на якій спадає магнітне поле розсіювання. Бібл. 15, рис. 7.

Ключові слова: тороїдальний надпровідний індуктивний накопичувач, параметричний аналіз, магнітне поле розсіювання.

Рассмотрена сверхпроводящая тороидальная магнитная система с катушками круглой формы. Исследована возможность использования идеализированной математической модели в виде сплошной токовой поверхности для проведения параметрического анализа магнитных систем с ограниченным количеством отдельных катушек. На основе сравнения величин безразмерных характеристик, рассчитанных для системы с отдельными катушками и для идеализированной модели, установлено, что относительное отклонение не превышает 10 %. Получены зависимости магнитного поля рассеяния для магнитной системы энергоемкостью 450 МДж от относительного размера сечения тора и количества катушек. Выполнена оценка характерного расстояния от тороидальной поверхности, на котором убывает магнитное поле рассеяния. Библ. 15, рис. 7.

Ключевые слова: тороидальный сверхпроводящий индуктивный накопитель, параметрический анализ, магнитное поле рассеяния.

Introduction. Recently, there is an increase in the interest of researchers to the possibility of using superconducting magnetic energy storage (SMES) to increase the sustainability of power systems and improve power quality as a promising high-tech way to solve a number of problems in the power industry [1-3]. This interest is due, among other things, to the successes in the use of superconducting magnetic systems with large accumulated energy in large-scale physical facilities for controlled thermonuclear fusion [4-6].

Investigations to identify areas of potential effective use of SMES to address the issues of improving the reliability and manageability of power transmission in the power systems of Ukraine have shown that it can be economically feasible to use them in the following areas: ensuring the dynamic stability of power plants, damping irregular fluctuations in the power system load, short-term

emergency frequency regulation large disturbances [7]. The values of SMES energy capacity for use in the specified areas of the power industry are approximately in the range of 100 – 10,000 MJ. For these applications, there are both several operating SMES and research-based SMES projects, taking into account specific power systems and their operating modes [8, 9]. Regarding the feasibility of SMES in the specified energy capacity range, the fact add optimism that the magnetic energy storage of toroidal configuration, intended for use in large-scale physical installations, primarily in the field of controlled thermonuclear fusion, have been developed, created and operated for many years.

To be able to use SMES in the power industry, one of the main factors is lower cost compared to alternative solutions. Here, an important characteristic is the

From (5) it can be seen that with an increase in the energy capacity of an magnetic energy storage, the required volume of the superconducting winding increases as $V_{sc} \sim W^{2/3}$. The volume of steel structures of the mechanical holding system is proportional to the first power of the field energy – $V_{st} \sim W$ [10, 14]. Therefore, at relatively low power consumption, within the limits of the values considered in the work, the volume of structural materials turns out to be much smaller than the volume of the superconducting winding [9, 14].

It follows from the above relations that such parameters as the size of the magnetic system, the total toroidal current, the volume of the superconducting material are determined not only by the stored energy of the magnetic field, but also by the dimensionless characteristics of the magnetic system k_W, k_B, k_I and related characteristics k_R, k_I, k_{sc} .

In an idealized model of a toroidal current surface, any of the listed dimensionless characteristics k_i depends only on the configuration of the torus section, which is characterized by a set of dimensionless initial parameters. For example, for a torus of a circular section, this may be the only parameter – the ratio of small $r = (\rho_2 - \rho_1)/2$ and large $R = (\rho_2 + \rho_1)/2$ (see Fig. 1) torus radii $\varepsilon = r/R$ – relative radial size of the torus section.

The dimensionless characteristics of a circular torus, expressed in terms of the dimensionless parameter ε , will be [4]

$$k_B = 1/(1 - \varepsilon), \quad k_W = 2 \left(1 - \sqrt{1 - \varepsilon^2} \right), \quad k_I = 2\pi\varepsilon, \quad (7)$$

$$k_R = \left[2\pi^2 (1 - \varepsilon)^2 \left(1 - \sqrt{1 - \varepsilon^2} \right) \right]^{-1/3},$$

$$k_{sc} = 4\pi\varepsilon \left[4\pi (1 - \varepsilon) \left(1 - \sqrt{1 - \varepsilon^2} \right) \right]^{-1/3}. \quad (8)$$

Systems composed of a set of momentless constant tension windings of a more complex *D*-shape form a torus, the section geometry of which is also described using one parameter [4]. It may be the same relative radial section size ε . To describe the section of a torus with racetrack windings, two independent dimensionless parameters are necessary [10]. An idealized model makes it possible to obtain visual results for determining the values of geometrical parameters at which one or another configuration has optimal indicators. Thus, the analysis shows that the minimum values of the large torus radius and the volume of the superconducting winding for the mentioned configurations of magnetic systems are achieved in the range of the dimensionless parameter $\varepsilon \sim (0.4 - 0.6)$ [10].

We now consider a magnetic system with a discrete toroidal winding in the form of a system of a limited number of coils with a rectangular section.

The transition from an idealized model to a model of a winding with individual coils greatly complicates the analysis. Now, the dimensionless characteristics k_B and k_W , and hence k_R, k_I, k_{sc} , also depend on additional

dimensionless initial values that characterize the geometry of the system: the number of coils N , the relative values of thickness Δ/R and the width h_c/R of coils, as well as the parameter which characterizes the presence of a gap between the coils $k_{st} = h_c/h_{st} \leq 1$, where h_{st} is the maximum width of the coil with no gap, when $h_b = 0$.

For a system with a discrete winding with additional data on the number of coils N and the value of k_{st} , the sectional dimensions of each coil Δ/R and h_c/R are also to be determined by given magnetic energy values W and the properties of the superconducting conductors B_m and j_m . That is, the dimensions of the section of the coils depend on the initial parameters of the storage, and at the same time, these dimensions affect the value of the dimensionless characteristics k_R, k_I, k_{sc} of the storage.

The most significant is that any dimensionless characteristic k_i is determined not only by the parameters of the torus section, but also depends on the initial parameters of the storage $k(\varepsilon, \dots, W, B_m, j_m, N, k_{st})$. This means that a parametric analysis cannot be carried out separately for the initial dimensional and dimensionless parameters. However, the task can be formulated not only as finding the mass and dimensional parameters for a particular storage capacity, but also based on obtaining corrections to the values of dimensionless characteristics that are valid for an idealized model. This allows to carry out a generalized analysis for the approximate values of quantities with a certain error, and to characterize its deviation by the value

$$\beta_i = \frac{k_{iN} - k_i}{k_i}, \quad (9)$$

where k_i is the value of the dimensionless characteristic when calculating with the help of an idealized model of a continuous current surface, k_{iN} is the same characteristic of the system with separate coils.

During the calculations, the following features of the system with a discrete winding were taken into account.

First, each value of the mass-dimensional parameters and dimensionless characteristics were found as a result of solving the problem with the following initial parameters: $\varepsilon, W, N, k_{st}, B_m, j_m$. Permissible values of the magnetic flux density and current density in the winding $B_m = 5 \text{ T}, j_m = 4 \cdot 10^7 \text{ A/m}^2$ were selected, which corresponds to the values for the wire based on the low-temperature NbTi superconductor.

Secondly, it was taken into account that for real windings the position of a point on the perimeter of the coil section (see Fig. 1) with the maximum value of the magnetic flux density B_m depends on the size of the section, i.e. is a function of the initial parameters. This point is shifted to a region near the angle of a rectangular section, and therefore the condition for finding its position was included in the system of equations for finding the geometry of the system.

Thirdly, the magnetic field of a system with discrete coils exists not only in a certain internal volume, as in an idealized model, but extends beyond its limits. Therefore, the calculation of the magnetic field energy was carried

out using integration over the volume occupied by the currents in accordance with the expression:

$$W = \frac{1}{2} \sum_i \sum_k W_{ik} = \frac{1}{2} \sum_i \sum_k \int_V A_i j_k dV, \quad (10)$$

where j_k is the current density of one of current systems; A_i is the magnetic vector potential created by another (at $i \neq k$) or the same (at $i = k$) system in the region of current flow.

When performing calculations, the asymptotic methods for calculating the magnetic field of massive circuits with current, described in detail in [15], were used to reduce the required amount of calculations. An iterative calculation procedure was used to determine the dimensionless characteristics.

As an example, Fig. 2 shows deviations β_B and β_W for dimensionless characteristics, respectively, k_B and k_W of SMES with round-shaped coils depending on energy capacity at different values of relative radial size ε . In order to show the general trends of deviations β_B and β_W , a wider range of values $\varepsilon = 0.2-0.8$ was chosen as compared to the minimum values of the large torus radius and the volume of the superconducting winding.

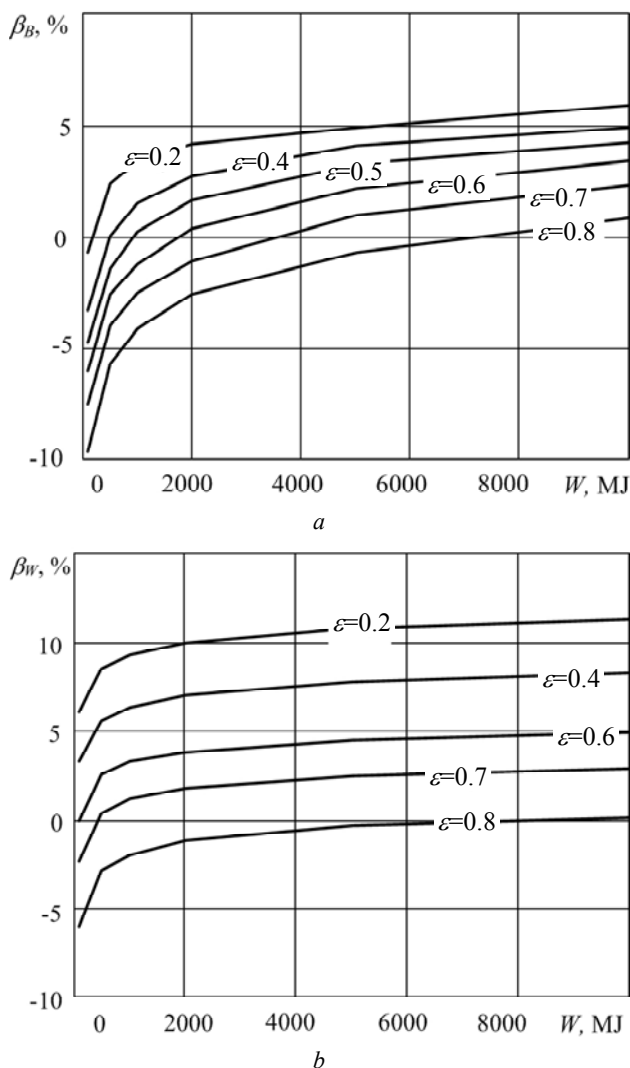


Fig. 2. Relative deviations β_B and β_W for the storage with round-shaped coils ($N = 36, k_{st} = 1$)

Figure 3 illustrates the effect of the number of circular storage's coils on the value of deviation β_{sc} from the value of the idealized model for the dimensionless characteristic k_{sc} , which determines the volume of the material of the superconducting winding. In this case, the calculation was carried out at a specific value of the energy capacity of SMES of 450 MJ, which is sufficient for the storage to perform the function of damping low-frequency irregular power flow oscillations along the high-voltage transmission line [9].

From presented in Fig. 2 dependencies it is seen that in the considered range of energy capacity and a significant number of coils $N = 36$, the calculation error for the idealized model does not exceed $\sim 10\%$.

From Fig. 3 it can be seen that the error in calculating the volume of the superconducting winding also does not exceed 10 % for storages with a smaller number of coils.

The indicated order of the error in calculating the mass-dimensional parameters of the magnetic system using the idealized model is also valid when varying other initial parameters for all the dimensionless characteristics under consideration. This indicates the possibility of using an idealized model at the first stage of the investigation. More accurate calculation can be performed after selecting approximate parameters of the storage.

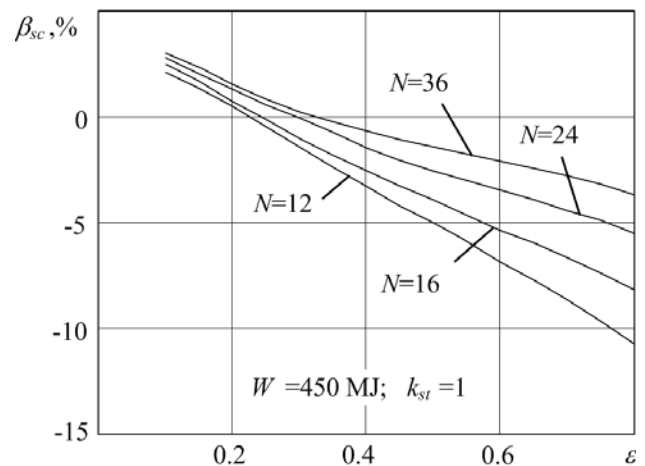


Fig. 3. Relative deviations β_{sc} for the storage with round-shaped coils

The field of scattering of a toroidal system with a limited number of superconducting coils. Magnetic flux density created by the surface current flowing over the toroidal current surface has only an azimuthal component and is concentrated inside the toroidal volume, in other words, there is no field of scattering in the idealized model.

For a real magnetic system, which is a system of individual coils with axial lines located on the surface of the torus, the magnetic field extends beyond the toroidal surface. A qualitative picture of the magnetic flux density lines in the xOy plane of the storage with eight coils is shown in Fig. 4.

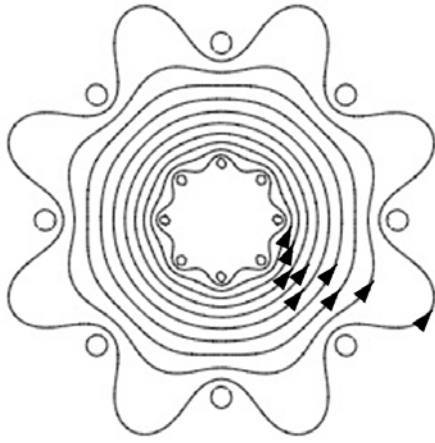


Fig. 4. Lines of the magnetic flux density

Outside the toroidal surface, only a «buckling» of the field in the region between the coils is shown for lines with a common magnetic flux density direction, which coincides with the field direction in the central part of the torus. However, for a field of scattering in areas adjacent to the planes in which the coils lie, the magnetic flux density vector has the opposite direction. Moreover, outside the toroidal winding, the averaged values along both directions are the same. This follows from the zero value of the circulation of the magnetic flux density vector along a circle of radius ρ exceeding the outer radius of the torus $\rho > \rho_2 + \Delta/2$

$$\oint_l \mathbf{B} dl = \rho \int_0^{2\pi} B_\varphi d\varphi = 0, \quad (11)$$

where φ is the azimuth angle.

For definiteness in the investigation of the field of scattering, the calculation results are given for the distribution of the magnetic flux density along the radius ξ , passing between the coils in the xOy plane, as shown in Fig. 1.

Since, as was shown, the geometrical dimensions of the magnetic energy storage, including the cross-sectional dimensions of the coils, depend on the initial parameters, the distribution of the field of scattering was calculated, as before, for the storage's energy capacity of $W = 450$ MJ and the properties of the superconducting wire based on NbTi.

Figure 5 shows the dependencies of the relative value of the magnetic flux density B/B_m on the relative distance ρ/ρ_m (solid curves) at points in space beyond the volume bounded by the toroidal surface for $\rho > \rho_2 + \Delta/2$ (see Fig. 1); ρ_m is the distance from the vertical axis of the torus to the point at which the magnetic flux density takes the maximum value B_m . These dependencies make it possible to estimate the value of the field of scattering for different values of the relative size of the section of the torus ε and, accordingly, different maximum radial sizes of the torus.

The flux density of the magnetic field of scattering for all ε decreases sharply away from the surface of the toroidal storage. At small values of ε near the toroidal surface, the value of the magnetic flux density is greater. This is explained by the fact that for small ε the magnetic

flux density within the relatively small transverse size of the torus, changing inversely to the radius, drops to smaller values for ρ_2 than for larger ε .

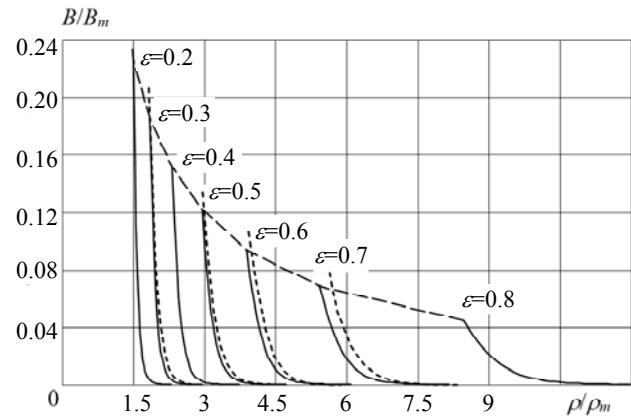


Fig. 5. Field of scattering of the toroidal magnetic system with the number of coils $N = 16$ and $k_{st} = 1$

At the same time, the field decrease rate is the highest at small ε . This character of the dependence is due to the fact that at the outer radius of ρ_2 for small ε the coils diverge relative to each other to a lesser extent than for large ε . The characteristic size $\Delta\rho$, on which the field of scattering significantly decreases, can be estimated as the distance between the coils on the radius ρ_2 . So, from Fig. 1 it is shown that this distance is approximately

$$\Delta\rho \approx 2\rho_2 \sin \frac{\pi}{N} - h_c = 2R(1 + \varepsilon) \sin \frac{\pi}{N} - h_c. \quad (12)$$

The relative distance from the toroidal surface on which the field decreases

$$\frac{\Delta\rho}{\rho_m} \approx 2 \left(\frac{1 + \varepsilon}{1 - \varepsilon} - k_{st} \right) \sin \frac{\pi}{N}, \quad (13)$$

substantially depends on the relative cross-sectional size of the torus section ε , the number of coils N , and also on the coupling coefficient k_{st} .

The values obtained from (13) are consistent with the data on the reduction of the field in the magnetic system with real-section coils shown in Fig. 5.

It is convenient to present the dependencies of the magnetic fields of scattering with a different number of coils for a specific value of ε . In Fig. 6, dependencies are presented for $\varepsilon = 0.6$ and $k_{st} = 1$.

It can be seen that the external magnetic field decreases the faster with distance from the toroidal surface, the greater the number of coils used, in other words, the smaller the discreteness of the superconducting winding.

In the previous two cases, the calculations were carried out with the exact coupling of the coils near the radius $\rho_1 - \Delta/2$, and the discreteness was most pronounced at the radius ρ_2 . However, it is almost impossible to ensure accurate coupling of coils in a particular system. Figure 7 presents the results of calculations on the effect of the coupling coefficient on the fields of scattering for $N = 16$, $\varepsilon = 0.6$ for different values of the coupling coefficient $k_{st} = 1, 0.67$ and 0.5 .

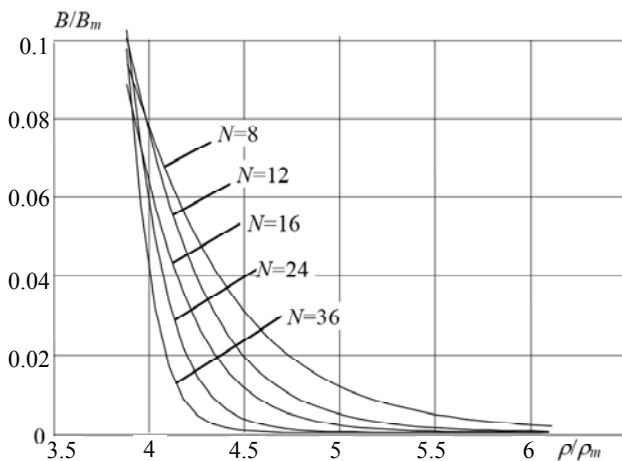


Fig. 6. The influence of the number of coils on the value of the field of scattering ($\varepsilon = 0.6$ and $k_{st} = 1$)

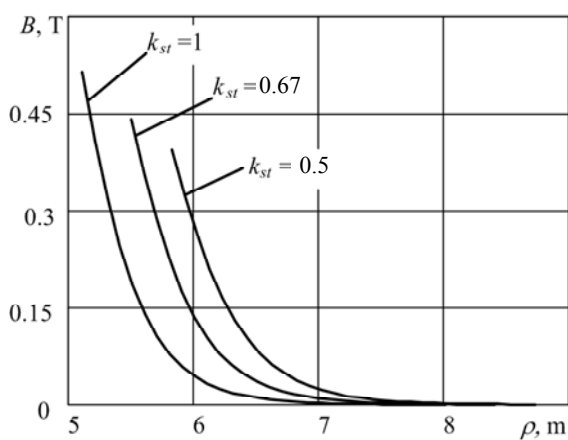


Fig. 7. Influence of the parameter k_{st} on the value of the field of scattering

The fields of scattering will be the smaller, the closer the coils are located to each other. In Fig. 7 dependencies are built in named units, which makes it possible to estimate the real values of the magnetic flux density and the distances covered by the fields for a storage with energy capacity of $W = 450$ MJ.

The calculation of fields of scattering using the complete model with a discrete winding is rather time-consuming. To simplify the analysis, various approximate mathematical models can be used. However, as noted in [4], the nature of the approximate winding models significantly influences the results of the field calculation, especially near current-carrying parts. Thus, the use of current filaments as a model is associated with the appearance of features at the locations of the filaments, which introduces significant perturbations in the local field under consideration. However, the estimation of the field of scattering can be performed in the region between the coils at a certain distance from them.

Taking into account that the field of scattering decreases rapidly with distance from the winding, to estimate it in the xOy plane, it is enough to use a simple plane-parallel model of a system of unidirectional current filaments. The position of the vertical current filaments is determined by the intersection of the axial lines of the

coils with the plane. The calculation results for some values of the relative size of the sections of the torus ε are shown in Fig. 5 by dashed lines. It can be seen that such a rough model allows, however, obtain preliminary results of the value of the field of scattering.

Conclusions.

1. In toroidal magnetic systems with a winding consisting of individual superconducting coils, it is advisable to carry out parametric analysis using dimensionless characteristics similar to those used for an idealized mathematical model of a toroidal current surface.

2. The dimensionless characteristics that show the influence of the geometrical configuration of the magnetic system on the dimensions of the toroidal winding, the mass or volume of the material of the superconducting winding, in the considered energy capacity range are only approximately independent on the total accumulated field energy and properties of the superconducting winding. At the same time, the relative deviations of the dimensionless characteristics calculated by the two models do not exceed 10 %, which makes it possible to apply an idealized model at the first stage of the development of a superconducting storage.

3. In contrast to the idealized model, the magnetic field of a toroidal system composed of individual coils spreads beyond the toroidal surface and decreases the faster, the smaller the relative radial size of the torus section, the greater the number of coils used and the closer they are to each other.

REFERENCES

1. Vyisotskiy V.S., Syitnikov V.E., Yliushyn K.V., Kovalev L.K., Kovalev K.L., Eshoshkyna L.A. Superconductivity in Electromechanics and Power Engineering. *Electricity*, 2005, no.7, pp. 31-40. (Rus).
2. Devotta J.B.X., Rabbani M.G. Application of superconducting magnetic energy storage unit in multi-machine power systems. *Energy Conversion & Management*, 2000, vol.41, pp. 493-504. doi: 10.1016/S0196-8904(99)00100-4.
3. Matsukawa T., Nakamura H., Nomura S., Sato Y., Tsuji-Ito S., Shimada R. Conceptual design of SMES system equipped for IPP plant. *IEEE Transactions on Applied Superconductivity*, 2000, vol.10, no.1, pp. 788-791. doi: 10.1109/77.828349.
4. Thome R.J., Tarrh J.M. *MHD and Fusion Magnets. Field and Force Design Concepts*. New York, A Wiley-Interscience Publication, 1982. 316 p.
5. Duchateau J.L., Journeaux J.Y., Grivil B. Tore Supra Superconducting Toroidal Magnetic Field System. *Fusion Science and Technology*, 2009, vol.56, no.3, pp. 1092-1123. doi: 10.13182/FST09-A9170.
6. ITER Physics Basis. *Nuclear Fusion*, 1999, vol.39, no.12. doi: 10.1088/0029-5515/39/12/301.
7. Avramenko V.M., Aristov Yu.V., Vasetskiy Yu.M., Mazurenko I.L., Chernenko P.O. Some areas of effective use of superconducting magnetic energy storage (SPIN) in power systems of Ukraine. *Technical electrodynamics. Thematic issue «Problems of modern electrical engineering»*, 2008, chapter 3, pp. 43-48. (Ukr).
8. Zhou X., Chen X.Y., Jin J.X. Development of SMES Technology and Its Applications in Power Grid. *Proceedings of*

2011 *IEEE International Conference on Applied Superconductivity and Electromagnetic Devices*. Sydney, Australia, December 14-16, 2011, pp. 260-269. doi: **10.1109/ASEMD.2011.6145115**.

9. Vasetsky Yu.M., Mazurenko I.L., Pavlyuk A.V. Damping of irregular low-frequency load fluctuations using a superconducting magnetic energy storage. *Electricity*, 2014, no.2, pp. 10-17. (Rus).

10. Mazurenko I., Pavlyuk A., Vasetsky Yu. Parameters of superconducting magnets with racetrack-shaped coils and support structure placed inside torus. *Przegląd Elektrotechniczny*, 2012, no.3a, pp. 67-69.

11. But D.A., Aliyevskiy B.L., Mazyrin S.R., Vasyukevich P.V. *Nakopiteli energii* [Energy storage]. Moscow, Energoatomizdat Publ., 1991. 400 p. (Rus).

12. Pavlyuk A. magnetic fields and parameters of toroidal superconducting magnets with limited number of coils. *Works of the Institute of Electrodynamics of the National Academy of Sciences of Ukraine*, 2013, no.34, pp. 94-105. (Ukr).

13. Dimitrov I.K., Zhang X., Solovyov V.F., Chubar O., Li Q. Rapid and Semi-Analytical Design and Simulation of a Toroidal Magnet Made With YBCO and MgB2 Superconductors. *IEEE Transactions on Applied Superconductivity*, 2015, vol.25, no.5, pp. 1-8. doi: **10.1109/TASC.2015.2448455**.

14. Brechna H. *Superconducting magnet systems*. Berlin, Springer, 1973. 590 p.

15. Vasetsky Yu.M. *Asimptoticheskie metody resheniia zadach elektrodinamiki v sistemakh s massivnymi krivolineinymi provodnikami* [Asymptotic methods for solving electrodynamic problems in systems with bulky curvilinear conductors]. Kyiv, Naukova dumka Publ., 2010. 271 p. (Rus).

Received 18.02.2019

Yu.M. Vasetsky¹, Doctor of Technical Science, Professor,
I.L. Mazurenko¹, Candidate of Technical Science,
S.L. Bondarevskiy², Candidate of Technical Science, Associate Professor,

¹ The Institute of Electrodynamics of the NAS of Ukraine,
56, prospekt Peremogy, Kiev-57, 03057, Ukraine,
phone +380 44 3662562,
e-mail: yuriy.vasetsky@gmail.com

² Kryvyi Rih National University,
11, V. Matusevycha Str., Kryvyi Rih, 50027, Ukraine,
phone +380 67 3165975,
e-mail: parapet1979@googlemail.com

How to cite this article:

Vasetsky Yu.M., Mazurenko I.L., Bondarevskiy S.L. Parametric analysis and stray fields of toroidal superconducting magnetic energy storage. *Electrical engineering & electromechanics*, 2019, no.3, pp. 30-36. doi: **10.20998/2074-272X.2019.3.05**.

M.I. Baranov

REFINED SELECTION OF ALLOWABLE CROSS-SECTIONS OF ELECTRICAL CONDUCTORS AND CABLES IN THE POWER CIRCUITS OF INDUSTRIAL ELECTRICAL EQUIPMENT TAKING INTO ACCOUNT EMERGENCY OPERATING MODES

Purpose. Implementation and clarification of the existing engineering approach for determination in industrial power engineering for allowable sections of cable-conductor products (CCP) S_{ii} of electric wires and cables in the circuits of electrical equipment of the general industrial installations characterized flowing in malfunction of current $i_k(t)$ of short circuit (SC) with different amplitude-temporal parameters (ATPs). Methodology. Scientific and technical bases of electrical power engineering, electrophysics bases of technique of high voltage and high pulse currents, theoretical bases of the electrical engineering. Results. The results of the developed engineering approach are resulted in the calculation determination on the condition of thermal resistibility of CCP permissible sections of S_{ii} of the uninsulated wires, insulated wires and cables with copper (aluminum) cores (shells), polyvinyl chloride (PVC), rubber (R) and polyethylene (PET) insulation, on which in malfunction of their operation the current $i_k(t)$ of SC can flow with the set by normative documents of ATP. It is shown that divergence between the values of basic calculation coefficient of C_{ik} by existing and offered to the engineering calculations selection of permissible sections of S_{ii} of cores (shells) of the tested wires and cables for normal of their operating time at the nominal current load of CCP makes no more (3-8) %, and in the mode of de-energizing of CCP arrives at to (9-26) %.. Analytical correlation is got for the specified calculation determination of integral of action of J_{ak} of current $i_k(t)$ of SC (Joule integral) in the power circuits of the tested electrical equipment. It is set that in the circuits of the general industrial installations (for permanent time of slump of $T_a=20$ ms of aperiodic constituent of current of SC) maximum possible amplitudes of density of $\delta_{ilm} \approx I_{mk}/S_{ii}$ of SC current at time of his disconnecting $t_{kc}=100$ ms for the uninsulated wires with copper (aluminum) cores make according to approximately 0.64 (0.36) $\kappa A/mm^2$, for cables with copper (aluminum) cores (shells), PVC and R insulation – 0.47 (0.30) $\kappa A/mm^2$, and for cables with copper (aluminum) cores (shells) and PET insulation – 0.39 (0.25) $\kappa A/mm^2$. At time of disconnecting $t_{kc}=160$ ms of SC current in the circuits of electrical equipment ($T_a=20$ ms) permissible amplitudes of current density of δ_{ilm} of SC for the unsuolated wires with copper and aluminum cores are accordingly about 0.52 (0.29) $\kappa A/mm^2$, for cables with copper (aluminum) cores (shells), PVC and R insulation of 0.39 (0.25) $\kappa A/mm^2$, and for cables with copper (aluminum) cores (shells) and PET insulation – 0.32 (0.21) $\kappa A/mm^2$. Originality. First by a calculation the specified numeral values of sections of S_{ii} and amplitudes of density δ_{ilm} of SC current are determined for the uninsulated wires, insulated wires and cables with copper (aluminum) cores shells), PVC, R and PET insulation. New analytical correlation is offered for the calculation estimation of thermal resistibility of tested CCP to the action of current of SC. Practical value. The obtained results will be useful in the increase of thermal resistibility of CCP with copper (aluminum) cores (shells), PVC, R and PET insulation, widely applied in the power circuits of electrical equipment of the general purpose industrial installations. References 6, tables 6.

Key words: electric power engineering, electric wires and cables of circuits of electrical installations of the general industrial purpose, calculation selection of allowable sections of wires and cables in the circuits of electrical equipment.

Надані результати розробленого інженерного електротехнічного підходу до уточненого розрахункового вибору гранично допустимих перерізів S_{ii} електричних неізолюваних дротів, ізолюваних дротів і кабелів з полівінілхлоридною (ПВХ), гумовою (Г) і поліетиленовою (ПЕТ) ізоляцією і мідними (алюмінієвими) жилами (оболонками) по умові їх термічної стійкості, по яких в силових колах електроустановок загальнопромислового призначення в аварійному режимі протікає струм $i_k(t)$ короткого замикання (КЗ) із заданими параметрами. На підставі цього підходу здійснений уточнений вибір перерізів S_{ii} для вказаних дротів (кабелів) силових кіл досліджуваного електрообладнання. Виконана розрахункова оцінка гранично допустимих амплітуд щільності δ_{ilm} струму $i_k(t)$ КЗ в даних дротах і кабелях силових кіл вказаних електроустановок. Отримані результати сприятимуть підвищенню термічної стійкості електричних неізолюваних дротів, ізолюваних дротів і кабелів з ПВХ, Г і ПЕТ ізоляцією і мідними (алюмінієвими) жилами (оболонками), які широко застосовуються в силових колах електроустановок загальнопромислового призначення. Бібл. 6, табл. 6.

Ключові слова: електроенергетика, електричні дроти і кабелі кіл електроустановок загальнопромислового призначення, розрахунковий вибір гранично допустимих перерізів дротів і кабелів в колах електрообладнання.

Приведены результаты разработанного инженерного электротехнического подхода к уточненному расчетному выбору предельно допустимых сечений S_{ii} электрических неизолированных проводов, изолированных проводов и кабелей с поливинилхлоридной (ПВХ), резиновой (Р) и полиэтиленовой (ПЭТ) изоляцией и медными (алюминиевыми) жилами (оболочками) по условию их термической стойкости, по которым в силовых цепях электроустановок общепромышленного назначения в аварийном режиме протекает ток $i_k(t)$ короткого замыкания (КЗ) с заданными параметрами. На основании этого подхода осуществлен уточненный выбор сечений S_{ii} для указанных проводов (кабелей) силовых цепей исследуемого электрооборудования. Выполнена расчетная оценка предельно допустимых амплитуд плотностей δ_{ilm} тока $i_k(t)$ КЗ в рассматриваемых проводах и кабелях силовых цепей указанных электроустановок. Полученные результаты будут способствовать повышению термической стойкости электрических неизолированных проводов, изолированных проводов и кабелей с ПВХ, Р и ПЭТ изоляцией и медными (алюминиевыми) жилами (оболочками), широко применяемых в силовых цепях электроустановок общепромышленного назначения. Библ. 6, табл. 6.

Ключевые слова: электроэнергетика, электрические провода и кабели цепей электроустановок общепромышленного назначения, расчетный выбор предельно допустимых сечений проводов и кабелей в цепях электрооборудования.

© M.I. Baranov

Introduction. Issues of a reasonable selection of cross sections of electrical wires and cables used in electrical equipment (electrical installations) of industrial electric power industry have been and are being given increased attention [1]. Particularly acute these issues arise during emergency operation of its electrical equipment, due to all types of short-circuit (SC) in electrical networks (ENs). No less dangerous for the reliable operation of electrical equipment powered from industrial power supply networks are modes of operation associated with the current overloads of its wide range of cable and conductor products (CCP). Most fires of CCP of circuits of electrical equipment of industrial electric power industry (at temperatures of current-carrying wires cores and cables of about 450 °C [1]), which lead to a prolonged de-energization of consumers of electrical energy, as well as to great material damage and loss of people lives, just related to similar modes of their operation. Of the possible emergency modes of operation of the EN (SC of various types, ignition of the CCP and other types of its damage), calculated to select their electrical equipment, including its components such as electrical apparatus, and accordingly its CCP is SC mode [2, 3]. In [1], a well-known electrical engineering approach was presented on the approximate selection in the field of industrial electric power industry of the minimum allowable S_{min} cross sections of various brands of electrical wires and cables for short-term modes of their operation from the condition of their thermal resistance to the action of SC current. The “bottleneck” in this engineering approach is the calculation finding of the Joule integral B_k for the SC current (integral of the SC current action), which determines the accuracy of calculating the values of the specified sections S_{min} . The graphic materials given in [1] (for example, Fig. 36.38) for three types of materials of wires cores and cables (copper, aluminum and steel) used in determining the final temperature θ_k of Joule heating by SC current of the current transmission parts of CCP do not fully describe the features of the process of approximate calculation of the numerical values of the specified integral B_k and allowable cross sections S_{min} (for example, selecting the amplitude-time parameters (ATPs) for these purposes of periodic and aperiodic components of the SC current, duration t_{kC} of the SC process, etc.). In addition, the absence in [1] of the analytical relation for the approximate determination of the temperature θ_k of Joule heating by the SC current of the current-carrying parts of the CCP makes it difficult for the wires and cables to check whether the condition of their thermal resistance to the SC current is met.

Therefore, in the field of industrial electric power engineering, when choosing the values of the minimum allowable cross sections S_{min} for the CCP of power circuits of electrical equipment, there is a need for a more detailed and refining calculation of the allowable cross sections S_{il} of electrical wires and cables containing metal cores ($i=1$) and return shells ($i=2$), as well as one or another belt and protective insulation.

The goal of the paper is to carry out the engineering approach refining the existing ones that

determines the minimum allowable cross sections S_{min} of the cable and conductor products in industrial power engineering for calculation selection of the maximum allowable cross sections S_{il} of electrical wires and cables in the power circuits of industrial electrical equipment taking into account the flow of three-phase short-circuit current $i_k(t)$ in emergency mode.

1. Problem definition. Consider uninsulated copper and aluminum wires commonly used in power circuits for electrical equipment for general industrial use, as well as insulated wires and cables with copper (aluminum) inner cores and outer shells having polyvinyl chloride (PVC), rubber (R) or polyethylene (PET) insulation [1, 4]. We assume that in the circular continuous or split copper (aluminum) cores and shells of the specified wires and cables of power circuits of electrical installations in atmospheric air with temperature of $\theta_0=20$ °C in the normal mode of their operation under the rated current load, alternate current flows in their longitudinal direction with frequency $f=50$ Hz, and the maximum long-term permissible temperature θ_{ll} of Joule heating for non- and insulated wires and cables with PVC, R and PET insulation does not exceed numerically the regulated by current requirements levels in 70 °C и 65 °C, respectively [1]. For the generality of the problem to be solved, let us agree that in the studied power circuits with CPP, their operation modes are possible, when their current-carrying parts are completely de-energized. As in [1], we believe that the thermal resistance of the considered electrical wires and cables is limited by the permissible short-term temperature θ_{IS} of heating the current-carrying parts of wires (cables) at three-phase SC in the EN of power supply system of the electrical installation under study. We believe that the values of θ_{IS} correspond to the known permissible short-term temperatures of heating of the CCP by AC SC currents of power frequency [1]. In this regard, the numerical temperature values θ_{IS} for uninsulated copper wires with tension less than 20 N/mm² will be 250 °C, and for uninsulated aluminum wires with tension less than 10 N/mm² – 200 °C [1]. For insulated wires and cables with copper and aluminum conductors, PVC and R insulation, the numerical values of the temperature θ_{IS} are 150 °C, and for the indicated CPP with PET insulation – 120 °C [1]. When selecting S_{il} sections, we assume that the SC current $i_k(t)$ is almost uniformly distributed over the cross section of the core and the shell of the wire (cable). One of the rationales of this assumption is that the minimum penetration depth Δ_i of the magnetic field (thickness of the skin layer) from the SC current $i_k(t)$ in the quasistationary approximation to the considered non-ferromagnetic conductive materials, determined from the calculated expression of the form $\Delta_i \approx [1/(\pi f \mu_0 \gamma_{0i})]^{1/2}$ [5], where γ_{0i} is the electrical conductivity of the core (shell) material of the CPP $\theta_0=20$ °C, and $\mu_0=4\pi \cdot 10^{-7}$ H/m is the magnetic constant, numerically for copper is approximately 9.3 mm, and for aluminum is 11.8 mm. It can be seen that these values of Δ_i turn out to be comparable with the real radii (thicknesses) of the current-carrying cores (shells) of wires and cables commonly used in electrical circuits of electrical installations for general industrial purposes. Let us take

advantage of the adiabatic nature of the taking place at acting durations of SC current $i_k(t)$ of no more than 1000 ms in the materials of cores (shells) of the CCP under consideration of the thermal processes, under which the influence of heat transfer from the surfaces of their current-carrying parts having the current temperature $\theta_{is} \geq \theta_0$ and their thermal conductivity of layers of their conductive materials and insulation on Joule heating of the current-carrying parts of the cores (shells) of wires (cables) is neglected. It is required by calculation in an approximate form taking into account the nonlinear nature of the change due to Joule heating of the indicated CCP of the specific electrical conductivity γ_i of the material of its cores (shells) and the condition of thermal resistance of the CCP to the action of SC current in expanded form to determine the permissible cross sections S_{il} of current-carrying parts for uninsulated copper (aluminum) wires, as well as for insulated wires and cables with copper (aluminum) cores (shells), PVC, R or PET insulation, widely used in power circuits of electrical installations of general industrial purpose and through which in emergency mode of operation of the EN the three-phase SC current $i_k(t)$ of the power frequency $f=50$ Hz with these or other specified ATPs flows.

2. The proposed refined approach to the selection of the allowable cross-sections S_{il} of wires and cables in circuits of electrical installations for general industrial purposes. From the heat balance equation for the current-carrying parts of the CCP of the circuits of indicated electrical installations in the adiabatic mode and the condition of their thermal resistance to current $i_k(t)$ of the adopted SC, the analytical expression for the refined calculation determination of the allowable cross sections S_{il} of the considered electrical wires and cables takes the following form [6]:

$$S_{il} = [J_{ak} / (J_{iIS} - J_{iII})]^{1/2} = J_{ak}^{1/2} / C_{ik}, \quad (1)$$

where $J_{ak} = B_k = \int_0^{t_{kC}} i_k^2(t) dt$ is the Joule (action) integral of

the SC current $i_k(t)$, $A^2 \cdot s$; J_{iIS} , J_{iII} are the current integrals for the current-carrying parts of the wires (cables), the permissible short-term temperature and the long-term permissible heating temperature of the material of which are θ_{IS} and θ_{II} , respectively, $A^2 \cdot s \cdot m^{-4}$; $C_{ik} = (J_{iIS} - J_{iII})^{1/2}$ is the coefficient, the numerical values of which will be listed below and compared with the known ones, $A \cdot s^{1/2} \cdot m^{-2}$.

2.1. Calculation of the current integrals J_{iIS} , J_{iII} and coefficient C_{ik} . For the calculation definition with engineering accuracy of the values of the current integrals in (1) J_{iIS} and J_{iII} used in [5] in the form of current or inertia integrals (see formula 4.56), whose integrand function, unlike the classical Joule integral, contains not the square of current $i_k(t)$, but the square of the density of the specified current $\delta_k(t)$ in electrically conductive materials of the CCP we use the following approximate analytical expressions [6]:

$$J_{iIS} = \gamma_{0i} \beta_{0i}^{-1} \ln[c_{0i} \beta_{0i} (\theta_{IS} - \theta_0) + 1]; \quad (2)$$

$$J_{iII} = \gamma_{0i} \beta_{0i}^{-1} \ln[c_{0i} \beta_{0i} (\theta_{II} - \theta_0) + 1], \quad (3)$$

where c_{0i} , β_{0i} are, respectively, the specific volumetric heat capacity and the thermal coefficient of the electrical

conductivity of the conductive material of the core (shell) of the wire (cable) of the considered power circuit of the electrical installation before the impact on the tested CCP of the emergency current $i_k(t)$ of the SC with arbitrary ATPs, quantified at $\theta_0=20$ °C.

Table 1 shows the numerical values of the used values of γ_{0i} , c_{0i} и β_{0i} for the main conductor materials of the current-carrying parts of the CCP at the temperature of the medium equal to $\theta_0=20$ °C [5, 6].

Table 1

The values of the characteristics of the main materials of the current-carrying cores (shells) of non- and insulated wires and cables of power circuits of electrical installations for general industrial use at $\theta_0=20$ °C [5, 6]

Material of the core (shell) of the wire (cable)	Numerical value of the characteristic		
	γ_{0i} , $10^7 \cdot (\Omega \cdot m)^{-1}$	c_{0i} , $10^6 \cdot J / (m^3 \cdot ^\circ C)$	β_{0i} , $10^{-9} \cdot m^3 / J$
Copper	5.81	3.92	1.31
Aluminum	3.61	2.70	2.14

Knowing the values of the indicated characteristics γ_{0i} , c_{0i} and β_{0i} (see Table 1), for given values of the normalized temperatures θ_0 , θ_{IS} and θ_{II} , using (2) and (3), the numerical values of the current integrals J_{iIS} , J_{iII} and the coefficient C_{ik} used in (1), can be relatively easy founded for a wide range of the CPP used in the power circuits of the considered electrical installations. Table 2 shows the numerical values of the desired coefficient C_{ik} for the main versions of the CPP used in the power circuits of electrical installations for industrial purposes.

Table 2

Refined values of the coefficient C_{ik} for non- and insulated wires (cables) with copper (aluminum) cores (shells) in the power circuits of electrical installations for general industrial purposes

Type of insulation in the wire (cable) of the circuit of the electrical installation	Material of the core (shell) of the wire (cable)	Numerical value of C_{ik} , $10^8 \cdot A \cdot s^{1/2} / m^2$	
		$J_{iII} \neq 0$	$J_{iII} = 0$
Without insulation	Copper	1.56	1.86
	Aluminum	0.88	1.09
PVC, R	Copper	1.16	1.51
	Aluminum	0.74	0.97
PET	Copper	0.96	1.36
	Aluminum	0.62	0.88

Note that in Table 2 the case, when $J_{iII} \neq 0$, corresponds to the rated load current of the CCP in the circuits of the electrical installations under study (the temperature of their current-carrying parts is θ_{II}), and the case $J_{iII} = 0$ – to the de-energization mode of the CCP (the temperature of their current-carrying parts before the flow of the SC current $i_k(t)$ through them equal to the ambient air temperature $\theta_0=20$ °C). To compare the obtained refined data for the coefficient C_{ik} (see Table 2), Table 3 shows its numerical values known according to [1], corresponding to the mode of operation of the CCP, when $J_{iII} \neq 0$.

Table 3

Known values of the coefficient C_{ik} for the main types of electrical wires and cables with copper (aluminum) cores in industrial electric power circuits under the action of SC current on them [1]

No.	Name of the wire (cable) and core	C_{ik} 10^8 $A \cdot s^{1/2}/m^2$
1	Copper wires (cores), uninsulated	1.70
2	Aluminum wires (cores), uninsulated	0.90
3	Cables (insulated wires) with PVC and R insulation and copper cores	1.20
4	Cables (insulated wires) with PVC and R insulation and aluminum cores	0.75
5	Cables (insulated wires) with PET insulation and copper cores	1.03
6	Cables (insulated wires) with PET insulation and aluminum cores	0.65

From the comparison of data of Tables 2, 3 it follows that at $J_{CII} \neq 0$, their corresponding numerical values for the coefficient C_{ik} , depending on the type of the CCP, differ by no more than (3-8)%, and for the mode of operation of the CCP in electrical installation circuits, when $J_{CII} = 0$, these differences increase and reach (9-26)%. In this regard, demonstratively executed on the basis of the mathematical relations (2) and (3), taking into account the nonlinear change in the specific electrical conductivity γ_i of the material of the cores (shells) of the CCP during its Joule heating by SC current $i_k(t)$, the calculation refinement of numerical values for the coefficient C_{ik} , directly used to determine by (1) the permissible cross sections S_{il} , is an electrotechnically justified and expedient action.

2.2. Calculation at the SC of the action integral J_{ak} of the emergency current. To do this, we first write an analytical relation describing the change in time t of the SC current $i_k(t)$ in the power circuits of electrical installations used in industrial electric power industry. According to [1, 3], ATPs of a given SC current $i_k(t)$ obey the following temporal dependence:

$$i_k(t) = I_{mk} [\exp(-t/T_a) - \cos(2\pi t/T_p)], \quad (4)$$

where I_{mk} is the amplitude of the steady-state SC current in the power circuit of the electrical installation $i_k(t)$; T_a , T_p are, respectively, the time constant of decay of the aperiodic component and the oscillation period of the periodic component of the SC emergency current $i_k(t)$ in the circuit under study.

It is interesting to note that from (4) at $T_p = 20$ ms and $t = 10$ ms, corresponding to the largest amplitude of the shock SC current in circuits of the EN, the well-known calculation formula for the shock coefficient k_s relating to the characteristic elements and parts of the electric power system (EPS) (for example, for synchronous generators, electric motors, etc.) follows [1]:

$$k_s = [1 + \exp(-0.01/T_a)]. \quad (5)$$

Note that for turbogenerators with power of (100-1000) MW, the numerical value of T_a is approximately 500 ms (see Table 35.5 in [1]). In this regard, for such electric power elements, the value of the shock coefficient k_s at SC will be numerically about 1.98. For distribution cable networks with voltage (6-10) kV, according to the

above-mentioned Table 35.5 of [1], the time constant of the decay of the aperiodic component of the SC current takes the numerical value $T_a \approx 10$ ms. In the latter case, according to (5), the shock coefficient is $k_s \approx 1.37$. As for the known maximum levels of SC currents in EPS networks, at nominal network voltage of $U_n = 110$ kV, the numerical value of the switching off current amplitude (in fact I_{mk}) is about 50 kA (see table 36.7 in [1]). At $U_n = 10$ kV in the SC mode, the amplitude of the switching off current in accordance with the data in Table 36.7 of [1] can reach a level of 125 kA.

Taking into account (1) and (4), the calculation expression for the desired integral of action J_{ak} of the SC current $i_k(t)$ in the circuit of the electric installation under consideration in the adopted approximation takes the following analytical form:

$$J_{ak} = I_{mk}^2 \left\{ 0.5 t_{kC} + 0.25 \pi^{-1} T_p \sin(2\pi t_{kC}/T_p) \times \right. \\ \times \cos(2\pi t_{kC}/T_p) - 2T_a^2 T_p^2 (T_p^2 + 4\pi^2 T_a^2)^{-1} \left[e^{-t_{kC}/T_a} \times \right. \\ \times [2\pi T_p^{-1} \sin(2\pi t_{kC}/T_p) - T_a^{-1} \cos(2\pi t_{kC}/T_p) + T_a^{-1}] \left. \right] + \\ \left. + 0.5 T_a (1 - e^{-2t_{kC}/T_a}) \right\} \quad (6)$$

From (6) it clearly follows that the value of the integral of action J_{ak} of the SC current $i_k(t)$ is directly proportional to the square of the amplitude I_{mk} of the steady-state SC current and duration (switch off time) t_{kC} of the SC. The greater the numerical values I_{mk} and t_{kC} , the greater will be the numerical values of the desired quantity J_{ak} . In Table 4 at $T_a = 20$ ms ($T_p = 20$ ms) for four fixed numerical amplitude values I_{mk} of the steady-state SC current (30, 50, 70 and 100 kA) and two numerical values of the duration t_{kC} of the SC specified by [1] (100 and 160 ms) the numerical values of the integral of action J_{ak} of the SC current $i_k(t)$, calculated by (6) are shown.

Table 4

Values of the integral action J_{ak} for the SC current $i_k(t)$ according to (4) flowing in the power circuits of electrical installations for general industrial purposes (at $T_a = 20$ ms)

Amplitude value I_{mk} of the steady-state SC current $i_k(t)$ in the power circuit of industrial electrical installation, kA	Values of the integral of action J_{ak} for the SC current $i_k(t)$ by (4), $A^2 \cdot s$	
	$t_{kC} = 100$ ms	$t_{kC} = 160$ ms
30	$5.4 \cdot 10^7$	$8.1 \cdot 10^7$
50	$15.0 \cdot 10^7$	$22.5 \cdot 10^7$
70	$29.4 \cdot 10^7$	$44.1 \cdot 10^7$
100	$60.0 \cdot 10^7$	$90.0 \cdot 10^7$

Having determined from (6) the numerical values of the integral of action J_{ak} of the SC current $i_k(t)$ (see Table 4) and knowing the numerical values of the coefficient C_{ik} (see Table 2), taking into account (1), the refined numerical values of the allowable cross-sections S_{il} of the current-carrying parts of the considered CCP in the power circuits of general-purpose electrical installations can be found. Using accepted assumptions, the allowable amplitudes of current density δ_{ilm} in the materials of the cores (shells) of the wires (cables) under study for the fault SC mode can be quantified from the ratio $\delta_{ilm} \approx I_{mk}/S_{il}$.

2.3. Results of the refined calculation selection of the permissible cross sections S_{il} and current densities

δ_{il} in wires and cables of circuits of electrical installations for general industrial purposes. Table 5 shows the results of the refined calculation by (1), taking into account the data of Table 2, 4 of the permissible cross sections S_{il} of current-carrying copper (aluminum) parts of wires and cables of power circuits for general industrial electrical installations at $J_{ill} \neq 0$, $t_{kC} = 100$ ms and the amplitude I_{mk} of the SC current changing discretely in the range (30-100) kA.

Table 5

Values of the permissible cross sections S_{il} for wires (cables) with copper (aluminum) cores (shells) in the power circuits of electrical installations of general industrial purpose with amplitude I_{mk} of the SC current $i_k(t)$ of 30-100 kA (for $t_{kC} = 100$ ms and $T_a = 20$ ms)

Type of insulation in the wire (cable) of the circuit of the electrical installation	Material of the core (shell) of the wire (cable)	Section value S_{il} , mm ²			
		Amplitude I_{mk} of the steady-state SC current, kA			
		30	50	70	100
Without insulation	Copper	47.11	78.51	109.91	157.02
	Aluminum	83.51	139.17	194.84	278.35
PVC, R	Copper	63.35	105.58	147.81	211.16
	Aluminum	99.30	165.51	231.71	331.01
PET	Copper	76.55	127.58	178.61	255.15
	Aluminum	118.52	197.54	276.55	395.08

From the data of Table 5 it follows that the permissible density amplitudes $\delta_{ilm} \approx I_{mk}/S_{il}$ of the SC current at its flow (switching off) time $t_{kC} = 100$ ms for uninsulated wires with copper and aluminum cores in the circuits of general industrial installations ($T_a = 20$ ms) are approximately 0.64 kA/mm² and 0.36 kA/mm², respectively, for cables with copper (aluminum) cores (shells), PVC and R insulation 0.47 (0.30) kA/mm², and for cables with copper (aluminum) cores (shells) and PET insulation 0.39 (0.25) kA/mm². Note that the indicated numerical values of the permissible amplitudes of the density δ_{ilm} of the SC current in the materials of the current-carrying parts of the wires (cables) do not depend on the amplitude level I_{mk} of the steady-state emergency current of power frequency 50 Hz in them.

Table 6 presents the results of the refined determination by (1) taking into account the data of Table 2, 4 for the case $J_{ill} \neq 0$ of permissible cross sections S_{il} of current-carrying copper (aluminum) parts of wires and cables of power circuits for general industrial purposes at $t_{kC} = 160$ ms and the amplitude I_{mk} of steady-state SC current changing discretely in the range (30-100) kA ($T_a = 20$ ms).

From the data of Table 6 we find that at the time of the SC current flow (switching off) $t_{kC} = 160$ ms, regardless of the numerical value of the current amplitude I_{mk} , the permissible density amplitudes $\delta_{ilm} \approx I_{mk}/S_{il}$ of the emergency current for uninsulated wires with copper and aluminum cores in electrical installation circuits of general purpose ($T_a = 20$ ms) is about 0.52 kA/mm² and 0.29 kA/mm², respectively, for cables with copper (aluminum) cores (shells), PVC and R insulation 0.39 (0.25) kA/mm², and for cables with copper (aluminum)

cores (shells) and PET insulation 0.32 (0.21) kA/mm². From the analysis of data of Table 5, 6 for the refined values of the permissible cross sections S_{il} of the current-carrying parts of the CCP in power circuits for general-purpose electrical equipment ($J_{ill} \neq 0$; $T_a = 20$ ms), we can conclude that for the indicated amplitudes I_{mk} of the steady-state SC current satisfying the range (30-100) kA, an increase in the switching off time t_{kC} of the SC current by 1.6 times (from 100 ms to 160 ms) leads to a decrease in the permissible density amplitudes δ_{ilm} of the SC current in the materials of the wires and cables under consideration by about 1.2 times. At the same time, the values of the permissible cross sections S_{il} copper (aluminum) cores and shells (return conductors) of the CCP under study increase by the same amount (~1.2 times). From here, practical recommendations supported by the above-mentioned refined engineering calculations of the values of S_{il} and δ_{ilm} follows for the operating conditions of electrical installations for general industrial purposes: in their power circuits to ensure the thermal stability of the CCP, the switching off time t_{kC} of the SC current (types of phase-applied relay protection and switches in EN) and practically selected values of the permissible cross-sections S_{il} of their current-carrying parts must be obligatory mutually agreed.

Table 6

Values of the permissible cross sections S_{il} for wires (cables) with copper (aluminum) cores (shells) in the power circuits of electrical installations of general industrial purpose with amplitude I_{mk} of the SC current $i_k(t)$ of 30-100 kA (for $t_{kC} = 160$ ms and $T_a = 20$ ms)

Type of insulation in the wire (cable) of the circuit of the electrical installation	Material of the core (shell) of the wire (cable)	Section value S_{il} , mm ²			
		Amplitude I_{mk} of the steady-state SC current, kA			
		30	50	70	100
Without insulation	Copper	57.69	96.15	134.61	192.31
	Aluminum	102.27	170.45	238.64	340.91
PVC, R	Copper	77.58	129.31	181.03	258.62
	Aluminum	121.62	202.70	283.78	405.40
PET	Copper	93.75	156.25	218.75	312.50
	Aluminum	145.16	241.93	338.71	483.87

2.4. Calculation estimation of the thermal stability of electrical wires and cables in circuits of electrical installations for general industrial purpose.

Within the framework of the proposed approach to the selection of the allowable cross sections S_{il} of wires (cables) in the power circuits of electrical installations for general industrial purposes, the calculation estimation of their thermal stability can be demonstratively carried out. For this purpose, as in [1, 6], we determine the thermal stability of the wires and cables under consideration in the circuits of the electrical installations under investigation according to the following thermophysical condition:

$$\theta_{iS} \leq \theta_{IS}, \quad (7)$$

where θ_{iS} , θ_{IS} are, respectively, the current (final) and permissible short-term temperature of heating of the current-carrying parts of the considered electrical wires and cables in the power circuits of the EN.

To find in (7) the values of the current or final temperature θ_{iS} of heating the material of the current-carrying parts of the CCP, determined by Joule heat from the action of the SC current $i_k(t)$ on it, we first use the well-known nonlinear dependence of the specific electrical conductivity γ_i of the material of the core (shell) of the wire or cable on the value of temperature θ_{iS} [5]:

$$\gamma_i = \gamma_{0i} [1 + c_{0i} \beta_{0i} (\theta_{iS} - \theta_0)]^{-1}. \quad (8)$$

It should be noted that the expression (8) in the temperature range from 20 °C to the melting temperature of materials of the cores (shells) of the CCP, according to experimental data from [5], approximates the temperature dependence of γ_i for copper and aluminum with an error of no more than 5 %. In addition, we note that, both earlier and in (8), the value γ_{0i} means the electrical conductivity γ_i of the material of the current-carrying parts of the CCP at temperature $\theta_0=20$ °C. Taking into account (8), the solution of a non-uniform differential equation of the first order for the final temperature θ_{iS} of Joule heating by SC current $i_k(t)$ of the material of the core (shell) of the CCP in the circuit of the electrical installation of general industrial purpose under the initial condition of the form $[\theta_{iS}(t=0) - \theta_{0i}] = 0$ can be written in the following approximate analytical form [6]:

$$\theta_{iS} = \theta_{0i} + (c_{0i} \beta_{0i})^{-1} \left[\exp(J_{ak} \gamma_{0i}^{-1} \beta_{0i} / S_{ii}^2) - 1 \right], \quad (9)$$

where θ_{0i} is the initial material temperature of the material of current-carrying parts of the CCP, equal depending on the operating mode of the power circuits of electrical equipment to $\theta_{ii} (J_{ii} \neq 0)$ or $\theta_0 = 20$ °C ($J_{ii} = 0$).

From (9) it can be seen that under the accepted assumptions, the known numerical values of the thermophysical characteristics γ_{0i} , c_{0i} and β_{0i} for the materials used in the current-carrying parts of the CCP (see data from Table 1 and [5]), and also for founded by (1) and (6) the numerical values of the permissible cross sections S_{ii} of copper (aluminum) cores (shells) of wires (cables) and the integral of action J_{ak} of the SC current $i_k(t)$, determination of the desired final temperature θ_{iS} does not cause any electrical engineering difficulties.

As one of the examples (*the first example*) of the practical implementation of the results obtained, we carry out at $\theta_{0i}=\theta_{ii}=70$ °C ($J_{ii} \neq 0$), according to (7) and (9), the calculation estimation of the thermal stability of uninsulated (bare) copper wire of the power circuit of general-purpose electrical equipment for the emergency case when $t_{kC}=160$ ms, $T_a=20$ ms and $I_{mk}=100$ kA. According to the calculated data (see Table 6), the permissible cross-section S_{ii} of the accepted wire is numerically approximately 192.31 mm². In this case, the value of the integral of action J_{ak} of the SC current $i_k(t)$ by (6) will be numerically about $9 \cdot 10^8$ A²·s (see Table 4). Then by (9) taking into account the data of Table 1, the final temperature θ_{iS} of the Joule heating by the emergency SC current $i_k(t)$ of the copper wire under consideration will be approximately numerically equal to 212.4 °C. It can be seen that this temperature value is less than the normalized permissible short-term temperature θ_{iS} of heating of checked for thermal resistance the copper wire of the power circuit of electrical equipment, which according to [1] is 250 °C at tension in it (wire) less than

20 N/mm². Therefore, we can conclude that condition (7) for the specified calculation case is satisfied.

Calculation estimation by (9) with the same initial data ($\theta_{0i}=\theta_{ii}=70$ °C; $t_{kC}=160$ ms; $T_a=20$ ms; $I_{mk}=100$ kA; $J_{ak}=9 \cdot 10^8$ A²·s) of the final temperature θ_{iS} of the Joule heating of a copper round core of the cable with PVC or R insulation (*the second example*) with the permissible cross section $S_{ii}=258.62$ mm² (see Table 6) shows that in this case it reaches a level of approximately 139.1 °C. This temperature is less than the normalized level of the permissible short-term temperature θ_{iS} of heating of tested for thermal resistance the cable with PVC (R) insulation, which is 150 °C [1]. As we see, the condition (7) is also satisfied for this calculation case. In this regard, it is reasonable to say that the carried out calculation estimates of the thermal resistance of both uninsulated copper wire and cable with copper core, PVC and R insulation of power circuits of electrical installations under study indicate the operability of the proposed electrical engineering approach to the refined calculation selection of the permissible cross sections S_{ii} of current-carrying parts of the CCP used in the power circuits of electrical equipment of industrial electric power industry.

Conclusions.

1. The proposed electrical engineering approach allows by the condition of thermal stability of CCP of power circuits of electrical equipment for general industrial purposes to provide a refined calculation selection of permissible cross sections S_{ii} of uninsulated wires, insulated wires and cables with copper (aluminum) cores (shells-screens) with PVC, R and PET insulation, the current-carrying parts of which in emergency mode of their operation can be affected by the current $i_k(t)$ of a three-phase SC in EPS with ATPs specified by standardizing documents.

2. It is shown that the discrepancy between the numerical values of the coefficient C_{ik} included in formula (1) and determining the values of the permissible cross sections S_{ii} of the current-carrying parts of the CCP in the circuits of electrical installations of general purpose, according to the existing and proposed electrical engineering approaches to the calculation selection of the permissible cross sections S_{ii} of the cores (shells) of the considered electrical wires and cables for their normal operation at $J_{ii} \neq 0$ (at rated current load of the CCP) is not more than (3-8)%, and at $J_{ii} = 0$ (in the mode of de-energizing of the CCP) it reaches up to (9-26) %.

3. An analytical relation (6) is obtained for a refined calculation determination of the value of the integral of action J_{ak} of the SC current $i_k(t)$ (Joule integral B_k) in the power circuits of the electrical equipment under study, which allows for given amplitudes I_{mk} of the steady-state SC current, duration (switching off time) of the SC process t_{kC} , time constant of the decay T_a of aperiodic component of the SC current $i_k(t)$ and oscillation period $T_p=20$ ms of the periodic component of emergency SC current to relatively easy find required for the calculation selection of the permissible cross sections S_{ii} of the current-carrying parts of the considered CCP the value of the integral J_{ak} .

4. It is established that in the first approximation in the power circuits of electrical equipment for general industrial purpose ($T_a=20\text{ms}$) the allowable density amplitudes $\delta_{ilm} \approx I_{mk}/S_{il}$ of the SC current $i_k(t)$ at its switching off time $t_{kc}=100\text{ ms}$ in EPS for uninsulated wires with copper (aluminum) cores are about 0.64 (0.36) kA/mm^2 respectively, for cables with copper (aluminum) cores (shells) and PVC (R) insulation 0.47 (0.30) kA/mm^2 , and for cables with copper (aluminum) cores (shells) and PET insulation 0.39 (0.25) kA/mm^2 . If in the EPS the switching off time t_{kc} of the SC current $i_k(t)$ in these circuits increases ($T_a=20\text{ ms}$), the permissible density amplitudes δ_{ilm} of the fault SC current are reduced and at $t_{kc}=160\text{ ms}$ for uninsulated wires with copper (aluminum) cores equal, respectively, approximately 0.52 (0.29) kA/mm^2 , for cables with copper (aluminum) cores (shells) and PVC (R) insulation 0.39 (0.25) kA/mm^2 , and for cables with copper (aluminum) cores (shells) and PET insulation 0.32 (0.21) kA/mm^2 .

5. A convenient in practical use analytical relation (9) has been proposed for carrying out, by condition (7), the calculation estimation of the thermal stability to the SC current $i_k(t)$ of indicated electrical wires and cables, widely used in power circuits for general-purpose electrical equipment.

REFERENCES

1. Orlov I.N. *Elektrotehnicheskij spravochnik. Proizvodstvo i raspredelenie elektricheskoy energii. Tom 3, Kn. 1* [Electrical

engineering handbook. Production and distribution of electric energy. Vol. 3, Book 1. Ed. I.N. Orlov]. Moscow, Energoatomizdat Publ., 1988. 880 p. (Rus).

2. Barybin Yu.G. *Spravochnik po proektirovaniyu elektricheskikh setey i oborudovaniya* [Handbook per planning electrical circuit and equipment]. Moscow, Energoatomizdat Publ., 1991. 464 p. (Rus).

3. Knyazevskiy B.A., Lipkin B.Yu. *Elekrosnabzhenie promyshlennykh predpriyatij* [Electric supply industrial organization]. Moscow, High school Publ., 1972. 432 p. (Rus).

4. Belorussov N.I., Saakjan A.E., Jakovleva A.I. *Elektricheskie kabeli, provoda i shnury. Spravochnik* [Electrical cables, wires and cords. Directory]. Moscow, Energoatomizdat Publ., 1988. 536 p. (Rus).

5. Knopfel' G. *Sverkhsil'nye impul'snye magnitnye polia* [Ultra strong pulsed magnetic fields]. Moscow, Mir Publ., 1972. 391 p. (Rus).

6. Baranov M.I. *Izbrannye voprosy elektrofiziki. Monografiya v 3 tomah. Tom 3: Teoriya i praktika elektrofizicheskikh zadach* [Selected topics of Electrophysics. Monograph in 3 vols. Vol. 3: Theory and practice of electrophysics tasks]. Kharkiv, Tochka Publ., 2014. 400 p. (Rus).

Received 17.12.2018

M.I. Baranov, Doctor of Technical Science, Professor, Scientific-&-Research Planning-&-Design Institute «Molniya», National Technical University «Kharkiv Polytechnic Institute», 47, Shevchenko Str., Kharkiv, 61013, Ukraine, phone +380 57 7076841, e-mail: baranovmi@kpi.kharkov.ua

How to cite this article:

Baranov M.I. Refined selection of allowable cross-sections of electrical conductors and cables in the power circuits of industrial electrical equipment taking into account emergency operating modes. *Electrical engineering & electromechanics*, 2019, no.3, pp. 37-43. doi: 10.20998/2074-272X.2019.3.06.

G.V. Bezprozvannykh, I.A. Mirchuk, A.G. Kyessayev

TECHNOLOGICAL PARAMETERS OF THE COOLING MODE OF POLYMER INSULATION OF POWER CABLES

Introduction. The cooling mode of polymer insulation after application to the extruder is one of the main factors determining cable performance. Theoretically, it is ideal to cool the insulation when the temperature of the cooling medium is equal to the melting point of the insulation material: in this case, the probability of formation of voids in the insulation is less. The cooling process is usually not subject to stringent requirements, since most insulating materials allow for quite sharp cooling. The exception is polyethylene, which requires gradual cooling. When the insulation is cooled in a cooling bath, the temperature decrease starts from the surface. In this regard, the cooling of the insulation of polyethylene is carried out in steps to a temperature at which the cooled extruded insulation will not be deformed or damaged on the receiving drum. Polyethylene is characterized by a large value of thermal expansion coefficient, the maximum value of which is in the temperature range (90-125) °C. As a result, there is an uneven reduction in the volume of the upper and inner insulation layers, especially for cables with a considerable insulation thickness. The rapid cooling of polyethylene leads to the formation of cracks, air inclusions both between the insulation and the conductive core, and in the layers located near the core. *Purpose.* The substantiation of the technological parameters of the cooling mode of power cables based on the calculation of the thermal equivalent circuit of a conductive core insulated with polyethylene in transient thermal mode. *Methodology.* The calculation of the temperature distribution in the thickness of extruded polyethylene insulation at different points in time, depending on the temperature of the cooling water, is made by the method of electrothermal analogies. There is a transition from the thermal equivalent circuit of power cables to the equivalent circuit of the discrete resistive equivalent circuit method, which is calculated using the nodal potential method. As a result of solving a three-diagonal system of linear algebraic equations by sweeping and finding at each discretization step (time step) thermal power fluxes in the branches of the thermal equivalent circuit, the temperature in the thermal capacitances determines the temperature in each insulation layer. *Practical value.* The duration of the transition process, corresponding to the achievement of the same temperature throughout the thickness of the insulation, can be considered as a criterion in determining the length of the cooling bath sections depending on the extrusion (reception) rate. References 12, figures 6.

Key words: cooling mode, polyethylene insulation, thermal equivalent circuit, discrete resistive equivalent circuit method, transient mode, nodal potentials method, system of linear algebraic equations, cooling bath length.

Обґрунтовано методику розрахунку режиму охолодження силових кабелів в перехідному тепловому режимі. Представлено теплову схему заміщення ізольованої струмопровідної жили. За допомогою методів дискретних резистивних схем заміщення і вузлових потенціалів отримано розподіл температури в товщі поліетиленової ізоляції в різні моменти часу в залежності від температури води, що охолоджує. Показано, що тривалість перехідного процесу, що відповідає досягненню однакової температури по всій товщині ізоляції, можна розглядати в якості критерію при визначенні технологічних параметрів охолодження. Бібл. 12, рис. 6.

Ключові слова: режим охолодження, поліетиленова ізоляція, теплова схема заміщення, метод дискретних резистивних схем заміщення, несталій режим, метод вузлових потенціалів, система лінійних алгебраїчних рівнянь, довжина ванни охолодження.

Обоснована методика расчета режима охлаждения силовых кабелей в переходном тепловом режиме. Представлена тепловая схема замещения изолированной токопроводящей жилы. С помощью методов дискретных резистивных схем замещения и узловых потенциалов получено распределение температуры в толще экструдированной полиэтиленовой изоляции в разные моменты времени в зависимости от температуры охлаждающей воды. Показано, что длительность переходного процесса, соответствующая достижению одинаковой температуры по всей толщине изоляции, можно рассматривать в качестве критерия при определении технологических параметров охлаждения. Библ. 12, рис. 6.

Ключевые слова: режим охлаждения, полиэтиленовая изоляция, тепловая схема замещения, метод дискретных резистивных схем замещения, неустойчивый режим, метод узловых потенциалов, система линейных алгебраических уравнений, длина ванны охлаждения.

Introduction. The cooling mode of polymer insulation after application in the extruder is one of the main factors determining cable performance. Theoretically, the cooling of the insulation is ideal at the temperature of the cooling medium equal to the melting point of the insulation material: in this case, the probability of formation of voids in the insulation is less [1-3]. In the process of cooling, heat from the surface of the insulation is removed with the help of air or water of lower temperature. The cooling process is mainly subject to the laws of convective heat transfer, and, here forced convection is usually observed due to the continuous axial

movement of the workpiece during the technological process. The process of temperature change over the thickness of the insulation or shell, that is, inside a solid, occurs according to the laws of heat conduction.

The cooling process is usually not subject to stringent requirements, since most insulating materials allow for quite sharp cooling. The exception is polyethylene, which requires gradual cooling. When the insulation is cooled in a cooling bath, the temperature decrease starts from the surface. In this regard, the cooling of insulation of polyethylene is carried out

© G.V. Bezprozvannykh, I.A. Mirchuk, A.G. Kyessayev

stepwise to a temperature at which the cooled extruded insulation will not be deformed or damaged on the receiving drum [2, 3]. At cable companies, extruded coating is cooled to temperatures (40...50) °C to comply with safety requirements [4].

The length of the cooling bath depends on the speed of extrusion, the diameter of the core (or cable) and the thickness of the insulation (shell). The length of the bath for cooling insulation based on crystalline polymers is longer than for cooling insulation of amorphous polymers, since the crystallization process is exothermic [2, 3].

The rewinding speed depends on the diameter of the extruded cables. So, for telephone cables, the conductor diameter of which does not exceed 1 mm, the reception speed is one of the highest and reaches 1200 m/min. As the diameter of the core increases, the reception speed decreases and for power cables it is about (6-30) m/min. At cooling of polyethylene insulation, speed is limited by the length of the cooling bath.

Existing methods for calculation of the cooling modes of extruded insulation allow one to calculate the cable rewinding speed at a known cooling bath length or the bath length at a given rewinding speed [5, 6] without taking into account the temperature distribution over the entire insulation thickness in transient thermal mode.

Problem definition. Technological parameters of the cooling mode affect the internal structure of the polymer: the lower the cooling rate, the higher the content of the crystalline phase in the polymer insulation. At rapid cooling, relaxation processes do not have time to complete, a violation of the internal morphological structure occurs, leading to the formation of a non-equilibrium structure of polymer insulation with a predominance of the amorphous phase [1-3]. The quantitative ratio of the crystalline and amorphous phases ultimately determines the thermal, mechanical and electrical characteristics of extruded insulation.

At sharp cooling, it is also possible the formation of internal voids in the thickness of extruded insulation. This process is most likely to occur when cooling polyethylene, in which the volume of the melt at temperature of 200 °C is practically 25% higher than at 20 °C: a sharp change in volume occurs near its melting point [7]. Polyethylene is characterized by a large value of thermal expansion coefficient, the maximum value of which is in the temperature range (90-125) °C. As a result, there is an uneven reduction in the volume of the upper and inner insulation layers, especially for cables with a considerable insulation thickness. The sharp cooling of polyethylene leads to the formation of cracks, air inclusions both between the insulation and the conductive core, and in the layers located near the core.

Thus, in [5] the degree of cable cooling is determined at a given temperature at the inlet to the bath and the temperature of the cooling water during convective heat exchange between the surface of the insulation and cooling water [8].

For power cables, it is important to obtain the temperature field distribution over the thickness of extruded polyethylene insulation, which is determined by the thermal conductivity of polyethylene insulation,

taking into account the temperature of heating of the conducting core and the temperature of the cooling water.

The goal of the paper is the justification of the technological parameters of the cooling mode of power cables based on the calculation of the thermal equivalent circuit of a conductive core insulated with polyethylene in transient thermal mode.

Thermal equivalent circuit of extruded insulated core in transient thermal mode. In the general case, the calculation of the temperature field over the thickness of the insulation when it is cooled is reduced to the specification of single-valued conditions: geometric conditions that characterize the shape and dimensions of the extruded conductive core; physical conditions characterizing thermal conductivity, heat capacity, density of the core, insulation and cooling medium, respectively; initial conditions characterizing the temperature distribution at the initial moment of time (at $t = 0$); boundary conditions characterizing the interaction of the extruded insulation under consideration with the environment [9].

To calculate the temperature distribution in the thickness of extruded polyethylene insulation at different times, depending on the cooling water temperature, we use the method of electrothermal analogies [9]. There is a complete analogy between the thermal and electrical equivalent circuits, which allows using the well-known methods of the theory of electrical circuits to calculate thermal circuits. The analogue of the potential in the thermal equivalent circuit is the temperature (T), and the analogue of the current is the heat flux (P) per unit length of insulation along its axis (per unit length of cable).

The thermal equivalent circuit of insulation of power cables (Fig. 1) is calculated using the method of discrete resistive equivalent circuits [9]. For this, thermal quantities will be replaced by their electrical counterparts. Then we calculate the thermal circuit and determine the desired temperature [9].

The thermal substitution circuit (Fig. 1) reflects: the heat capacity of the core C_g ; the temperature-dependent (non-linear) thermal resistances R_t and thermal capacitances C_i of each insulation layer (from 1 to M), the thermal resistance of heat transfer R_{to} from the surface of the wire insulation, as well as the effect of the source of heating of the wire to the medium temperature T_w .

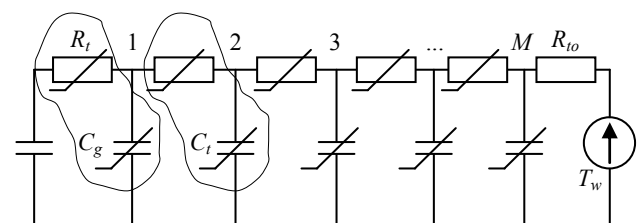


Fig. 1. Thermal substitution circuit of the extruded insulated core in transient thermal mode

To calculate the temperature field in the process of cooling of a moving insulated conductive core, we take the following assumptions:

- 1) an insulated core is considered symmetric about its axis;
- 2) the core moves at a constant speed;

- 3) the core material and insulation is isotropic;
- 4) changes in the size of the wire caused by shrinkage of the insulation are not take into account;
- 5) the heat transfer along the conductive core is neglected;
- 6) the internal sources of heat released during the phase transition of the polymer during cooling of the insulation are not take into account;
- 7) each element has constant electrical and physical characteristics in its volume.

Given the initial values of the temperature at the exit of extruded polyethylene insulation from the vulcanization chamber at time $t = 0$, namely: of a heated conductor, insulation (the temperature of which is the same throughout the thickness and on the surface), cooling water, it is possible to obtain the temperature distribution across the insulation thickness at different points in time.

The calculation technique. From the thermal equivalent circuit (Fig. 1), we turn to the equivalent circuit of the discrete resistive equivalent circuit (DREC) method (Fig. 2) [10], in accordance with which capacitances are represented by sources of EMF E_{cg} , E_{ct} and resistors R_{cg} , R_{ct} . The EMF sources «remember» the temperatures on the capacitances at the previous ($k-1$)th time («old» temperature). Finding a «new» temperature at the current k -th instant of time in time interval h is defined as

$$T_k \approx \frac{h}{C} \cdot P + T_{k-1}. \quad (1)$$

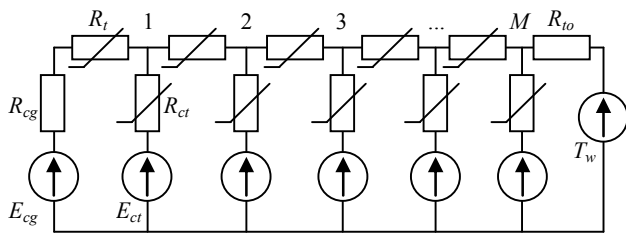


Fig. 2. Discrete resistive equivalent circuit of extruded insulated core in transient thermal mode

The calculation of the DREC is performed by the method of nodal potentials [9, 10]. The system of linear algebraic equations (SLAE) of the method of nodal potentials for the case of M nodes (the number of layers along the insulation thickness) has the form [9]

$$\begin{pmatrix} G_{11} & G_{12} & G_{13} & G_{14} & \dots & G_{1M} \\ G_{21} & G_{22} & G_{23} & G_{24} & \dots & G_{2M} \\ G_{31} & G_{32} & G_{33} & G_{34} & \dots & G_{3M} \\ G_{41} & G_{42} & G_{43} & G_{44} & \dots & G_{4M} \\ G_{51} & G_{52} & G_{53} & G_{54} & \dots & G_{5M} \\ \dots & \dots & \dots & \dots & \dots & \dots \\ G_{M-1,1} & G_{M-1,2} & G_{M-1,3} & G_{M-1,4} & \dots & G_{M-1,M} \\ G_{M1} & G_{M2} & G_{M3} & G_{M4} & \dots & G_{MM} \end{pmatrix} \begin{pmatrix} \varphi_1 \\ \varphi_2 \\ \varphi_3 \\ \varphi_4 \\ \varphi_5 \\ \dots \\ \varphi_{M-1} \\ \varphi_M \end{pmatrix} = \begin{pmatrix} J_1 \\ J_2 \\ J_3 \\ J_4 \\ J_5 \\ \dots \\ J_{M-1} \\ J_M \end{pmatrix}, \quad (2)$$

where $J_1 - J_M$ are the nodal «currents» (heat flow): $J_1 - J_{M-1} = 0$; $J_M = \frac{T_c}{R_{to}}$; $G_{11} = \frac{1}{R_t + R_{cg}} + \frac{1}{R_{ct}} + \frac{1}{R_t}$ is

the nodal conductivity of the first node (the sum of the conductivities of the branches converging at the first

node); $G_{22} = \frac{1}{R_t} + \frac{1}{R_{ct}} + \frac{1}{R_t}$ is the nodal conductivity of the second node;

$G_{33} = G_{22}$; $G_{44} = G_{22}$; $G_{55} = G_{22}$; ... $G_{(M-1)(M-1)} = G_{22}$;

$G_{MM} = \frac{1}{R_t} + \frac{1}{R_{ct}} + \frac{1}{R_{to}}$; $G_{12} = -\frac{1}{R_t}$ is the mutual

conductivity between the 1st and the 2nd nodes (taken with a minus sign the total conductivity between the 1st and the 2nd nodes); $G_{23} = G_{34} = G_{45} = \dots = G_{12}$;

$G_{13} = G_{14} = G_{15} = \dots = G_{1M} = 0$.

As a result of solution of the three-diagonal SLAE (2) by the method of sweeping and finding at each discretization step (time interval) thermal power fluxes in the branches of the thermal equivalent circuit, the temperatures in the thermal capacitances, the temperature is determined in each insulation layer. The order of the resolving system of linear algebraic equations is determined by the product of the number of nodes and the number of discretization steps.

The influence of technological modes of cooling and design parameters of cables on the temperature distribution across the thickness of extruded polyethylene insulation. The calculation of the temperature distribution over the thickness of the insulation is carried out with given thermal characteristics (thermal conductivity λ , specific heat capacity c , density ρ): for copper conductor $\lambda_g = 200$ W/(m·K); $c_g = 420$ J/(kg·K); $\rho_g = 8300$ kg/m³ [11, 12].

For polyethylene: the density is assumed to be $\rho_d = 940$ kg/m³; the dependences of the thermal conductivity and specific heat capacity on temperature are given as approximating functions [1, 7]:

$$\lambda_d = 0,35 \text{ W/(m·K) at } T \geq 120 \text{ }^\circ\text{C};$$

$$\lambda_d = 0,41 - 0,001 \cdot T \text{ at } T < 120 \text{ }^\circ\text{C};$$

$$c_d = 3150 \text{ J/(kg·K) at } T \geq 115 \text{ }^\circ\text{C};$$

$$c_d = 3750 - 4,78 \cdot T \text{ at } T < 115 \text{ }^\circ\text{C};$$

Thermophysical characteristics of cooling water required for the calculation of thermal resistance R_{to} : $\lambda_w = 0,24$ W/(m·K); $c_w = 5000$ J/(kg·K); $\rho_w = 1000$ kg/m³ [5].

The calculations are performed for initial insulation temperature of 200 °C at time $t = 0$ when extruded polyethylene insulation exits the vulcanization chamber.

1. The influence of the temperature of the cooling medium on the temperature distribution. Figure 3 shows the dynamics of the temporal variation of the temperature distribution in polyethylene insulation 2 mm thick (i is the layer number in the thickness of the insulation, measured from the core), depending on the cooling water temperature. The temperature of the water in the cooling bath is respectively:

- 30 °C (Fig. 3,a, curve 1 in Fig. 3,d);
- 60 °C (Fig. 3,b, curve 2 in Fig. 3,d);
- 90 °C (Fig. 3,c, curve 3 in Fig. 3,d).

The calculation results are obtained for a conductive copper core heated to 90 °C with cross section of 95 mm². As the calculations show (compare Fig. 3,c and Fig. 4), heating the core to 90 °C reduces the probability of formation of air cavities near the core, provides a more

uniform temperature distribution across the insulation thickness during the same transient time and improves adhesion of the polymer melt to the metal conductor.

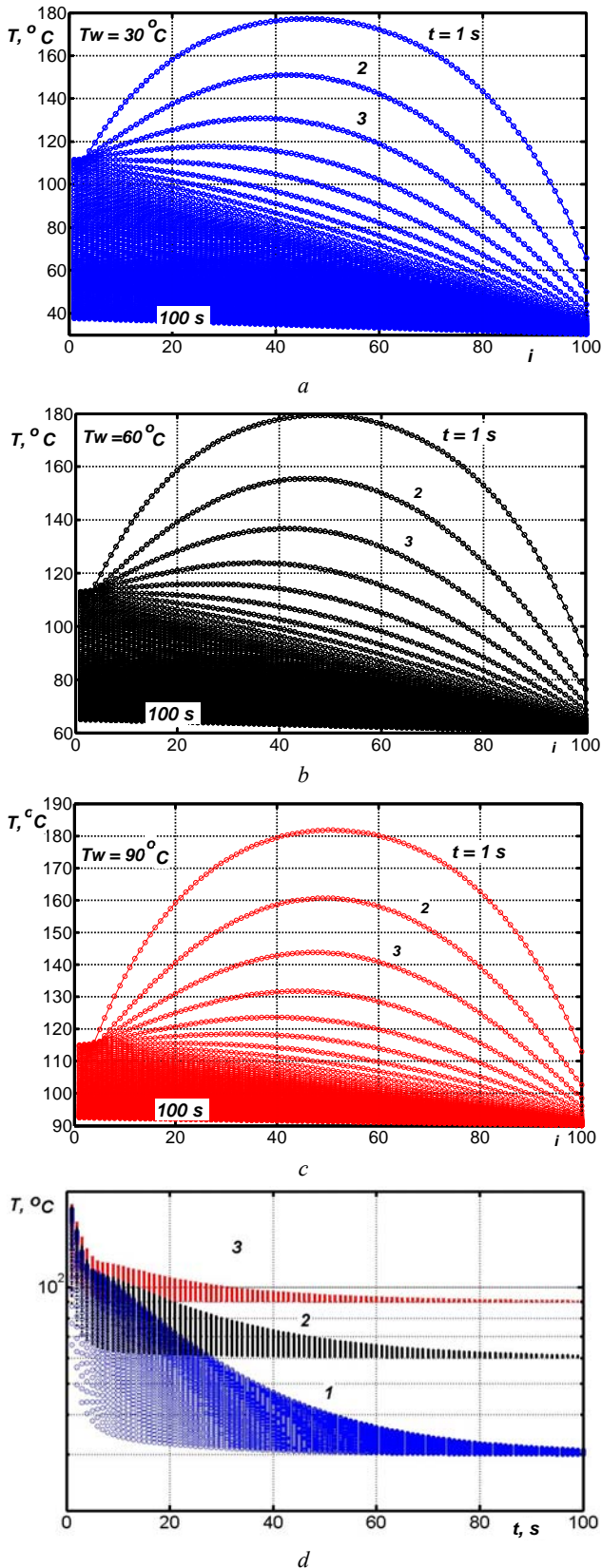


Fig. 3. The effect of cooling water temperature on temporal distribution dynamics of temperature through the thickness of polyethylene insulation

At cooling water temperature of 30 °C, the most sharp cooling of the insulation is observed (compare curve 1 with curve 3 in Fig. 3,d). The decrease in temperature starts from the surface of the insulation (see Fig. 3, layer $i = 100$ at $t = 1$ s). The surface layer, cooling over time $t = 5$ s, tends to reduce its volume, while the internal ones, which are not yet cooled, impede this reduction. In this case, the surface layer hardens under the action of radial pressure and is in a stretched state with frozen internal stresses. Upon subsequent cooling of the inner layers, their volume is reduced, but this occurs under conditions when the outer layers have already hardened. Volume reduction may occur unevenly, and at the most mechanically weak points, i.e. where insulation is last cooled.

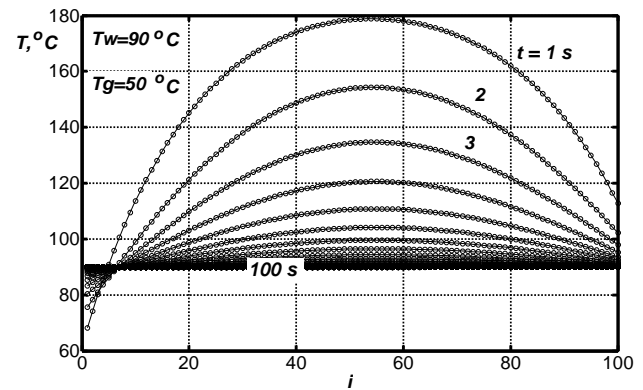


Fig. 4. Dynamics of temperature distribution over the thickness of the insulation at the temperature of the core equal to 50 °C

The probability of formation of bubbles and voids in the core, the temperature of which is higher in comparison with the outer layers of insulation, increases significantly. The time required to complete the transient thermal process in the first section of the cooling bath with water temperature of 90 °C (see Fig. 3,c, curve 3 in Fig. 3,d, curve 1 in Fig. 5) is about 100 s.

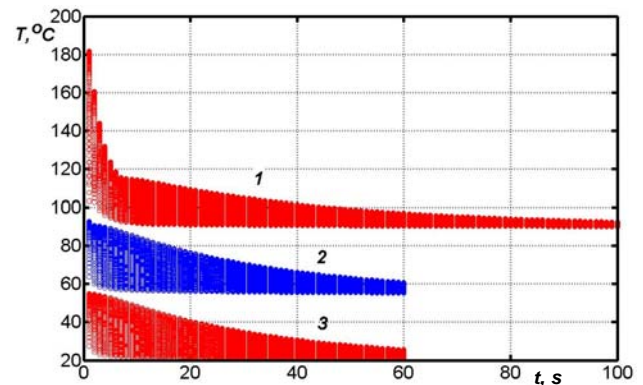


Fig. 5. Temporal diagram of the temperature distribution across the thickness of the polyethylene insulation with step cooling in a three-section bath

During this time, over the entire thickness of the insulation, practically the same temperature is established, equal to the cooling water temperature of 90 °C, which reduces the probability of formation of cavities and the concentrations of thermomechanical stresses in the thickness of the polyethylene insulation.

The transient time can be considered as a criterion to substantiate the relationship between the length L_1 (m) of the first section of the cooling bath and the reception speed v (m/s). For the case considered, the L_1/v value is 100 s. At a rewind speed of $v = 0,2$ m/s = 12 m/min, the length of the first section should be equal to 20 m. The length of the bath can be reduced at least twice with that same reception speed: at such a length, the temperature difference between the inner and outer layers of insulation does not exceed 10 °C (see Fig. 5, curve 1).

The insulation in the second and the third sections is cooled by water, the temperature of which is equal to 50 °C and 20 °C, respectively, in significantly less time (compare curve 1 and curves 2, 3 in Fig. 5). The length of the second section L_2 is 10 m, of the third (to ensure the insulation temperature of about 40 °C) is $L_3 = 4$ m. Thus, the total length of the three-section cooling bath will be 30 m. Such cooling mode parameters provide less probability of formation of voids, air inclusions and cracks in the thickness of the insulation. The results obtained are consistent with the data given in [1, 5].

2. The influence of cable design parameters on the temperature distribution across the thickness of extruded polyethylene insulation. The effect of the diameter of the conductive core on the temperature distribution across the insulation thickness at different points in time is shown in Fig. 6.

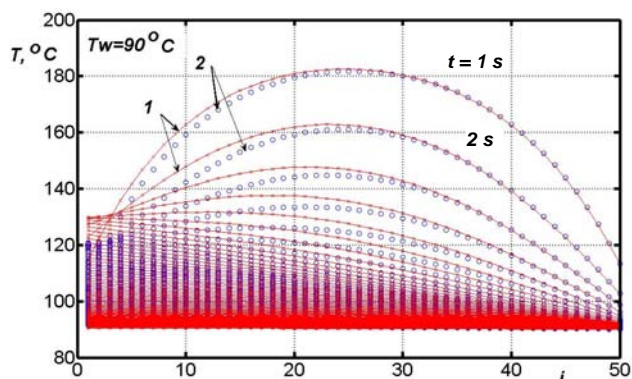


Fig. 6. The influence of the conductive core cross section on the temperature distribution across the thickness of the polyethylene insulation

The insulation thickness in both cases is 2 mm. Curve 1 corresponds to the cross section of a copper core of 95 mm², curve 2 – of 240 mm². At the initial cooling moment, for internal insulation layers located near the core of a larger cross section, the temperature is lower compared to the temperature distribution for insulation with a core of a smaller cross section. The difference is further leveled, which allows using a bath of the same length for cooling.

Increasing the thickness of the insulation leads to an increase in the time of the transient thermal process, and hence the length of the first cooling section (Fig. 7). To maintain the same length of the first section of the cooling bath when cooling cables with a greater insulation thickness, it is necessary to reduce the reception rate accordingly.

Figure 7 shows the effect of the number of layers on the temperature distribution: $M = 100$ (Fig. 7,a), $M = 300$

(Fig. 7,b). The core cross section is 95 mm², the insulation thickness is 6 mm. An increase in the number of layers along the insulation thickness improves the calculation accuracy by 8 %.

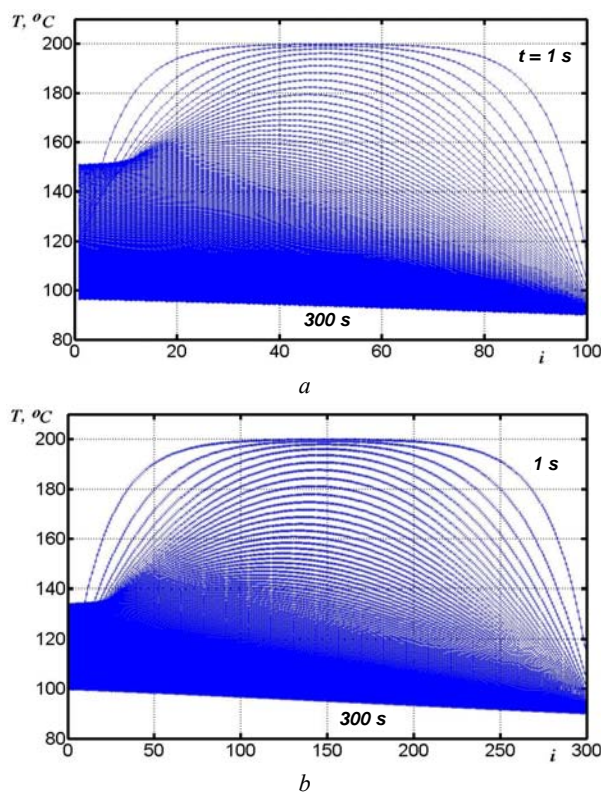


Fig. 7. The influence of the number of layers on the temperature distribution over the thickness of the insulation

Conclusions.

A technique is developed for calculation of the technological parameters of the cooling mode of power cables. The technique is based on the calculation of the thermal equivalent circuit of a conductive core insulated with polyethylene in transient thermal mode, taking into account the dependence on temperature of thermal resistance and heat capacity using methods of discrete resistive equivalent circuits and nodal potentials.

The duration of the transient, corresponding to achieving the same temperature throughout total thickness of the insulation of power cables of different designs, is substantiated. It is shown that the duration of the transient can be considered as a criterion in determining the length of the sections of the cooling bath, depending on the rate of extrusion (reception).

The influence of the diameter of the conducting core and the thickness of the polyethylene insulation on the cooling mode of the power cables is established.

The proposed technique can be applied to select technological cooling modes for other types of cables, for example, symmetric, radio frequency and optical cables.

REFERENCES

1. Leonov V.M., Peshkov I.B., Ryazanov I.B., Kholodnyy S.D. *Osnovy kabelnoy tehniki* [Basics of cable technology]. Moscow, Akademiya Publ., 2006. 432 p. (Rus).
2. Kim V.S. *Teoriya i praktika ekstruzii polimerov* [Theory and practice of polymer extrusion]. Moscow, Khimiya, KolosS Publ., 2005. 568 p. (Rus).

3. Rauvendaal K. *Ekstruziya polimerov* [Polymer extrusion]. Saint Petersburg, Professiya Publ., 2006. 768 p. (Rus).
4. Rao Natti S., Shott Nik R. *Tekhnologicheskie raschety v pererabotke plastmass* [Technological calculations in plastics processing]. Saint Petersburg, Professiya Publ., 2013. 200 p. (Rus).
5. Khrenkov N.N. Calculation of the cooling modes of a moving cable. *Cables and wires*, 2018, no.1, pp. 20-25. (Rus).
6. Voznyuk V.T., Kravchenko Yu.O., Mikulyonok I.O. Increase cooling corrugated polymer pipes. *Eastern-European Journal of Enterprise Technologies*, 2011, vol.5, no.8(53). –pp. 46-50. (Rus).
7. Kazakov A.V., Petrenko A.A. Mathematical modeling of the polymer melt. *Fundamental research*, 2015, no.10(part 2), pp. 264-267. (Rus).
8. Carslaw H.S., Jaeger J.C. *Conduction of heat solids. Second Ed.* Clarendon Press, London, 2003. 510 p.
9. Bezprozvannykh G.V., Naboka B.G. *Matematicheskie modeli i metody rascheta elektroizolatsionnykh konstruksii* [Mathematical models and methods of calculation of electrical designs]. Kharkiv, NTU «KhPI» Publ., 2012. 108 p. (Rus).
10. Demirchian K.S., Neiman L.R., Korovkin N.V., Chechurin V.L. *Teoreticheskie osnovy elektrotehniki: V 3-kh t. Uchebnik dlia vuzov* [Theoretical bases of electrical engineering. In 3 vols.]. St. Petersburg, Piter Publ., 2003. 463 p. (Rus).
11. Kozdoba L.A. *Elektricheskoe modelirovanie iavlenii teplo- i massoperenosa* [Electrical modeling of heat and mass transfer phenomena]. Moscow, Energiya Publ., 1972. 296 p. (Rus).
12. Ametistov E.V. *Teplo- i massoobmen. Teplotekhnicheskiiy eksperiment* [Heat and mass transfer. Thermal engineering experiment]. Energoatomizdat Publ., 1982. 512 p. (Rus).

Received 11.03.2019

*G.V. Bezprozvannykh¹, Doctor of Technical Science, Professor,
I.A. Mirchuk², Postgraduate Student,
A.G. Kyessayev¹, Candidate of Technical Science,
¹National Technical University «Kharkiv Polytechnic Institute»,
2, Kyrpychova Str., Kharkiv, 61002, Ukraine,
tel/phone +38 057 7076010,
e-mail: bezprozvannykh@kpi.kharkov.ua
²Private Joint Stock Company «Ukraine Scientific-Research
Institute of Cable Industry»,
2-P, Promychnennaya Str., Berdyansk, Zaporozhye Region,
71101, Ukraine,
tel/phone +38 066 8288554,
e-mail: garik710@ukr.net*

How to cite this article:

Bezprozvannykh G.V., Mirchuk I.A., Kyessayev A.G. Technological parameters of the cooling mode of polymer insulation of power cables. *Electrical engineering & electromechanics*, 2019, no.3, pp. 44-49. doi: 10.20998/2074-272X.2019.3.07.

M.I. Boyko, A.V. Makogon

THE MICRO- AND NANOSECOND DISCHARGES IN GAS BUBBLES FOR WATER DISINFECTION AND PURIFICATION

Purpose. Comparison of electrical circuits of experimental plants for obtaining micro- and nanosecond discharges in gas bubbles in water and comparing the experimental results obtained for disinfecting water using such discharges. *Methodology.* To obtain high-voltage pulses on the load in the form of a gas bubbles and a layer of water with a frequency of more than 2000 pulses per second, a method of generating micro- and nanosecond pulses using high-voltage pulse generators based on a pulse transformer (PT) according to Tesla, with a transistor opening switch IGBT in the low-voltage part of the circuit. A current-limiting resistor with a resistance $R_{cl} = 24 \text{ k}\Omega$ is used to protect the transistor switch at microsecond discharges. At nanosecond discharges, a multi-gap spark gap is used to sharpen the front of high-voltage pulses. We used a capacitive voltage divider with a division factor of $K_d = 7653$ to measure voltage pulses, a shunt with a resistance of $R_s = 2.5 \text{ }\Omega$ for measuring current pulses. RIGOL DS1102E digital oscilloscope with a 100 MHz bandwidth was used as a recording device. *Results.* The effect of micro- and nanosecond discharges in gas bubbles on microorganisms was experimentally investigated. It was possible to reduce the biochemical oxygen consumption of water during microsecond discharges, reduce the turbidity of water, and improve its organoleptic qualities. The energy released in a single pulse with microsecond discharges $W_u \approx 17 \text{ mJ}$, with nanosecond discharges $W_n \approx 7.95 \text{ mJ}$. At nanosecond discharges, complete inactivation of *E.coli* bacteria was achieved. The disinfecting and purifying action of nanosecond pulses is better compared to microsecond pulses due to an increase in the amplitude of the pulsed voltage up to 30 kV, and a pulsed current of up to 35 A. *Originality.* The possibility of effective microbiological disinfection of water using nanosecond discharges in gas bubbles at low specific energy consumption has been experimentally shown. *Practical value.* The obtained experimental results on water disinfection using micro- and nanosecond discharges offer the prospect of industrial application of installations using such discharges for disinfecting and purification wastewater, swimming pools, and post-treatment of tap water. References 9, figures 3.

Key words: high-voltage generator, micro- and nanosecond pulses, discharge in gas bubbles in water, disinfection and water purification by discharges, inactivation of microorganisms.

Мета. Порівняння електричних кіл експериментальних установок для одержання мікро- та наносекундних розрядів в газових бульбках у воді і порівняння одержаних експериментальних результатів знезараження води за допомогою таких розрядів. *Методика.* Для отримання високовольтих імпульсів на навантаженні у вигляді бульбк газу і шару води з частотою більше 2000 імпульсів за секунду запропоновано спосіб генерації мікро- та наносекундних імпульсів з використанням генераторів імпульсів високої напруги на основі імпульсного трансформатора за схемою Тесла з транзисторним розмикаючим перемикачем IGBT в низьковольтній частині кола. Резистор, що обмежує струм, з опором $R_{cl} = 24 \text{ кОм}$ використовується для захисту транзисторного перемикача при мікророзрядних розрядах. При наносекундних розрядах багатозазорний іскровий розрядник використовується для загострення фронту імпульсів високої напруги. Ми використовували ємнісний ділник напруги з коефіцієнтом ділення $K_d = 7653$ для вимірювання імпульсів напруги, шунт з опором $R_s = 2,5 \text{ Ом}$ – для вимірювання імпульсів струму. В якості записуючого пристрою використовувався цифровий осцилограф RIGOL DS1102E зі смугою пропускання 100 МГц. *Результати.* Експериментально досліджено вплив мікро- і наносекундних розрядів в газових бульбках на мікроорганізми. Вдалося зменшити біохімічне споживання кисню водою при мікророзрядних розрядах, знизити мутність води, покращити органолептичні показники. Енергія, що виділяється в одному імпульсі при мікророзрядних розрядах, складає $W_u \approx 17 \text{ мДж}$, а при наносекундних розрядах – $W_n \approx 7,95 \text{ мДж}$. При наносекундних розрядах досягнуто повної інактивації бактерій *E.coli*. Знезаражуюча і очищуюча дія наносекундних імпульсів краща порівняно з мікророзрядними імпульсами із-за збільшення амплітуди імпульсної напруги до 30 кВ, а імпульсного струму до 35 А. *Наукова новизна.* Експериментально показана можливість ефективного мікробіологічного знезараження води за допомогою наносекундних розрядів в газових бульбках при малих питомих витратах енергії. *Практична значущість.* Одержані експериментальні результати щодо знезараження води за допомогою мікро- і наносекундних розрядів відкривають перспективу промислового застосування установок з використанням таких розрядів для знезараження і очистки стічних вод, басейнів та доочистки водопровідної води. Бібл. 9, рис. 3.

Ключові слова: високовольтний генератор, мікро- і наносекундні імпульси, розряд в газових бульбках у воді, знезараження та очистка води розрядами, інактивація мікроорганізмів.

Цель. Сравнение электрических схем экспериментальных установок для получения микро- и наносекундных разрядов в газовых пузырях в воде и сравнение полученных экспериментальных результатов обеззараживания воды при помощи таких разрядов. *Методика.* Для получения высоковольтных импульсов на нагрузке в виде пузырьков газа и слоя воды с частотой более 2000 импульсов в секунду предложен способ генерации микро- и наносекундных импульсов с использованием генераторов импульсов высокого напряжения на основе импульсного трансформатора по схеме Тесла с транзисторным размыкающим переключателем IGBT в низковольтной части цепи. Токоограничивающий резистор с сопротивлением $R_{cl} = 24 \text{ кОм}$ используется для защиты транзисторного переключателя при микросекундных разрядах. При наносекундных разрядах многозазорный искровой разрядник используется для обострения фронта импульсов высокого напряжения. Мы использовали емкостный делитель напряжения с коэффициентом деления $K_d = 7653$ для измерения импульсов напряжения, шунт с сопротивлением $R_s = 2,5 \text{ Ом}$ – для измерения импульсов тока. В качестве записывающего устройства использовался цифровой осциллограф RIGOL DS1102E с полосой пропускания 100 МГц. *Результаты.* Экспериментально исследовано влияние микро- и наносекундных разрядов в газовых пузырях на

© M.I. Boyko, A.V. Makogon

микроорганизмы. Удалось уменьшить биохимическое потребление кислорода воды при микросекундных разрядах, снизить мутность воды, улучшить органолептические показатели. Энергия, выделяемая в одном импульсе при микросекундных разрядах, составляет $W_{\mu} \approx 17$ мДж, а при наносекундных разрядах – $W_n \approx 7,95$ мДж. При наносекундных разрядах достигнута полная инактивация бактерий *E.coli*. Обеззараживающее и очищающее действие наносекундных импульсов лучше по сравнению с микросекундными импульсами из-за увеличения амплитуды импульсного напряжения до 30 кВ, а импульсного тока до 35 А. Научная новизна. Экспериментально показана возможность эффективного микробиологического обеззараживания воды при помощи наносекундных разрядов в газовых пузырях при малых удельных затратах энергии. Практическая значимость. Полученные экспериментальные результаты по обеззараживанию воды при помощи микро- и наносекундных разрядов открывают перспективу промышленного применения установок с использованием таких разрядов для обеззараживания и очистки сточных вод, бассейнов и доочистки водопроводной воды. Библи. 9, рис. 3.

Ключевые слова: высоковольтный генератор, микро- и наносекундные импульсы, разряд в газовых пузырях в воде, обеззараживание и очистка воды разрядами, инактивация микроорганизмов.

Introduction. In the modern world, researchers are constantly searching for new energy-saving technologies for disinfection and water treatment. One of the most promising and relevant technologies in this direction is the technology of water treatment using micro- and nanosecond discharges in gas bubbles [1-3].

The use of short electric pulses of voltage (current) for water treatment allows to avoid large ohmic losses due to its heating, to increase the electrical strength of the discharge gap, thereby obtaining high electric fields with intensity of $E \geq 30$ kV/cm in a load in the form of a gas bubble water layer. High electric fields inactivate microorganisms in water, causing irreversible pore formation in the cell membranes of microorganisms, as well as affecting the intracellular contents, including the impact on their RNA and DNA [4].

Pulsed electrical discharge is also a source of broadband radiation. It follows from [5, 6] that such radiation has damaging effects on bacteria, leading to their degradation and destruction, and, thereby, increasing the efficiency of microbiological disinfection of water.

Micro- and nanosecond discharges in gas bubbles inside the treated volume of water cause the formation of active microparticles with a high value of oxidative potential, measured in volts. The highest value of the oxidation potential for ozone (O_3) is 2.07 V, for atomic

oxygen (O) is 2.42 V, for hydroxyl (OH) is 2.85 V, and for hydrogen peroxide (H_2O_2) is 1.77 V [7].

Ozonation is widely used for disinfection of drinking water, as well as water in swimming pools. However, OH hydroxyls, which are formed in discharges in the presence of water, have a higher oxidative potential and are able to destroy persistent chemical compounds, unlike ozone [8]. The use of OH can improve the efficiency of disinfection and chemical treatment of water. The lifetime of OH particles in the air is hundreds of microseconds. Therefore, radicals should be created in the immediate vicinity of the surface of the separation of water and gas bubbles in it [1, 9].

Installations using this type of discharge can be widely used for the treatment of wastewater, waters of swimming pools and the purification of tap water.

The goal of the work is a comparison of the electrical circuits of experimental installations for obtaining micro- and nanosecond discharges in gas bubbles in water, as well as a comparison of the experimental results obtained for disinfecting water using such discharges.

Electric circuits of experimental installations.

Figures 1,a,b show the electric circuits of experimental installations for water treatment using micro- and nanosecond discharges in gas bubbles [2, 3].

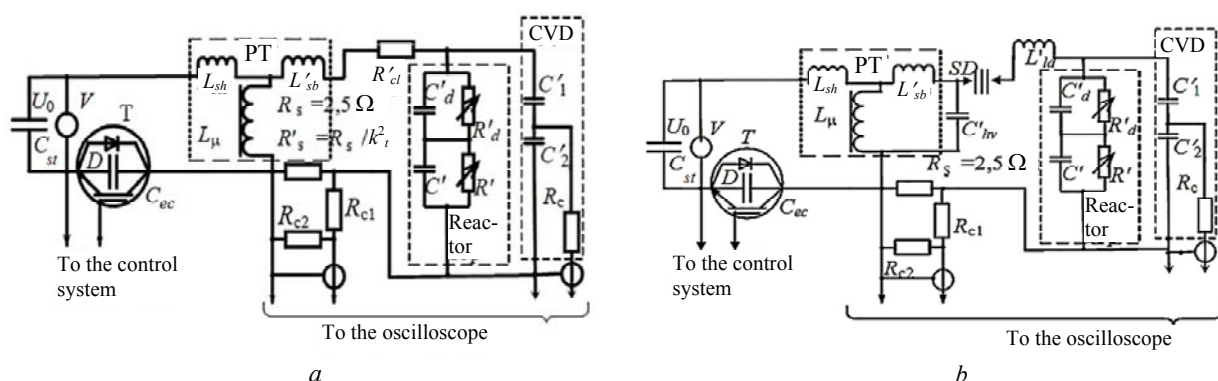


Fig. 1. Electric circuits of experimental water treatment plants using discharges in gas bubbles: a – microsecond; b – nanosecond

In Fig. 1,a,b, the capacitance C_{st} is charged from the mains (220 V, 50 Hz) to the voltage U_0 . T is the transistor switch of IGBT-transistors of type IRG4PH50UD, operating as a breaker. Pulse transformer (PT) according to the Tesla scheme is presented in the form of an equivalent circuit, where L_{μ} is the magnetization inductance; L_{sh} , L'_{sb} are the primary leakage inductance

and reduced secondary leakage inductance; D are the reverse diodes of the IGBT-key built into the transistors; $C_{ec} \geq 1$ nF is the «emitter collector» capacitance of the IGBT-key; $C'_d < C_{ec} \ll C_{st}$; R'_s is the reduced resistance of the measuring shunt in the high-voltage circuit of the generator; $R_{c1} = 300 \Omega$, $R_c = 60 \Omega$ are the matching resistances of the shunt $R_s = 2.5 \Omega$; C'_1 , C'_2 are the reduced

capacitances of high-voltage and low-voltage arms of capacitive voltage divider (CVD) with matching resistance R_c . Here, the unreduced (i.e. real) values of the capacitances were $C_1 \approx 2.7 \cdot 10^{-12}$ F, $C_2 = 20.4 \cdot 10^{-9}$ F, and the division ratio of CVD is $K_d \approx 7650$. In the electric circuit of the reactor, C_d , R_d are the capacitance and nonlinear active resistance of the discharge gap (DG), and C , R are the capacitance and nonlinear resistance of the water layer between the DG and a low-voltage (grounded) electrode (C'_d , R'_d , C' , R'' are the reduced to the primary winding of PT values of these quantities), respectively.

Principal differences between the electric circuits of experimental installations. In the diagram in Fig. 1, *a* a current-limiting resistor with resistance $R'_{cl} = 24$ k Ω is used to protect the transistor switch by current. The dissipation of active power on the resistor leads to additional ohmic losses. $C_{st} = 940$ μ F (2 capacitors TAMICON 470 μ F in parallel), T is the transistor switch consisting of 2 transistors connected in parallel. In the diagram in Fig. 1, *b* $C_{st} = 4230$ μ F (9 capacitors TAMICON 470 μ F in parallel), the transistor switch T

consists of four parallel-connected transistors. The pulse duration, the front and the shape are determined by the discharge circuit $C_{hv} - SD - L_{ld} - (R_d$ in parallel with $C_d) - (R$ in parallel with $C) - R_{sh} - C_{hv}$. The sharpening of the pulse front occurs when a multichannel multigap spark discharger SD operates. The distance between the gaps is 1 mm, it is possible to adjust, the number n of gaps is $1 \leq n \leq 5$. The pulse duration is determined by the presence in the discharge circuit of a low-inductance capacitive energy storage device $C_{hv} = 150$ pF assembled from six KВИ-2 capacitors with capacitance of 100 pF each, calculated for voltage 20 kV (two consecutive chains of three capacitors in parallel). All voltage from C_{hv} is applied to series-connected discharger SD and discharge gap DG in the reactor – a gas bubble in water. The inductance L_{ld} of the load discharge circuit is $L_{ld} \approx 0.5$ μ H.

Experimental results. Figures 2, *a, b* show oscillograms of voltage (current) pulses obtained at disinfecting water treatment using micro- and nanosecond discharges.

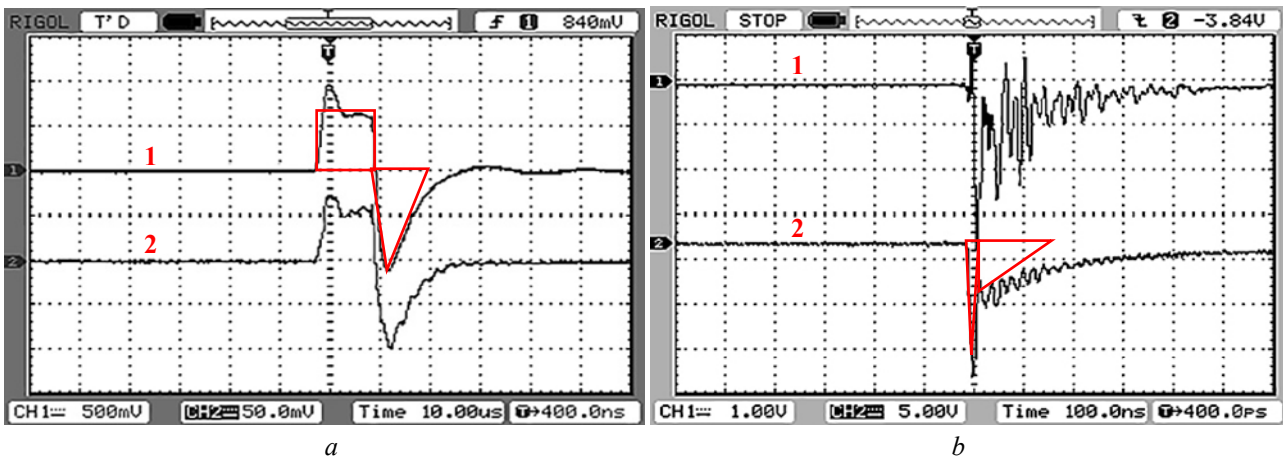


Fig. 2. Oscillograms of voltage (curves 1) and current (curves 2) pulses:
a – at microsecond discharges; *b* – at nanosecond discharges

At microsecond discharges (see Fig. 2, *a*), the voltage amplitude reaches 8 kV, and the current amplitude is 0.2 A at a pulse repetition rate of $f \approx 2200$ Hz. The division along the process axis is 4 kV/div for voltage oscillograms, and 0.1 A/div for current oscillograms. Oscillograms of voltage and current in the load (in the form of a working chamber with water processed by microsecond discharges) have the shape of bipolar pulses.

At nanosecond discharges, the amplitude (see Fig. 2, *b*) of the voltage across the load reaches 30 kV, and the amplitude of the current is 35 A at a pulse repetition rate of $f \approx 2200$ Hz. The division along the process axis for voltage oscillograms is 7.9 kV/div, and for current oscillograms it is 11.7 A/div. At nanosecond discharges, the shape of the voltage and current pulses in the load is close to the decaying exponent with a steep front and superimposed oscillations. A capacitive voltage divider with division factor $K_d = 7653$ was used to register voltage pulses, and a shunt with resistance $R_s = 2.5$ Ω ($R_{c1} = 300$ Ω , $R_{c2} = 60$ Ω – matching shunt resistances) was used to register current pulses. A RIGOL DS1102E digital

oscilloscope with a bandwidth of 100 MHz was used as a recording device.

Current and voltage on the oscillograms of Fig. 2, *a, b* are close in shape and practically not shifted relative to each other in time. In the first approximation, we can assume that the load is active and all the energy W is released in the working chamber. Calculate the energy W , based on the relation of the form

$$W = \int_0^t U(t) \cdot i(t) dt.$$

For the estimated calculation of energy, we represent the positive part of the pulses in Fig. 2, *a* in the form of two rectangular regions with sides along the time axis $t_1 \approx 10$ μ s, and negative one in the form of two triangular regions with the same base size along the time axis $t_2 \approx 10$ μ s. Then the pulse energy W_μ is defined as the sum of the areas of the selected areas $W_\mu \approx U \cdot I \cdot t_1 + 0.5 \cdot U \cdot I \cdot t_2 \approx 6000$ V \cdot 0.15 A \cdot $10 \cdot 10^{-6}$ s + $0.5 \cdot 8000$ V \cdot 0.2 A \cdot $10 \cdot 10^{-6}$ s $\approx (0.009 + 0.008)$ J ≈ 17 mJ.

Oscillograms of Fig. 2, *b* with nanosecond pulses for the estimated calculation of the pulse energy are divided

into triangular areas. The first two triangular regions are selected at the front when the current and voltage on the load reach maximum values during $t_1 \approx 10$ ns. To take into account the pulse energy released in the load on the flat part of the pulse decay, we choose the second two triangular regions with duration along the time axis $t_2 \approx 150$ ns, where the amplitudes of voltage and current reach values $U_2 \approx 6$ kV, $I_2 \approx 6$ A, respectively. The energy W_n released in each nanosecond pulse, we define as the sum of the areas of selected areas $W_n \approx 0.5 \cdot U_1 \cdot I_1 \cdot t_1 + 0.5 \cdot U_2 \cdot I_2 \cdot t_2 \approx (0.5 \cdot 30000 \cdot 35 \cdot 10 \cdot 10^{-9} + 0.5 \cdot 6000 \cdot 6 \cdot 150 \cdot 10^{-9}) \approx (0.00525 + 0.0027) \text{ J} \approx 7.95 \text{ mJ}$.

The ratio of the energy W_μ released in the load at each microsecond pulse to the energy W_n released in the load at each nanosecond pulse in this work is equal to $W_\mu/W_n \approx 17/7.95 \approx 2.1$.

By increasing the electric strength of the discharge gap in gas bubbles at nanosecond pulses, it was possible to obtain pulsed voltages with amplitude of 30 kV on the

load. The operation of the circuit without protective resistance, an increase in the electrical strength of the gap and a decrease in the capacitance resistance of water at nanosecond pulses allowed, compared to microsecond pulses, to increase the current amplitude 175 times and to reach its value of 35 A. Therefore, the disinfecting and cleaning action of nanosecond pulses is better than with microsecond pulses. And this is achieved at a significantly lower energy in the nanosecond pulse. In microsecond pulses, most of the energy is consumed less efficiently: the degree of water disinfection is less, and unwanted heating of water is more.

Figures 3, *a, b* show the luminescence at nanosecond and microsecond discharges in gas bubbles in water. It has been established that the intensity of luminescence at nanosecond discharges is greater (see Fig. 3, *a*) due to the increase in their amplitudes of the pulsed voltage and current in gas bubbles.



a



b

Fig. 3. Discharges in a gas bubble: *a* – nanosecond pulses; *b* – microsecond pulses

A series of experiments on microbiological disinfection and purification of water using micro- and nanosecond discharges in gas bubbles was carried out. During water purification (the sample was taken from the Kharkiv river in a volume of 3 liters) using microsecond discharges in gas bubbles (see Fig. 2, *a*), the processing time was 10 minutes, the volume of processing was 1.5 liters (three portions of 0.5 l each). The treated water was filtered with a paper filter before being sent to the laboratory (Communal Enterprise «Sanepidservice», Kharkiv). Biochemical oxygen consumption decreased from 3.84 mgO₂/dm³ (in the control sample) to 3.67 mgO₂/dm³ (in the treated samples), at a rate of ≤6 mgO₂/dm³, i.e. it was possible to additionally clean the fairly clean source water. The turbidity of water has decreased, the organoleptic properties of water have improved. When processing the water temperature increased by 17-20 °C.

When treating tap water contaminated with *E.coli* bacteria with a dilution of 10⁸ in 3 liters of water (at the Communal Enterprise «Sanepidservice», Kharkiv), using nanosecond discharges (see Fig. 2, *b*) in gas bubbles, the processing time was 7 minutes, the volume of the processed material 1.5 l (three portions of 0.5 l), complete (100 %) inactivation of bacteria has been achieved. The temperature of the treated water increased by 7-8 °C.

The estimated energy released in the load when treating water using discharges in gas bubbles in the case of using nanosecond discharges was about 2.1 times less than when using microsecond discharges. Therefore, the heating of water at nanosecond discharges is also less. The pulse repetition rate was the same for both processing modes, including nano- and microsecond discharges, respectively.

Conclusions. The results of the experiments on the disinfection and purification of water using micro- and nanosecond discharges in gas bubbles showed the promise of further study and practical application of these types of discharges. Nanosecond discharges seem to be more promising for industrial applications. When using nanosecond discharges, complete inactivation of *E.coli* bacteria is achieved, water heating is insignificant, and the intensity of broadband radiation at such discharges, compared with microsecond discharges, is higher due to large amplitudes of pulsed currents and amplitudes of pulsed electric field strengths. The energy in the pulse with nanosecond discharges is 2.1 times less than with microsecond discharges.

REFERENCES

1. Gershman S., Mozgina O., Belkind A., Becker K., Kunhardt E. Pulsed Electrical Discharge in Bubbled Water. *Contributions*

- to *Plasma Physics*, 2007, vol.47, no. 1-2, pp. 19-25. doi: **10.1002/ctpp.200710004**.
2. Boyko N.I., Makogon A.V. Experimental plant for water purification with the help of discharges in gas bubbles. *Technical Electrodynamics*, 2017, no.5, pp. 89-95. doi: **10.15407/techned2017.05.089**.
3. Boyko N.I., Makogon A.V. Generator of high-voltage nanosecond pulses with repetition rate more than 2000 pulses per second for water purification by the discharges in gas bubbles. *Technical Electrodynamics*, 2018, no.4, pp. 37-40. doi: **10.15407/techned2018.04.037**.
4. Boyko M.I., Makogon A.V., Marynin A.I. Energy efficiency of the disinfection treatment of liquid foodstuffs by high-voltage pulse effects. *Electrical engineering & electromechanics*, 2018, no.3, pp. 53-60. doi: **10.20998/2074-272X.2018.3.07**.
5. Trofimova S.V., Ivanova I.P., Bugrova M.L. The analysis of structural changes of prokaryotic and eukaryotic cell under the influence of plasma spark radiation. *Fundamental research*, 2013, no.4(part 1), pp. 130-133. (Rus).
6. Ivanova I.P., Trofimova S.V., Piskaryov I.M., Burkhina O.E., Sysoeva V.A., Karpel Vel Leitner N. The Study of Biocidal Mechanisms of Spark Discharge Plasma Radiation. *Modern Technologies in Medicine*, 2012, no.3, pp. 12-18. (Rus).

7. Available at: http://www.chem.msu.su/rus/handbook/redox/elem_dat/o.html (accessed 13 June 2018). (Rus).
8. Nazarenko O.B., Shubin E.G. Investigation of Electric Discharge Treatment of Water for Ammonium Nitrogen Removal. *Proceedings of the 2nd Environmental Physics Conference*, 18-22 Feb. 2006, Alexandria, Egypt, pp. 85-90.
9. Iavorovskii N.A., Kornev Ya.I., Preis S.V., Pel'tsman S.S., Khaskel'berg M.B., Chen B.N. Pulsed barrier discharge as a method of water treatment: active particles-oxidizing agents in the water-air flow. *Bulletin of the Tomsk Polytechnic University*, 2006, vol.309, no.2, pp. 108-113. (Rus).

Received 27.02.2019

M.I. Boyko¹, Doctor of Technical Science, Professor,
A.V. Makogon¹, Postgraduate Student,
¹National Technical University «Kharkiv Polytechnic Institute»,
2, Kyrpychova Str., Kharkiv, 61002, Ukraine,
phone +380 57 7076245,
e-mail: qnaboyg@gmail.com

How to cite this article:

Boyko M.I., Makogon A.V. The micro- and nanosecond discharges in gas bubbles for water disinfection and purification. *Electrical engineering & electromechanics*, 2019, no.3, pp. 50-54. doi: **10.20998/2074-272X.2019.3.08**.

D.G. Koliushko, S.S. Rudenko, A.V. Plichko, V.I. Shcherbinin

MODERNIZATION OF THE COMPLEX TYPE IK-1U FOR MEASURING THE IMPEDANCE OF THE GROUNDING DEVICE OF A LIGHTNING ARRESTER AND SUPPORTS OF TRANSMISSION LINES

Purpose. The creation of a measuring device for determining the impedance of the grounding of lightning arresters and supports of overhead lines under the influence of aperiodic pulses with the parameters 1.2/50 μ s, 8/20 μ s and 10/350 μ s. Methodology. For this purpose, electrical engineering theory, transient modeling software and natural modeling methods are used. Results. The parameters of the electrical circuits of the additional forming unit were determined to create lightning current pulses with parameters of 10/350 μ s using the IK-1U measuring complex. According to the simulation results, a layout of the forming unit in the form of an attachment and the IK-1U complex with the upgraded power supply system were created. Oscillograms of the front and pulse duration are obtained. The specified model was tested when performing electromagnetic diagnostics of the state of the RFP for more than 100 operating electrical substations. Originality. The measuring complex IK-1U was improved, which made it possible to determine the impulse impedance of the grounding device of lightning arresters when exposed to a current of 10/350 μ s, 8/20 μ s and of voltages 1.2/50 μ s. Practical value. Upgraded device allows measurements in accordance with modern international requirements. References 9, tables 1, figures 3.

Key words: impedance, grounding device, lightning current (voltage) pulse, measuring complex.

Метою роботи є створення вимірювального приладу для визначення опору заземлювальних пристроїв (ЗП) блискавоквідводів та опор повітряних ліній електропередачі (ЛЕП) при дії аперіодичних імпульсів напруги з параметрами 1,2/50 мкс та струму з параметрами 8/20 мкс і 10/350 мкс. Для цього використано теорію електротехніки, програмні засоби моделювання перехідних процесів та методи натурного моделювання. Було визначено параметри елементів електричного кола додаткового формуючого блоку для створення грозових імпульсів струму з параметрами 10/350 мкс за допомогою вимірювального комплексу типу ІК-1У. Вдосконалено комплекс типу ІК-1У, що дозволило визначити імпульсний опір ЗП блискавоквідводів та опор ЛЕП при дії імпульсів струму 10/350 мкс, 8/20 мкс та напруги 1,2/50 мкс. Модернізований прилад дозволяє проводити вимірювання відповідно з сучасними міжнародними вимогами. Бібл. 9, табл. 1, рис. 3.

Ключові слова: опір, заземлювальний пристрій, грозовий імпульс струму (напруги), вимірювальний комплекс.

Целью работы является создание измерительного прибора для определения сопротивления заземляющих устройств (ЗУ) молниеотводов и опор воздушных линий электропередачи (ЛЭП) при воздействии аперiodических импульсов напряжения с параметрами 1,2/50 мкс и тока с параметрами 8/20 мкс и 10/350 мкс. Для этого использовано теорию электротехники, программные средства моделирования переходных процессов и методы натурного моделирования. Были определены параметры элементов электрической цепи дополнительного формирующего блока для создания грозовых импульсов тока с параметрами 10/350 мкс с помощью измерительного комплекса типа ИК-1У. Усовершенствован комплекс типа ИК-1У, что позволило определять импульсное сопротивление ЗУ молниеотводов и опор ЛЭП при воздействии импульсов тока 10/350 мкс, 8/20 мкс и напряжения 1,2/50 мкс. Модернизированный прибор позволяет проводить измерения в соответствии с современными международными требованиями. Библ. 9, табл. 1, рис. 3.

Ключевые слова: сопротивление, заземляющее устройство, грозовой импульс тока (напряжения), измерительный комплекс.

Problem definition. Provision of permissible values of the parameters of grounding devices (GDs) of electric power stations and substations, separately installed lightning arresters and overhead line's supports within the limits defined by regulatory documents, is a prerequisite for the reliability of the operation of expensive equipment and electrical safety of personnel. In order to control the state of the GDs of electric power stations and substations in Ukraine, the method of electromagnetic diagnostics is the most widespread [1, 2]. One of the procedures of its experimental stage is to determine the impedance of lightning arresters, installed separately, and the supports of overhead lines with lightning protection cables. In the domestic normative document [3] there is no concept of «impulse impedance of the GD», but in international requirements, in particular in [4-6], the impedance of the lightning arresters and overhead lines' supports is defined as «the ratio of the peak value of the voltage to the GD to the peak value of the current, which flows in the GD, under the action of the current pulse with the given time parameters».

In the world, there are a number of devices that allow to determine the impulse impedance of the GD. The paper [7] describes a powerful stationary generator that generates pulses of artificial lightning current with amplitude $\pm(100-200)$ kA for fundamental and applied research. The papers [8, 9] provide a detailed analysis of the most commonly used portable devices, including: Polish WG-407, WG-507 and MRU-200, Japanese PET-7, ZED-meter of the US, Ukrainian IK-1U and Russian impedance meter [8]. At the same time, it should be noted that among the listed devices, only three allow measurements when simulating a thunderstorm pulse, namely: WG-507 with pulse 4/10 μ s, MRU-200 – 4/10 μ s and 10/350 μ s, and IK-1U with pulses of 1.2/50 μ s and 8/20 μ s. Other devices allow measurements to be made under the influence of pulses of current or voltage with non-normalized parameters with pulse duration of several to hundreds of microseconds and a front from tens of nanoseconds to 1 microsecond. For example, PET-7 generates a pulse with a gain of 1 μ s and a duration of 256 μ s

© D.G. Koliushko, S.S. Rudenko, A.V. Plichko, V.I. Shcherbinin

or ZED-meter – a rectangular pulse duration $1.4 \mu\text{s}$. Among the above-mentioned, the complex IK-1U has the largest measuring current, the value of which in the short-circuit mode is 25 A while for other ones measuring current is in the range from 0.5 A to 5 A. The maximum energy of the measuring pulse of the IK-1U device, which is 0.3 J, lies in the middle of the range compared with other instruments for which it varies from 0.017 J to 1 J [8].

The complex IK-1U developed by the specialists of the Scientific-&Research Planning-&-Design Institute «Molnlya» of the NTU «KhPI» is designed to measure the impulse impedance of lightning arresters, standing separately, and the impedance of the transmission lines without disconnecting the lightning protection cable. The IK-1U device is entered in the state register and consists

of a generator of aperiodic pulses ГАИ-3 (see item 1 in Fig. 1) and a pulse voltmeter ВИ-6М (see item 2 in Fig. 1). In accordance with the current international requirements [4-6], for simulating the direct lightning strike, it is necessary to check the reaction of the GD to the pulse voltage of $1.2/50 \mu\text{s}$ and the current pulse $10/350 \mu\text{s}$, and to simulate the pulsed currents induced in the metal structures and communications of the object with distant lightning strikes – $8/20 \mu\text{s}$. The carried out analysis shows that there are no devices in the world that can carry out universal measurements in all three of the above modes.

The goal of the work is the creation of a measuring device for determining the impedance of GDs of lightning arresters and overhead lines' supports during the action of the aperiodic pulses of $8/20 \mu\text{s}$, $10/350 \mu\text{s}$ and $1.2/50 \mu\text{s}$.

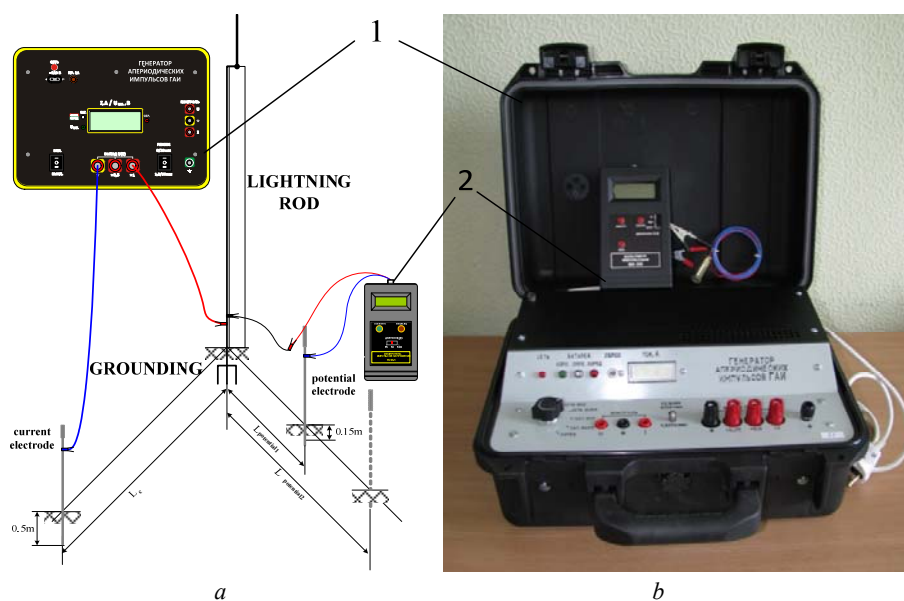


Fig. 1. Scheme of measurements (a) and external view (b) of the complex type IK-1U

Research materials. There are two ways to achieve this goal:

- development of a new device, which can operate in three modes of formation of the specified pulses;
- improvement of the existing instrument.

The first way involves the need to develop a new circuit design solution. Here, in the case of generating a current pulse with amplitude of 25 A at $10/350 \mu\text{s}$ temporal parameters, as in the device IK-1U for a mode of $8/20 \mu\text{s}$, the capacity of the capacitors of the device should increase from $2.35 \mu\text{F}$ to $7500 \mu\text{F}$ while maintaining the operating voltage of 1 kV with a corresponding change in the forming elements. That is, the new device will have such mass-sized dimensions, which will be either stationary, or mounted on the automotive base. This will greatly complicate its use in field conditions as part of the implementation of electromagnetic diagnostics of the GDs.

The second way is to improve the existing complex of type IK-1U due to «stretching» the duration of the current pulse in the mode of $8/20 \mu\text{s}$ at reducing its amplitude. This can be achieved by developing a special forming unit and expanding the pulse voltmeter measurement range. In addition, this will minimize costs

by maintaining the main circuitry solutions of the generator.

The forming unit of the device is proposed to be executed in the form of a set of RLC-elements, which should be connected to the output of the generator of the complex IK-1U in the mode of $8/20 \mu\text{s}$, which will allow the use of already developed complexes without their further elaboration. The following assumptions were made to evaluate the parameters of the elements of the forming unit of the complex: due to the fact that the period of follow-up of the pulses of IK-1U significantly exceeds the required pulse duration of $350 \mu\text{s}$ (the frequency of follow-up of about 3 Hz), we can consider the generator IK-1U as a capacitive energy storage device C1 with a known discharge circuit (see Fig. 2,a). In the $8/20 \mu\text{s}$ mode, the capacity is $2.35 \mu\text{F}$, the initial voltage on the capacitor C1 is 1000 V, the inductance $L1 = 56 \mu\text{H}$, and the resistance of R1-R4 is 1 Ω , 7.5 Ω , 6 Ω and 9 Ω , respectively. Resistor R1 acts as a load. Determination of the parameters of elements of the forming block of the complex was performed on the basis of the calculation model in the demo version of the MicroCap software complex. To increase the duration of the current pulse to $350 \mu\text{s}$, a high inductive throttle L2 was used, to provide a

10 μ s front a forming capacitor C2 and a resistor R5 were introduced, and the resistor R6 smoothes the oscillation processes that arise in the discharge circuit.

Nominal values of L2, C2 and R6 elements were determined in the Transient Analysis mode, taking into account the existing nominals of real elements. The results of the simulation of the IK-1U complex with a forming block in the mode of 10/350 μ s (see Fig. 2,b,c) show compliance with the set conditions for temporal parameters, with the amplitude of current not to exceed 1.1 A, and the maximum voltage on the elements of the block will be: L2 and R6 – 600 V, C2 – no more than 10 V, and R5 – no more than 5 V. Obtained values were used when selecting existing elements. As C2, two consecutive connected polar capacitors with capacity of 47 μ F and operating voltage 25 V each, resistor R6 – 1.2 k Ω type MJIT-0,125, throttle of our own manufacturing (due to the absence of industrial ones with inductance of 18 mH) with resistance less than 0.5 Ω , operating voltage up to 500 V and current of 1.1 A.

As can be seen from the pulse simulation results, the pulse duration is 341 μ s at amplitude of 1.04 A, pulse front of about 12.8 μ s, which, with allowance of ± 20 % [5], practically meets the set requirements. Thus, with the help of simulation, the parameters of the elements of the forming block for the current pulse 10/350 μ s were determined using the standard generator of the measuring complex IK-1U. In addition, it is proposed to use modern power supply elements and capacitor types during manufacturing of new complexes on the basis of the IK-1U device and, respectively, to improve the charging unit and to add a voltage control module. This will reduce the number of large size capacitors from 21 to 4, extend the service life of the battery pack of the IK-1U, increase the ease of mounting and replacing the batteries. The proposed changes allow to significantly reduce the total weight of the complex (from 14 kg to 5.5 kg). In addition, the transition to a more modern elemental base allows to free space in the case and to mount a forming unit of 10/350 μ s into the existing complex IK-1U, as its integral module.

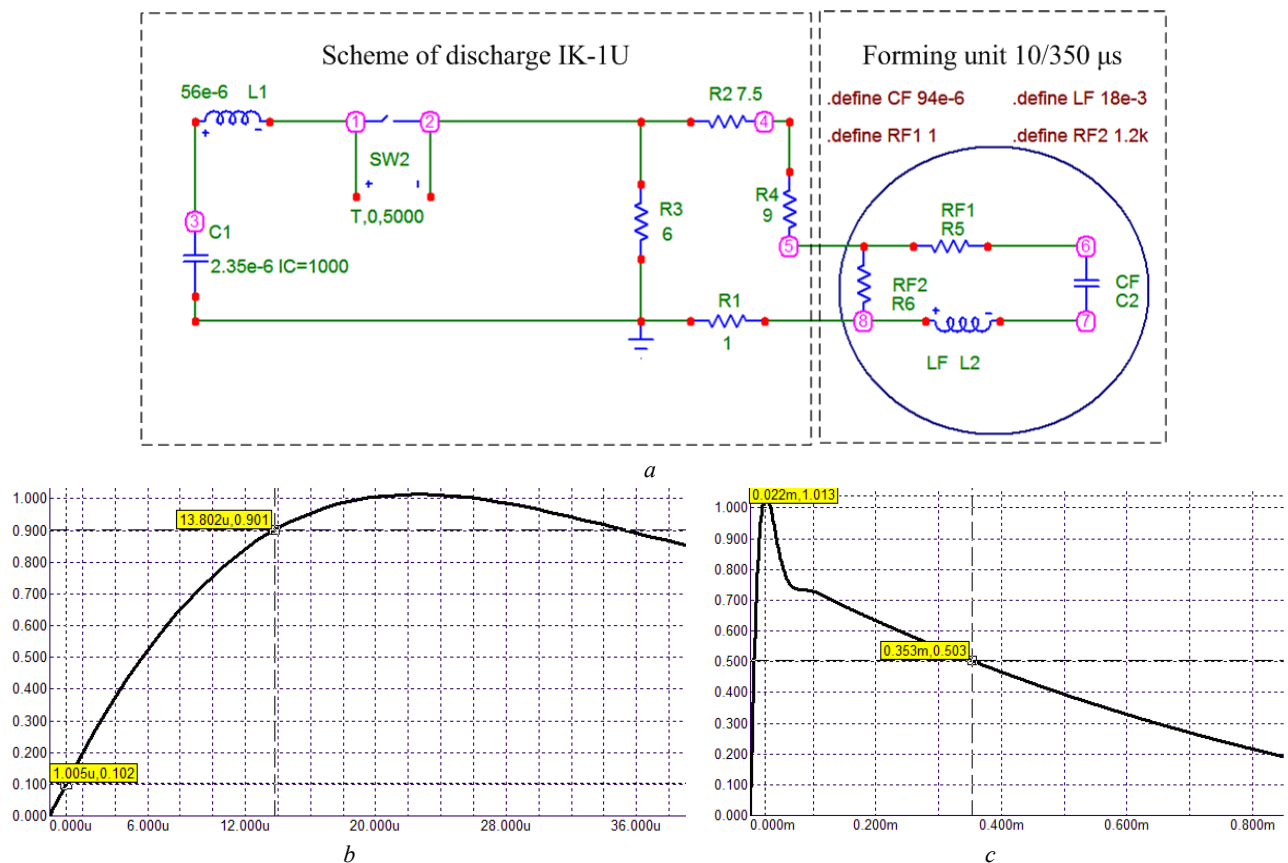


Fig. 2. Electrical circuit of the IK-1U class with the forming block (a) and the result of simulating the front of the pulse current (b) and its duration (c) in the software complex MicroCap

Table 1 shows the technical characteristics of the advanced complex IK-1U with the forming unit.

According to the simulation results, a layout of the forming unit in the form of an additional block and a complex of IK-1U with a modernized power supply system was created (see Fig. 3,a). Figures 3,b,c present the oscillograms of the front and the duration of the current pulse.

The indicated layout has been tested at performing electromagnetic diagnostics of the state of the GDs of

over 100 active electrical substations of Ukraine.

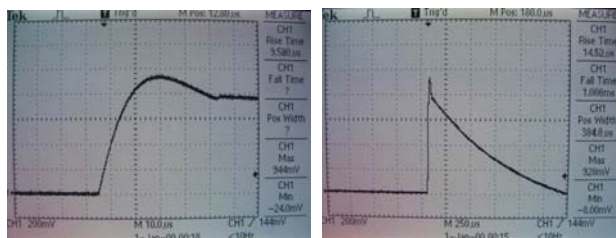
Thus, the use of the forming unit in the complex IK-1U allows to obtain a current pulse with the following temporal parameters: the duration of the front 10 \pm 2 μ s at the level of 0.1-0.9 from the amplitude and pulse duration 350 \pm 35 μ s at the level of 0.5 from the amplitude. Completion of the modernization of the complex type of IK-1U allowed to obtain the necessary result at a minimum cost with the possibility of using existing systems.

Table 1

Characteristics of the complex IK-1U	
Name of the parameter or characteristic	Value
Front of the pulse (at the levels 0.1-0.9 of the amplitude), μs	1.2 ± 0.1 ; 8 ± 0.8 ; 10 ± 2.0
Duration of the pulse (at the level 0.5 of the amplitude), μs	50 ± 5 ; 20 ± 4 ; 350 ± 35
Maximum amplitude of generated voltage pulses (in the mode of 10/350 μs), V	1000 (600)
Voltage pulses amplitude measurement range, V	0.5 – 200
Maximum amplitude of generated pulses (in the mode of 10/350 μs), A	25 ± 5 (1 ± 0.05)
Range of measurements of current pulse amplitude, A	0.1 – 25
Relative error of measurement of amplitude of pulses of current and voltage %, no more	10
Power supply	from the network; from the built-in battery



a



b

c

Fig. 3. External view of the forming unit in the form of an additional block with IK-1U (a) and the oscillograms of the current pulse front (b) and its duration (c)

Conclusions.

1. An analysis of the existing devices for measuring the impedance of the GDs is carried out and the need to create a device with test pulses of current of 8/20 μs , 10/350 μs and of voltage of 1.2/50 μs is shown.

2. The parameters of the elements of the forming block for the current pulse 10/350 μs are determined at utilization of an existing standard generator of the measuring complex of the type IK-1U.

How to cite this article:

Koliushko D.G., Rudenko S.S., Plichko A.V., Shcherbinin V.I. Modernization of the complex type IK-1U for measuring the impedance of the grounding device of a lightning arrester and supports of transmission lines. *Electrical engineering & electromechanics*, 2019, no.3, pp. 55-58. doi: 10.20998/2074-272X.2019.3.09.

3. The practical implementation of the forming block and the complex of type IK-1U with a modern element base is realized. The testing of their operation has been carried out on more than 100 active power facilities of Ukraine.

4. An autonomous power supply unit has been upgraded, which greatly reduced the mass and overall dimensions of the complex, as well as will allow the forming block to be mounted directly into the housing of the complex IK-1U.

REFERENCES

1. *Natsional'nyy standart Ukrainy. SOU 31.2-21677681-19:2009. Viprobuvannya ta kontrol' prystroyiv zazemlennya elektroustanovok. Tipova instruktsiya* [National Standard of Ukraine SOU 31.2-21677681-19:2009. Test and control devices, electrical grounding. Standard instruction]. Kyiv, Minenergovugillya Ukrainy Publ., 2010. 54 p. (Ukr).
2. Koliushko D.G., Rudenko S.S. Analysis of methods for monitoring of existing energy objects grounding devices state at the present stage. *Electrical engineering & electromechanics*, 2019, no.1, pp. 67-72. doi: 10.20998/2074-272X.2019.1.11.
3. *Pravyla ulashtuvannja elektroustanovok* [Electrical Installation Regulations]. Kharkiv, Fort Publ., 2017. 760 p. (Ukr).
4. *IEC 61024-1:1990*. Protection of structures against lightning. Part 1: General principles.
5. *IEC 62305-1*. Risk management. Protection against lightning. Part 1. General principles.
6. *IEC 61643-1:2005*. Low-voltage surge protective devices – Part 1: Surge protective devices connected to low-voltage power distribution systems – Requirements and tests.
7. Baranov M.I., Koliushko G.M., Kravchenko V.I., Rudakov S.V. A powerful high-voltage generator of aperiodic impulses of current of artificial lightning with the peak-temporal parameters rated on an international standard IEC 62305-1-2010. *Electrical Engineering & Electromechanics*, 2015, no.1, pp. 51-56. doi: 10.20998/2074-272X.2015.1.10.
8. Kolobov V.V., Barannik M.B., Selivanov V.N. A new device for measuring tower grounding resistance using the impulse method. *Trudy Kolskogo nauchnogo tsentra RAN*, 2016, no.5, pp. 39-55. (Rus).
9. Djura D.A., Selivanov V.N. Instruments to measure impulse response of grounding *Trudy Kolskogo nauchnogo tsentra RAN*, 2013, no.4, pp. 56-66. (Rus).

Received 18.02.2019

D.G. Koliushko¹, Candidate of Technical Science, Senior Research Associate,

S.S. Rudenko¹, Candidate of Technical Science, Senior Research Associate,

A.V. Plichko¹, Research Associate,

V.I. Shcherbinin², Candidate of Physics and Mathematics Science, Senior Research Associate,

¹ National Technical University «Kharkiv Polytechnic Institute», 2, Kyrpychova Str., Kharkiv, 61002, Ukraine, phone +380 57 7076671, e-mail: nio5_molniya@ukr.net

² National Science Center «Kharkov Institute of Physics and Technology»,

1, Akademicheskaya Str., Kharkov, 61108, Ukraine.

O.P. Lazurenko, O.M. Moroz, S.O. Tymchuk, O.O. Miroshnyk, O.A. Savchenko

OPTIMIZATION OF DESIGN PARAMETERS OF AUTOTRANSFORMERS IN ICE MELTING SCHEME WITH NON-INDUCTIVE CIRCUIT ON 6-10 KV OVERHEAD POWER LINES

Purpose. The purpose of the paper is to determine the basic electrical characteristics and to develop a calculation method and algorithm for optimizing the design parameters of autotransformers intended for use in a melting ice scheme with a non-inductive circuit on 6-10 kV overhead power lines. *Methodology.* The development of the technical and economic model and the method for calculation of the design parameters of the autotransformer for melting ice is performed on the basis of a systematic approach. *Optimization of structural characteristics of autotransformers is carried out using a combined algorithm based on the spatial grid method, adapted to the case of a mixed space of discrete and continuous independent variables, and the specifics of the technical and economic model of the autotransformer. The proposed combined optimization algorithm is implemented in the Delphi environment. Results.* Based on the required specific melting power, the main electrical characteristics of autotransformers intended for use in the melting ice scheme with a non-inductive circuit on 6-10 kV overhead lines, which were the basis for optimizing their design parameters, have been calculated. *The technical and economical model of autotransformer for melting ice, which is defined by nine independent variables and describes its cost and technical parameters, is developed. On the basis of the obtained electrical characteristics, optimization of the design parameters of a series of autotransformers is carried out, which includes three standard sizes, differing in maximum length of the transmission line. Originality.* A method of calculation of structural parameters of autotransformers for ice melting is proposed, the peculiarity of which is the use of the criterion of the minimum of the cost of the active part and taking into account the conditioned by the circuit of connection of the autotransformers the technical restrictions of errors on the value and angle of secondary current, which are important from the point of view of ensuring the permissible deviation of the specific power of melting ice. *Practical value.* Optimal correlations of geometrical sizes and electromagnetic loads of autotransformers for ice melting, their cost indicators, as well as the main design characteristics of the magnetic circuit and windings are established. *Results of design calculation of autotransformers are sufficient for introduction of their serial production in industrial conditions.* References 11, tables 2, figures 4.

Key words: overhead power line, melting of ice, autotransformer for melting of ice, technical and economic model, optimization of design parameters.

Мета. Метою статті є визначення електричних характеристик та розроблення методу розрахунку і алгоритму оптимізації конструктивних параметрів автотрансформаторів, призначених для використання в схемі плавлення ожеледі з безіндуктивним контуром на повітряних лініях електропередач 6-10 кВ. *Методологія.* Розроблення техніко-економічної моделі та методу розрахунку конструктивних параметрів автотрансформатора плавлення ожеледі виконано на засадах системного підходу. *Оптимізація конструкції автотрансформаторів плавлення ожеледі проведена з використанням комбінованого алгоритму на основі методу просторової сітки. Результати.* Одержано електричні характеристики та оптимізовано конструктивні параметри серії автотрансформаторів, призначених для використання в схемі плавлення ожеледі з безіндуктивним контуром на повітряних лініях електропередач 6-10 кВ. *Наукова новизна.* Запропоновано метод розрахунку конструктивних параметрів автотрансформаторів плавлення ожеледі, особливістю якого є використання критерію мінімуму вартості активної частини та врахування зумовлених схемою вмикання автотрансформаторів технічних обмежень похибок за величиною та кутом вторинного струму. *Практичне значення.* Результати конструктивного розрахунку автотрансформаторів плавлення ожеледі є достатніми для впровадження їх серійного виробництва в промислових умовах. Бібл. 11, табл. 2, рис. 4.

Ключові слова: повітряна лінія електропередач, плавлення ожеледі, автотрансформатор плавлення ожеледі, техніко-економічна модель, оптимізація конструктивних параметрів.

Цель. Целью статьи является определение электрических характеристик и разработка метода расчета и алгоритма оптимизации конструктивных параметров автотрансформаторов, предназначенных для использования в схеме плавки гололеда с безиндуктивным контуром на воздушных линиях электропередачи 6-10 кВ. *Методология.* Разработка технико-экономической модели и метода расчета конструктивных параметров автотрансформатора плавки гололеда выполнена на основе системного подхода. *Оптимизация конструкции автотрансформаторов плавки гололеда проведена с использованием комбинированного алгоритма на основе метода пространственной сетки. Результаты.* Получены электрические характеристики и оптимизированы конструктивные параметры серии автотрансформаторов, предназначенных для использования в схеме плавки гололеда с безиндуктивным контуром на воздушных линиях электропередачи 6-10 кВ. *Научная новизна.* Предложен метод расчета конструктивных параметров автотрансформаторов плавки гололеда, особенностью которого является использование критерия минимума стоимости активной части и учет обусловленных схемой включения автотрансформаторов технических ограничений погрешностей по величине и углу вторичного тока. *Практическое значение.* Результаты конструктивного расчета автотрансформаторов плавки гололеда достаточны для внедрения их серийного производства в промышленных условиях. Библ. 11, табл. 2, рис. 4.

Ключевые слова: воздушная линия электропередачи, плавка гололеда, автотрансформатор плавки гололеда, технико-экономическая модель, оптимизация конструктивных параметров.

Introduction. At present, the most effective way to protect 6-10 kV overhead transmission lines (OTL), which are widely used in some countries, from the effect

of the ice is to melt it [1]. The technology of melting ice is to use a certain melting scheme, which, based on the law of Joule-Lenz, allows to achieve the allocation of thermal

energy in the unit of the length of the OTL wire, sufficient for melting of deposits within a reasonable time, usually about 1 hour. In order to determine the appropriate amount of thermal energy, in this work the term «specific power of melting ice» is used.

In melting schemes of ice, electrical power melting installations of ice-and-frost deposits (IFDs) are often used, which harmonize the parameters of the power system with the parameters of the lines [2]. An example of such an installation is the autotransformer for melting ice (AMI), which is activated by the melting scheme proposed in [3]. As it is known, the use of autotransformers compared with transformers, due to the electrical connection between the windings, can significantly reduce the power of the electric apparatus. In addition, the feature of the proposed melting scheme is the use of a non-inductive circuit, which reduces the reactive component of the load of the autotransformer to almost zero.

To date, autotransformers, suitable for use in the proposed melting scheme of ice with a non-inductive circuit, are absent. Therefore, there is the task of determining the electrical characteristics of such autotransformers as well as developing a calculation method and algorithm for optimizing their design parameters.

The analysis of existing methods for the calculation of power transformers and autotransformers of industrial series [4-6] showed that they are based on the use of the criterion of reduced costs, which allows to establish the optimal ratio between capital and current costs to the transformer. This approach is not appropriate for autotransformers for melting ice, as they have a small total annual operating time (up to 50-100 h). Consideration in the method of calculating the AMI of current costs will lead to unnecessary complication of its technical and economic model and increase the optimization time of the algorithm. In addition, the existing calculation methods do not take into account determined by the AMI connection circuit the limiting of the angle between the primary and secondary current (angular error limitation) and the relative difference between the primary and the secondary current (current error limit), which are important for the AMI from the point the view of providing the required specific power of melting ice.

The preliminary analysis showed that the dependencies of the parameters of the AMI on the discrete and continuous independent variables is nonlinear, therefore the task of optimizing the design of such an autotransformer is the problem of nonlinear programming. There is a fairly large number of algorithms for solving these problems [7-10]. However, the general methods of solving the problems of nonlinear programming in the mixed space of discrete and continuous variables have not been developed to date. A characteristic drawback of existing methods is that they are not universal. The use of certain artificial techniques allows to reduce the task to any particular type. One of such technique is the transformation of independent variables to one type, such as continuous [10]. But such a technique can give significant errors in the inverse

transformation of variables. Transformation of variables to a discrete form is more acceptable, since continuous variables can be discretized with a small step and obtain a solution with a given accuracy, but with high computation costs. However, in the case of the multi-extremity of the objective function and the presence of nonlinear constraints on the permissible domain of solutions, practically all methods of discrete programming are reduced to a continuous enumeration of discrete variables. In [11] an approach to the solution of the problem of nonlinear programming for the case of discrete and continuous variables in the general formulation is proposed. The advantage of this approach is to take into account the specifics of a particular system and its mathematical model, in connection with which it was adopted as the basis for developing a combined algorithm for optimizing the design parameters of autotransformers for melting ice.

The goal of investigations is to determine the electrical characteristics and to develop a calculation method and algorithm for optimizing the design parameters of autotransformers intended for use in a melting scheme of ice with a non-inductive circuit on 6-10 kV overhead power lines.

Calculation of electrical parameters of autotransformers for melting ice. To optimize the design parameters of AMI, it is necessary to calculate their desired electrical characteristics. In [3] an analysis of electrical processes in the melting scheme of ice on the basis of autotransformer with a non-inductive secondary circuit was carried out. It is shown that the proposed scheme allows in melting ice mode to increase the equivalent active resistance of the OTL in number of times

$$k_R = \frac{(1+k_I)^2(1-a)+a}{a(1-a)k_I^2}, \quad (1)$$

where k_I is the coefficient of transformation of the AMI by current; a is the coefficient of ratio of active resistance of the external and internal parts of the wire

$$a = \frac{R}{R_e}, \quad (2)$$

where R , R_e are the active resistances according to the entire wire and its outer part.

Inductive resistance of the line at the same time practically does not change.

In the AMI series, there were three standard sizes that differ in maximum length of the OTL. Each AMI is intended for the melting of deposits on the OTL with a length from a certain value of l_{\min} to a value of l_{\max} . In order to provide the required specific melting power on the OTL with any length within the limits of $l_{\min} \div l_{\max}$, adjustment of the coefficient k_R is foreseen. It will also allow to quickly regulate the amount of thermal energy emitted in the wires of the OTL when weather conditions change, to affect the melting time of IFDs.

As the estimated calculations have shown, in order to obtain the required values of the specific melting power, the equivalent active resistance of the OTL should be much larger than the equivalent inductive resistance, so the latter can be neglected. Then the value of the

coefficient k_R to be provided by the AMI can be determined based on the required value of the specific melting ice power $P_0=56$ kW/km [1] based on the expression

$$k_R \approx \frac{U^2}{3P_0 R_0 l^2}, \quad (3)$$

where U is the nominal voltage of the line, kV; R_0 is the specific active resistance of the wire, Ω/km ; l is the OTL length, km.

Then, based on the expressions obtained in [3], the basic electrical parameters of the AMI were calculated. The calculation results are shown in Table 1. Nominal currents and voltages of windings of the AMI were taken equal to the maximum of values possible during the operation of each autotransformer. In addition, Table 1 shows the allowable values of errors in the values of the

secondary current and its phase relative to the primary current. The limitation of this error is due to the switching circuit of the autotransformers [3] and is necessary in terms of providing a tolerable deviation of the specific melting power of ice, which influences on the time of melting of deposits and, consequently, the success of this process. For those specified in Table 1 limit values of errors, the possible deviation of power losses in the wire is $\pm 10\%$.

Technical and economic model of autotransformer. To calculate the AMI, the basics of the methods used to calculate power transformers and autotransformers are used, with some differences. So, since the cost of operating APO, as mentioned above, can be neglected, then as an indicator of their optimization it is proposed to use a relatively simple criterion for the minimum cost of the active part $C \rightarrow \min$.

Table 1

Results of calculation of the main electrical characteristics of autotransformers for melting ice which are the basis for optimizing their design parameters

Size of the AMI	AMI parameters								
	Length of the line for which the AMI is assigned, km	Range of the line length, km	Coefficient of increasing the active resistance (for wire cross section of 70 mm ²)	Nominal transformation rate by current	Nominal current of primary/secondary windings, A	Nominal power, kVA	Nominal voltage of the primary winding, V	Permissible errors	
								by the value of secondary current, %	by the phase of secondary current, el. degrees
Size No. 1	4÷10	4÷4.7 4.7÷5.4 5.4÷6.3 6.3÷7.4 7.4÷8.6 8.6÷10	75.6 55.9 41.6 30.2 22.4 16.5	0.28 0.34 0.41 0.51 0.63 0.79	110/182	2000	6000	-5.4	±10
Size No. 2	4÷16	4÷4.7 4.7÷5.4 5.4÷6.3 6.3÷7.4 7.4÷8.6 8.6÷10 10÷11.7 11.7÷13.7 13.7÷16	75.6 55.9 41.6 30.2 22.4 16.5 12.0 8.8 6.6	0.28 0.34 0.41 0.51 0.63 0.79 1.04 1.40 1.99	174/182	3200	6000	-5.4	±10
Size No. 3	4÷25	4÷4.7 4.7÷5.4 5.4÷6.3 6.3÷7.4 7.4÷8.6 8.6÷10 10÷11.7 11.7÷13.7 13.7÷16 16÷18.5 18.5÷21.5 21.5÷25	75.6 55.9 41.6 30.2 22.4 16.5 12.0 8.8 6.6 4.8 4.1 3.5	0.28 0.34 0.41 0.51 0.63 0.79 1.04 1.40 1.99 3.23 4.67 7.83	207/182	3200	6000	-5.4	±10

As noted above, the APO must be provided with an appropriate level of error – by angle and by current

$$f_I \leq f_{Ia}, \quad (4)$$

$$\delta_I \leq \delta_{Ia}. \quad (5)$$

AMI must also be characterized by certain values of the overheating temperature of the windings (primary Δt_1 and secondary Δt_2) above the ambient air, which should not be greater than the permissible value for the accepted class of insulation F of the AMI $\Delta t_a = 140$ °C (taking into account the greatest possible temperature of air during melting ice time $t_{air} = 0$ °C)

$$\Delta t_1 \leq \Delta t_a, \quad (6)$$

$$\Delta t_2 \leq \Delta t_a. \quad (7)$$

The check for heating the windings during a short circuit was carried out after a detailed calculation of the AMI.

Thus, the task of designing an optimal AMI is to minimize the target function taking into account the given constraints. The technical and economic model of the optimal design of the AMI has the form of the system:

$$\begin{cases} C \rightarrow \min; \\ f_I \leq f_{Ia}; \\ \delta_I \leq \delta_{Ia}; \\ \Delta t_1 \leq \Delta t_a; \\ \Delta t_2 \leq \Delta t_a. \end{cases} \quad (8)$$

AMIs are intended to be performed as three-phase, cast-insulated and with spatial non-breaking magnetic system, which allows for the equalization of the magnetization currents, and hence of the AMI errors, in all three phases, which in turn eliminates the difference in power losses in the melting mode in the wires of various phases [6]. To manufacture the core of the AMI, cold-rolled anisotropic steel grade 3405, which is characterized by acceptable magnetic properties at a moderate price, is accepted. The insulation distances of the AMI were based on existing experience in designing transformers and operating standards.

The analysis showed that independent variables, which can describe the design of the AMI, include: d – the diameter of the rod of the autotransformer; b_1, b_2, h_1, h_2 – the dimensions of the wiring of the primary and secondary windings; n_1, n_2 – the number of parallel wires in windings; N_{11} – the number of layers of the primary winding; B – the magnetic flux density in the rods of the magnetic system. For the three-phase AMI, dependencies for the target function, as well as the main characteristics, including those that are subject to limitation, on independent variables, are obtained. With the exception of minor differences, they correspond to well-known expressions, which are in the specialized literature on the design and calculation of power transformers, in particular [4-6]. Due to the considerable cumbersome nature of these dependencies and their obviousness, they are not given in this paper.

Optimization of design parameters of autotransformers for melting ice. The initial data for optimization of the design parameters of AMI are their

electrical characteristics, shown in Table 1, as well as the parameters of the selected electrical materials.

The analysis of independent variables shows that among the variables that are discretely variable, two groups can be distinguished. The first one is the variables that can take values from the standard-size series (d, h_1, h_2, b_1, b_2), the second one is integer variables (N_{11}, n_1, n_2). The third group is a continuous variable, B . Thus, there are three groups of variables in the problem, for variation of which one can use schemes of different methods.

The approach was based on the spatial grid method proposed in [11]. This approach does not impose any restrictions on the type of variables, nor on the efficiency criterion. The enlarged structure of the combined algorithm represents three nested to each other stages (Fig. 1).

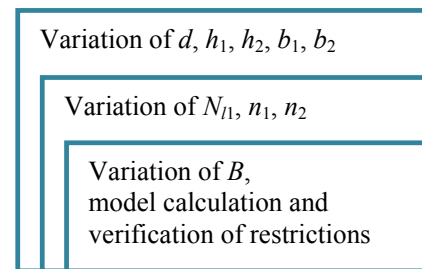


Fig. 1. Structure of the combined algorithm for optimization of the AMI

The first (external) stage of the algorithm implements the change of those independent variables that take values from the standard-size series, that is, the transformer structure for the internal stages is fixed. At this stage, it makes sense to replace the variables. The scope of the values of each variable is limited to the standard-size series in the form

$$\begin{cases} d = \{d_i\}, i=1, \dots, n_d; \\ h_1 = \{h_{1j}\}, j=1, \dots, n_h; \\ h_2 = \{h_{2p}\}, p=1, \dots, n_h; \\ b_1 = \{b_{1k}\}, k=1, \dots, n_b; \\ b_2 = \{b_{2m}\}, m=1, \dots, n_b. \end{cases} \quad (9)$$

Each element of a standard-size series corresponds to its serial number (index). Taking into account the unequivocal correspondence of the index to the element of a standard-size series, it is possible to accept their indexes as independent variables of optimization. The optimization task at this stage can be solved in the space of integer variables i, j, p, k, m .

The second (middle) stage implements the change of integer independent variables.

At the third (internal) stage, the variation of a continuous variable is performed, since, for fixed design parameters, the target function is continuous. In the internal cycle, the calculation of the target function of the system and verification of restrictions on the permissible decision area are performed.

The structure of the stages in which for each combination of the values of independent variables of the external stage the optimal for these combinations solution of internal stages is found, leads to the implementation of

the Bellman principle of optimality at the level of the structure of the algorithm.

To determine the possibility of application at different stages of the optimization algorithm of methods other than the grid method, a study was carried out on the dependence of the target function on independent variables. Analyzing the nature of the dependence of the target function on the variable B (Fig. 2,a), it can be noted that in this case the function is unimodal. To find the minimum of the target function in the third stage of the combined algorithm, one can use the scheme of the unidirectional search method, and the principle of minimax is implemented for moving from the maximum value of B to the minimum, since the minimum of the target function is near the maximum value of B . The maximum value of the magnetic flux density was

assumed to be equal to $B = 1.8$ T, since larger values for the accepted steel grade lead to a significant increase in the magnetic field strength, which, in turn, causes an increase in the magnetization current and, as a consequence, the errors of the autotransformer. Greater values of the magnetic flux density also cause a sharp increase in specific losses in steel and its intense heating. To take into account the restrictions of the functional type, imposed on the area of values of the target function, it is rationally to use the penalty function. In this case, it can be quite simple, for example, a constant whose value is clearly greater than the real values of the target function. Taking into account the apparent simplicity, the block diagram of the third stage of the combined algorithm of optimization is not given.

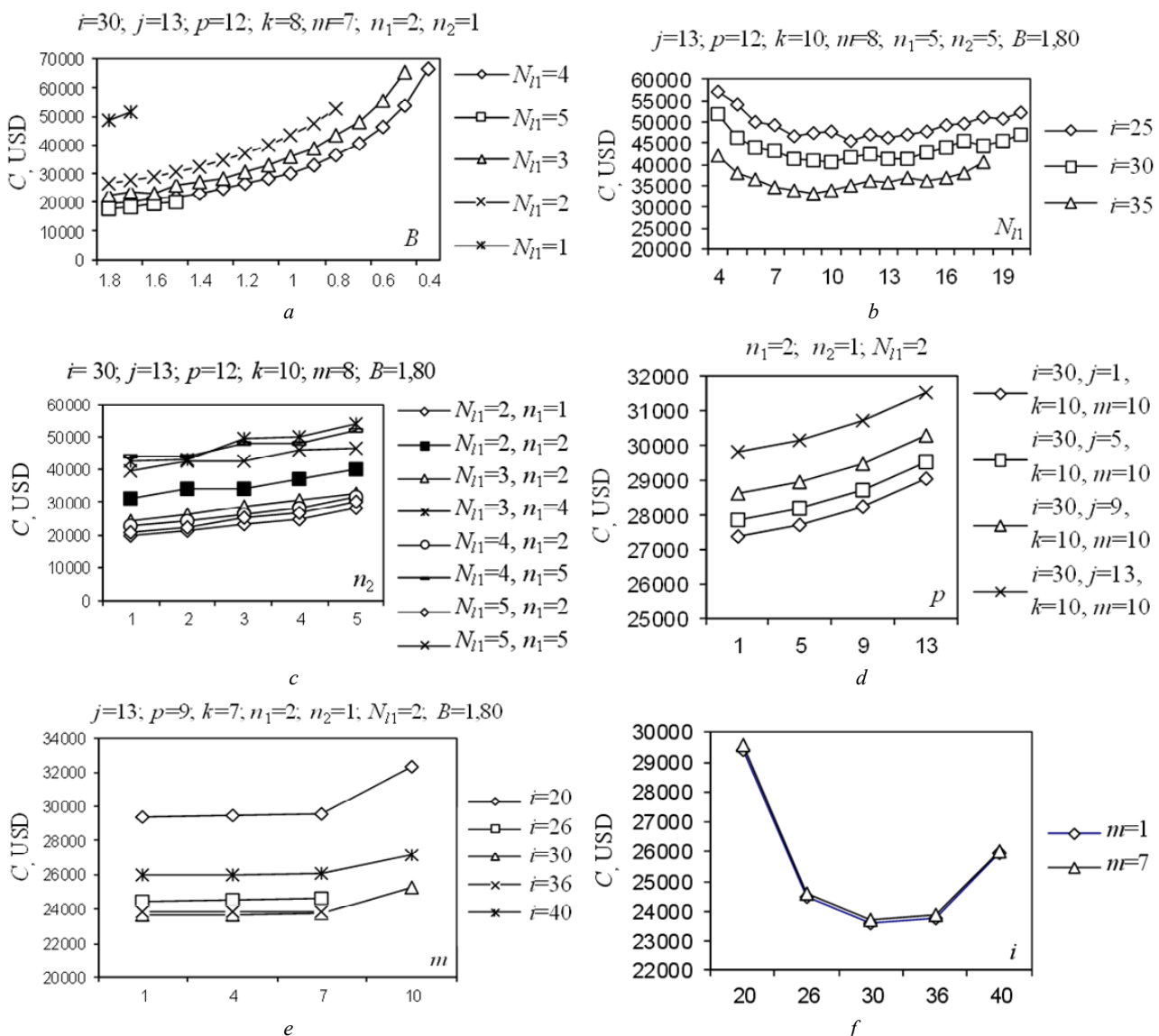


Fig. 2. Preliminary investigations of the target function C (USD)

Analysis of the nature of the dependence of the target function on the variables N_{I1}, n_1, n_2 (Fig. 2,b,c) shows that in this case the target function is not unimodal. Therefore, at the second stage of the combined algorithm of optimization, one should use the

scheme of any method for finding the global optimum. The range of variation of variables at this stage is relatively small. Therefore, the advantage was given to the method of scanning (the variant of the method of full overview of the combinations of values of variables).

Table 2

Results of optimization of design parameters of autotransformers for melting ice

AMI parameters	Parameter value for the standard-sized AMI		
	No. 1	No. 2	No. 3
<i>Magnetic system:</i>			
Rod diameter, mm	380	450	560
Rod length, mm	1464	1604	1998
Distance between axes of the rods, mm	694	793	927
Total steel mass, kg	5082	7931	14952
Magnetic flux density in steel, T	1.80	1.80	1.78
<i>Windings:</i>			
Number of layers of primary winding	3	4	1
Number of layers of secondary winding	1	2	6
Number of wires of primary winding	2	4	4
Number of wires of secondary winding	2	1	3
Radial wire size of the winding I, mm	5.60	5.60	4.50
Axial wire size of the winding I, mm	11.20	11.20	6.30
Radial wire size of the winding II, mm	2.00	3.15	5.60
Axial wire size of the winding II, mm	4.00	11.20	6.30
Number of turns of the primary winding	180	130	71
Maximum number of turns of the secondary winding	142	260	555
Overheating temperature of the primary winding, °C	138	133	112
Overheating temperature of the secondary winding, °C	140	134	139
Current density in the primary winding, A/mm ²	0.88	0.69	1.83
Current density in the secondary winding, A/mm ²	11.27	5.14	1.70
<i>Nominal electrical parameters:</i>			
Primary current, A	110	174	207
Secondary current, A	182	182	182
Error in the value of secondary current, %	-1.0	-1,5	-3.3
Error in the angle of secondary current, electric degrees	0.9	1,3	2.8
<i>General AMI parameters:</i>			
Autotransformer mass, kg	7915	12812	24980
Cost of autotransformer, USD	18159	29328	57319

Consideration of functional type restrictions occurs automatically, since for each combination of values of variables N_{11} , n_1 , n_2 the task of the third stage of optimization is solved, where restrictions have already been taken into account. The algorithm of the scanning method is well known and its block diagram is also not given.

A bit more interest is the definition of the optimization method for the first stage of the combined algorithm. The scope of the change of the independent variables is quite large (for example, $i = 1, \dots, 56$), which makes the scanning method ineffective. At the same time, analysis of the nature of the dependence of the target function on independent variables at this stage (Fig. 2, *d, e, f*) shows that this function is quasi-convex. This fact gives the right to depart from the scheme of the method of full overview of the combinations of values of variables. It is proposed to apply a scheme of spatial grid method with a variable step, adapting it for the case of integer variables (the grid step can not be small).

In the general case, the convergence of the spatial grid method depends on the choice of the initial step of the grid and the law by which this step varies with the narrowing of the search optimum. Calculation investigations of the convergence of the developed variant of the algorithm of the spatial grid method (Fig. 3, 4) showed that the convergence practically does not depend on the value of the initial step of the grid, but the rate of convergence essentially depends on. The minimum search time for the optimum corresponds to the value of the initial step of the grid, in which the number of nodes in the grid will be equal to one of the numbers of the Fibonacci series, namely, the number of nodes in the variable $i - 8$, by $j, p, k, m - 5$ the calculation time is about 7 minutes. Relative to the law of reducing the step of a grid, then in this case the most studied method of dichotomy is applied.

The proposed combined optimization algorithm was implemented in the Delphi environment. Results of optimization of design parameters of AMI are given in Table 2.

As can be seen from the results of the calculation, the permissible range of solutions for each AMI is primarily due to the overheating temperature of the windings, which in some cases almost corresponds to the permissible. The relatively high value of the permissible overheating temperature $\Delta t_a = 140$ °C, which is associated with the features of the AMI operation (calculation air temperature $t_{air} = 0$ °C), as well as the external placement of the secondary winding, resulted in rather high values of the density of the current in it. The magnetic flux density in the core of the AMI is close to the maximum. For the standard size of the autotransformer No. 3, the magnetic flux density was slightly lower, which is explained by the activity of the limit on the current error.

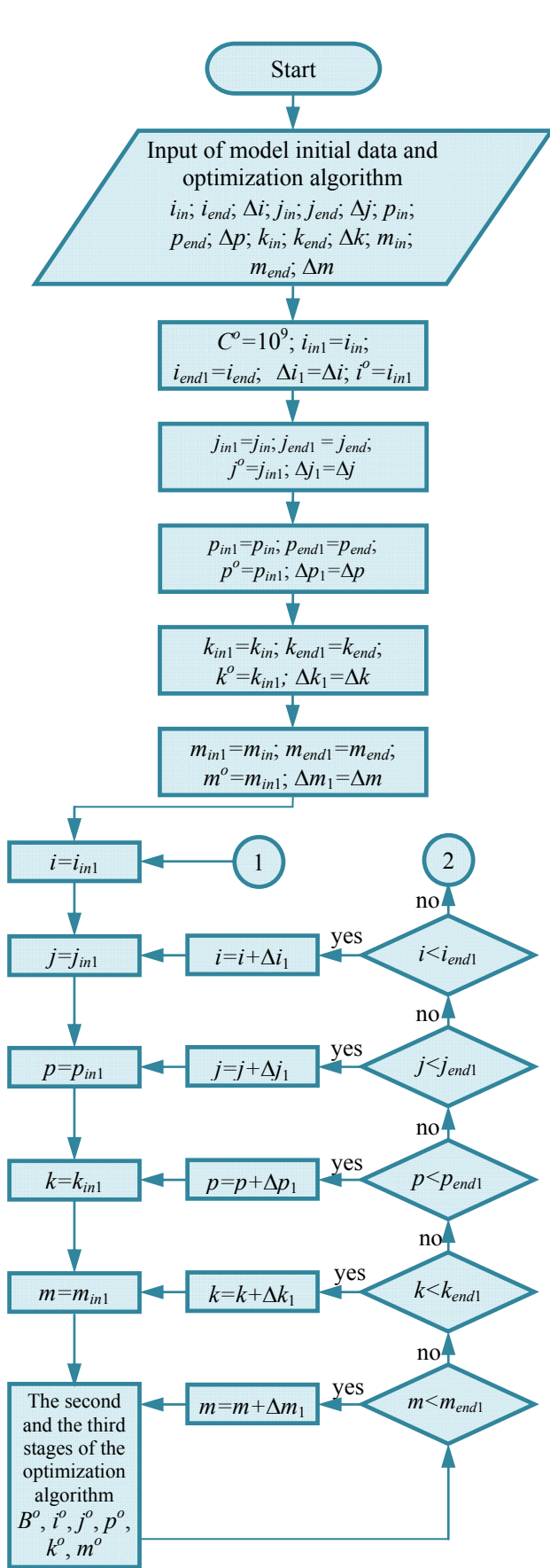


Fig. 3. Block diagram of the first stage of the combined algorithm

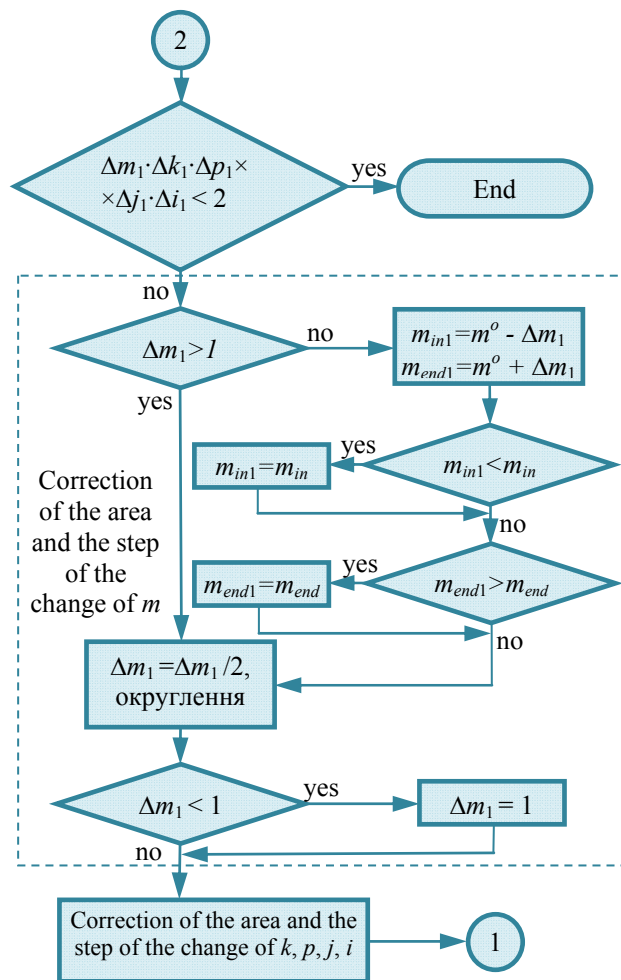


Fig. 4. Block diagram of the first stage of the combined algorithm (continuation)

Conclusions.

1. The electrical characteristics of autotransformers intended for use in the melting ice scheme with a non-inductive circuit on 6-10 kV overhead lines, which were the basis for optimization of their design parameters, have been calculated.

2. The technical and economic model of autotransformer for melting ice, which is described by nine independent variables, is developed. The method of calculation and the combined algorithm of optimization of design parameters of autotransformers for melting ice is proposed. The feature of the proposed method of calculation is the use of the criterion of the minimum value of the cost of active part and the account of the conditioned by the circuit of connecting autotransformers the technical restrictions of errors on the value and angle of secondary current.

3. Based on the obtained electrical characteristics, the design parameters of autotransformers intended for use in the melting ice scheme with a non-inductive circuit on 6-10 kV overhead power lines are optimized. In the series of autotransformers, there are three standard sizes, which differ in maximum length of the transmission line. The current density in the primary winding of autotransformers is about 1 A/mm², whereas in the secondary one varies in the range from 1.7 to 11.3 A/mm², which is explained by different conditions of cooling of

windings. Magnetic flux density in magnetic circuits is about 1.8 T. The results of the design calculation are sufficient for the introduction of batch production of autotransformers for melting ice in industrial conditions.

REFERENCES

1. Farzaneh M. *Atmospheric Icing of Power Networks*. Berlin, Springer, 2008. 381 p.
2. *Scientific and technical report on the topic «Choice of methods and development of suitable schemes for the melting of ice on the OPL of various voltage classes in the Moldovan energy system»*. Chisinau, STC «Techinformenergo» Publ., 2001. 132 p. (Rus).
3. Bilash I.P., Savchenko O.A. Analysis of electrical processes in the device for protecting air power lines from deposits of ice and frost. *Bulletin of Kharkiv State Technical University of Agriculture*, 2003, no.19, vol.1, pp. 91-98. (Ukr).
4. Biki M.A. *Proektirovanie silovykh transformatorov. Raschety osnovnykh parametrov* [Design of power transformers. Calculations of the main parameters]. Moscow, Znak Publ., 2013. 612 p. (Rus).
5. Del Vecchio R.M., Poulin B., Feghali P.T., Shah D.M., Ahuja R. *Transformer design principles: with applications to core-form power transformers*. New York, CRC Press, 2001. 599 p.
6. Tikhomirov P. M. *Raschet transformatorov* [Calculation of transformers]. Moscow, Energoatomizdat Publ., 1986. 582 p. (Rus).
7. Bazaraa M.S., Sherali H.D., Shetty C.M. *Nonlinear programming: theory and algorithms*. New Jersey, John Wiley & Sons, 2006. 853 p.
8. Timchuk S. A., Sirotenko M. A. The search algorithm for optimal reliability increasing system parameters in 10 kV branched distribution networks. *Eastern-European Journal of Enterprise Technologies*, 2015, vol.6, no.8(78), pp. 4-10. (Rus). doi: **10.15587/1729-4061.2015.54626**.
9. Borodakii Yu.V., Zagrebaev A.M., Kritsyna N.A., Kuliabichev Yu.P., Shumilov Yu.Yu. *Nelineinoe programmirovaniye v sovremennykh zadachakh optimizatsii* [Nonlinear programming in modern optimization problems]. Moscow, NIiAU «MIFI» Publ., 2011. 244 p. (Rus).
10. Ruban A.I., Mikhalev A.S. Global optimization with selective averaging of mixed variables: continuous and discrete with the ordered possible values. *Science Bulletin of the Novosibirsk State Technical University*, 2017, no.3(68), pp. 126-141. (Rus). doi: **10.17212/1814-1196-2017-3-126-141**.
11. Timchuk S.A. A method for constructing an algorithm for solving a nonlinear programming problem. *Bulletin of Kharkiv State Technical University of Agriculture*, 2004, no.23, pp. 128-134. (Rus).

Received 12.02.2019

O.P. Lazurenko¹, Candidate of Technical Science,
O.M. Moroz², Doctor of Technical Science,
S.O. Tymchuk², Doctor of Technical Science,
O.O. Miroshnyk², Doctor of Technical Science,
O.A. Savchenko², Candidate of Technical Science,
¹National Technical University «Kharkiv Polytechnic Institute»,
2, Kyrpychova Str., Kharkiv, 61002, Ukraine,
phone +380 57 7076585, e-mail: lazurenkoap@i.ua
²Kharkiv Petro Vasylenko National Technical University of
Agriculture,
44, Alchevskyyh Str., Kharkiv, 61002, Ukraine,
phone +380 57 7123432, e-mail: savoa@ukr.net

How to cite this article:

Lazurenko O.P., Moroz O.M., Tymchuk S.O., Miroshnyk O.O., Savchenko O.A. Optimization of design parameters of autotransformers in ice melting scheme with non-inductive circuit on 6-10 kV overhead power lines. *Electrical engineering & electromechanics*, 2019, no.3, pp. 59-66. doi: **10.20998/2074-272X.2019.3.10**.

I.V. Nizhevskiy, V.I. Nizhevskiy

CALCULATION ESTIMATION OF OVERVOLTAGE ON INSULATION OF THE EQUIPMENT OF A SUBSTATION AT THE LIGHTNING STRIKE IN ITS LIGHTNING ARRESTER

Purpose. The complex approach to calculating thunderstorm overvoltage on substation equipment is considered when lightning strikes in a lightning rod. **Methodology.** The conditions of safe passage of lightning current through a lightning arrester are formulated. **Results.** It is shown that the calculation of the permissible length of air insulating gaps in the substation is based on the breakdown of the air tension, which is assumed to be 500 kV/m. This leads to an error in calculating the length of the air gap and, as a consequence, the probability of its breakdown, the value of which is used to calculate the indicator of the lightning resistance of the substation. A technique is proposed for calculating the permissible voltage on the transformer case when a lightning strike strikes the lightning receptacle of the transformer portal. On the basis of the nonlinear pulsed electric strength of the ground, the specified minimum permissible ground distance between the grounding rod of the lightning rod and the nearest point of the protected device is obtained. **Originality.** Refined calculation of the length of the minimum breakdown gap in the air and in the ground. **Practical value.** The proposed approach makes it possible to calculate thunderstorm overvoltage on substation equipment. References 11, tables 4, figures 6.

Key words: lightning overvoltage, substation, lightning arrester, volt-second characteristic, insulator string, electric field, air gap, permissible voltage, transformer case, pulsed electric strength.

Розроблено інженерний підхід до розрахунку грозових перенапруг на обладнанні підстанції при ударі блискавки в блискавковідвід. Сформульовані умови безпечного для обладнання проходження струму блискавки по блискавковідводу. Показано, що розрахунок допустимої довжини повітряних ізоляційних проміжків на підстанції базується на основі пробивної напруженості повітря, яка прийнята рівною 500 кВ/м. Це призводить до помилки розрахунку довжини повітряного проміжку l , як наслідок, ймовірності його пробою, значення якої використовується для розрахунку показника грозоупорності підстанції. Як приклад розглянута методика розрахунку допустимої напруги на корпусі трансформатора при ударі блискавки в блискавкоприймач трансформаторного порталу. На основі нелінійної імпульсної електричної міцності ґрунту отримано уточнену мінімально допустиму відстань в землі між заземлювачем блискавковідводу і найближчою до нього точкою пристрою, що захищається. Наводяться аналітичні вирази для розрахунків. Бібл. 11, табл. 4, рис. 6

Ключові слова: грозові перенапруги, підстанція, блискавковідвід, вольт-секундна характеристика, гірлянда ізоляторів, електричне поле, повітряний проміжок, допустиме напруження, корпус трансформатора, імпульсна електрична міцність.

Разработан инженерный подход к расчету грозовых перенапряжений на оборудовании подстанции при ударе молнии в молниеотвод. Сформулированы условия безопасного для оборудования прохождения тока молнии по молниеотводу. Показано, что расчет допустимой длины воздушных изоляционных промежутков на подстанции базируется на основе пробивной напряженности воздуха, которая принята равной 500 кВ/м. Это приводит к ошибке расчета длины воздушного промежутка l , как следствие, вероятности его пробоа, значение которой используется для расчета показателя грозоупорности подстанции. В качестве примера рассмотрена методика расчета допустимого напряжения на корпусе трансформатора при ударе молнии в молниеприемник трансформаторного портала. На основе нелинейной импульсной электрической прочности ґрунта получено уточненное минимальное допустимое расстояние в земле между заземлителем молниеотвода и ближайшей к нему точкой защищаемого устройства. Приводятся аналитические выражения для расчетов. Библ. 11, табл. 4, рис. 6

Ключевые слова: грозовые перенапряжения, подстанция, молниеотвод, вольт-секундная характеристика, гирлянда изоляторов, электрическое поле, воздушный промежуток, допустимое напряжение, корпус трансформатора, импульсная электрическая прочность.

Introduction and problem definition. On the globe, as noted in [1], there are at the same time about 2000 thunderstorm foci, in which about 100 lightning discharges occur every second. Many countries, including Ukraine, have thunderstorm maps that are based on long-term meteorological observations and are periodically updated. This allows to improve the methods for calculating lightning overvoltage in electrical installations. Analysis of studies and publications shows that the task of protecting electrical equipment of substations (SS) from thunderstorm overvoltage during direct lightning strikes is under consideration of many domestic and foreign scientists. Coordination of insulation under conditions of limiting overvoltage, as well as reflection of modern materials on the problem

under consideration are presented in [2]. The operation of insulating structures at lightning and internal overvoltage in electrical systems and their limitation are considered in [1]. However, the continued research of many scientists leads to the need to improve calculations to limit lightning overvoltage. To determine the length of the insulating air gap $l_{a.g}$ between the support or portal body and the flexible bus or equipment, dependency curves $U_{50\%} = f(l_{a.g})$ are often used. The dependence of the 50 % discharge voltage of the air gap on its length at positive and negative polarity of lightning pulses is given, for example, in [3]. These dependencies have a weak nonlinearity. Consequently, the value of the breakdown electric field

strength of air in long air gaps decreases with an increase in their length which must be taken into account in the calculations when determining the length of the gap. Not accounting of this, i.e. the adoption of the value of the permissible electric field strength in the air gap constant and equal to 500 kV/m can lead to inaccuracy in determining its length and, accordingly, to reduce it, which increases the probability of breakdown of the specified gap. In addition, the neglect of possible overlaps of the air insulation of the substation after the end of the current increase leads to an underestimation of the danger of lightning currents with relatively low amplitudes at a large slope and the duration of their pulses [4]. More accurate results for determining the dielectric strength of the insulation under the so-called non-standard voltages can be obtained using the methods described in [5–7], which also makes it possible to clarify the lengths of the discharge gaps.

The goal of the paper is the development of an engineering methodology for calculating lightning overvoltage on substation equipment at a lightning strike in its lightning arrester.

Formulation of conditions for limiting thunderstorm overvoltage and their implementation.

The intensity of thunderstorm activity in the location of the protected object is characterized by the average number of thunderstorm hours per year $N_{l,h}$. Another characteristic of thunderstorm activity is the average number of lightning strikes n_{ls} per 1 km² of the earth's surface per 100 thunderstorm hours. On the territory of Ukraine $n_{ls} = 6.7$ 1/km² per 100 thunderstorm hours.

Protecting objects from direct lightning strikes is performed using lightning arresters of various designs. A lightning arrester is a device towering above the protected object, through which the lightning current, bypassing the protected object, is diverted into the ground. A lightning arrester consists of a lightning rod, directly receiving a lightning strike, a down-conductor (mast, gantry, rack fitting, strip) and a grounding device (GD). These extended elements have an inductance that also determines the distribution of the voltage along them. In addition, the resistance of the GD depends on its geometric dimensions and the specific resistance of the soil ground ρ in which it is located, as well as on the parameters of the lightning current pulse: oblique front, front slope a , front duration τ_f , pulse duration τ_p , amplitude I_l . When lightning current flows from the GD, the current density through the grounding rods is high, so high electric field strengths are created in the ground at the surface of the electrodes, exceeding the ground breakdown strength E_b . Zones of high conductivity are formed around the electrodes (primarily due to ionization processes, a dense network of streamers, etc.), increasing their effective dimensions. As a result, the resistance of the GD decreases. The rapid increase in lightning current at the pulse front creates a voltage drop across the inductance of an extended GD, which limits current drainage from more distant parts of it. In this case, the resistance of the GD, on the contrary, increases. As a result of the influence of one or another factor (the formation of an ionization zone and streamer channels or

a voltage drop across the inductance), the resistance of the GD to the lightning current flowing down from it R_p (without taking into account of inductance) or Z_p (taking into account of inductance) differs from GD resistance to power frequency current R_g measured at alternating voltage and relatively small current.

The resistance of the horizontal GD to the current of power frequency R_g is determined by the well-known formula [8]:

$$R_g = \frac{\rho}{2\pi \cdot l} \cdot \left[\ln \frac{l^2}{2r \cdot h_g} + 0.5 \ln \left(1 + \frac{4h_g^2}{l^2} \right) \right], \quad (1)$$

where l is the GD length, m; r is the GD radius, m; h_g is the GD depth of laying in the ground, m.

The resistance of a horizontal beam GD to pulsed current (of lightning) at the point of entry of lightning current for its instant of its maximum is calculated using the approximate formula [9]:

$$Z_p(0, \tau_f) = \frac{R_g + \frac{L_0 \cdot l}{3 \cdot \tau_f}}{n \cdot \eta}, \quad (2)$$

where L_0 is the specific inductance (per unit length of the GD electrode, $\mu\text{H}/\text{m}$); n is the number of horizontal beams; η is the mutual shielding factor.

The maximum voltage at the point of entry of lightning current to the GD is calculated by the formula:

$$U_{\max} = I_l \cdot Z_p(0, \tau_f). \quad (3)$$

The voltage at the end of the horizontal GD when lightning current enters its beginning is calculated by the formula [9]:

$$U(l, \tau_f) = \frac{I_l}{n} \cdot \left(R_g - \frac{L_0 \cdot l}{6 \cdot \tau_f} \right). \quad (4)$$

The relative decrease in voltage at the end of the horizontal GD depending on its length is calculated by the formula:

$$X\% = \frac{U(l, \tau_f)}{U_{\max}} \cdot 100\%. \quad (5)$$

Protection of outdoor switchgear for 110 kV and more from direct lightning strikes is usually performed with rod lightning arresters, lightning rods of which, as a rule, are installed on the outdoor switchgear structures. The installation of lightning rods on portals located near transformers or shunt reactors is allowed if a number of requirements are met. First of all, the lightning current spreading from the point of connection of the current release to the GD of the SS should be provided not less than in two or four directions of grounding lines. Secondly, two or three vertical electrodes with a length of 3-5 m should be installed at a distance of not less than the electrode length along the grounding line from the point of connection of the current release. It is known [9] that when exposed to pulsed lightning currents, there is a decrease in the proportion of current flowing from distant grounding sites, i.e. non-equipotentiality occurs, which increases with the length of the electrode. This phenomenon is associated with the value of the inductance of the steel electrode and its dependence on the equivalent frequency and amplitude of the flowing

current. The specific inductance of the grounding electrode of the GD is determined by the well-known formula [1, 9, 10]:

$$L_0 = 0.2 \cdot \left[\ln \left(\frac{2l}{d} - 0.31 \right) \right], \quad (6)$$

and the total inductance of an electrode of length l in this case is determined as

$$L_e = L_0 \cdot l. \quad (7)$$

Passing the lightning current through a lightning arrester on the SS will be safe for the equipment if it is based on the following calculations.

Calculation of permissible overvoltage on the insulator string. The pulsed discharge voltage of the insulator string must be greater than the voltage that arises during operation between the point of attachment of the string to the portal and the point of attachment of the flexible tire to the string. This means that the allowable voltage that occurs on a string of insulators during its operation must lie below the volt-second characteristic of the string, determined by the well-known formula [1]:

$$U(t) = A \cdot \sqrt{1 + \frac{T_0}{t}}, \quad (8)$$

where t is the time, μs ; A and T_0 are the constants.

The values of the constants are determined by substituting in (8) of the test voltages with full (at $t = 10 \mu\text{s}$) and cut (at $t = 2 \mu\text{s}$) pulses. Thus, for example, for a 110 kV string of seven IIC12-A insulators, we have test voltages $U_{2\mu\text{s}} = 600 \text{ kV}$ and $U_{10\mu\text{s}} = 480 \text{ kV}$. Substituting these values into formula (8), we obtain a system of two equations with unknown constants A and T_0 . Based on the solution of this system of equations with respect to the constants A and T_0 , the volt-second characteristic of the string is described by the expression:

$$U(t) = 444.994 \cdot \sqrt{1 + \frac{1.636}{t}}. \quad (9)$$

The reverse overlap of the insulator string on the portal with the lightning rod occurs at critical current I_c , which is found from the equality of the portal potential and the 50 % pulse discharge voltage of the insulator string according to the formula [1]:

$$I_c \cdot R_p + a \cdot L_0 \cdot h = U_{50\%}, \quad (10)$$

where R_p is the resistance of the GD of the substation to pulsed current (of lightning); h is the height of the fixing point of the string on the portal.

The critical value of the current I_c , at which the reverse overlap of the insulator string occurs, is obtained from the expression (10) in the following form:

$$I_c = \frac{U_{50\%} - a \cdot L_0 \cdot h}{R_p}. \quad (11)$$

Calculation of the permissible length of air gaps. The shortest distance in the air between the lightning arrester and the substation equipment nearest to it should be not less than permissible. The calculation of this distance is based on the determination of the maximum potential at a specific point of the lightning arrester (mast, portal, or separately laid current-carrying release), which is located at distance h_1 from the connection point of the current release (portal) to the GD of the SS. For the

considered form of a lightning current pulse, the maximum potential at a particular point of a lightning arrester occurs at the time of the maximum lightning current and is determined by the formula

$$U_{\max} = I_l \cdot R_p + a \cdot L_T \cdot h_1. \quad (12)$$

where L_T is the inductance of a unit length of the current release.

In engineering calculations, the specific value of L_T is assumed to be $L_T = 1.7 \mu\text{H/m}$ for both the separately laid current-carrying release and for metal lightning arresters of a lattice design. Voltage $E_a \cdot l_a$ is applied to the air gap of l_a length, where E_a is the permissible electric field strength in the air.

Since the number of lightning strikes in SS is relatively small, in (12) as the calculated values of the parameters I_l and a the following numerical values are taken: $I_l = 60 \text{ kA}$ and $a = 30 \text{ kA}/\mu\text{s}$. In addition, the permissible electric field strength in air E_a is taken in calculations to be 500 kV/m . Based on the above, the shortest distance through the air can be written as follows:

$$l_a \geq \frac{I_l \cdot R_p + a \cdot L_T \cdot h_1}{E_a}. \quad (13)$$

Substituting the above values into the formula (13), we obtain the permissible distance in air

$$l_a \geq \frac{60 \cdot R_p + 30 \cdot 1.7 \cdot h_1}{500} \approx 0.12 \cdot R_p + 0.1 \cdot h_1. \quad (14)$$

For example, when $R_p = 10 \Omega$ and $h_1 = 10 \text{ m}$ from (14) we find that $l_a = 2.2 \text{ m}$. It is well known that the air gap, which has uniform electric field, has the greatest electrical strength. If the considered gap has uniform electric field at small distances, then, with the same electrodes, an increase in the distance between them leads to an increase in the inhomogeneity of the electric field, and with a further increase in the distance, the electric field in the gap becomes highly heterogeneous. Consequently, at large distances between the electrodes, the breakdown electric field strength of air in the gap decreases [3], i.e. to prevent breakdown, an increase in the distance between the electrodes is necessary. Therefore, when the distances between the electrodes, measured by meters, used in practice the numerical value of the breakdown electric field strength of air of 500 kV/m should be refined. The longer the air gap, the smaller this value will be. A preliminary assessment shows that an increase in the length of this gap leads to a nonlinear decrease in the breakdown electric field strength.

For example, for a breakdown of an air gap of 6 m in length with breakdown electric field strength of 500 kV/m , voltage of 3000 kV must be applied. However, proceeding from the curves $U_{50\%} = f(l_{a.g})$ [3], the breakdown of such a gap will occur at voltage of about 2834 kV , i.e. at voltage of 5.5% less. Here, the breakdown electric field strength of air in the considered gap will be 472.3 kV/m . Based on the breakdown electric field strength of air of 472.3 kV/m , we determine the allowable distance by air by the formula (13), which is 2.31 m , which is 11 cm (or 5%) more than at the accepted electric field strength of 500 kV/m .

Calculation of the allowable voltage on the transformer case. The shortest distance along the GD line from the point of connection of the current release (portal) to it to the point of connection to the GD of the transformer case must be not less than the permissible value. The fulfillment of this condition is investigated by calculating the voltage on the case of a transformer connected to the GD of the SS, with different specific ground resistance and lightning pulse parameters.

As an example, consider a 110/6 kV power transformer, which is installed at the transformer portal.

To ensure the specified reliability of the transformer during the thunderstorm season, it is necessary to determine the distance L along the line of the GD electrode from the point of connection of the current release of the lightning arrester to the grounding point of the transformer case at which the voltage on the case does not exceed the allowable value (dielectric strength of external insulation). In this case, as the allowable voltage, we take the test voltage of the external insulation of a power transformer with lightning pulses. Test voltages of electrical equipment during thunderstorm pulses, reduced to normal atmospheric conditions, are presented in Table 1. Here, the numerator represents the value of the total pulse, and the denominator presents the value of the cutoff one.

Table 1

Test voltages of lightning pulses [1]

Acting voltage value, kV		Maximum value of the thunderstorm pulse, kV
Class	Maximum working	Power, voltage and current transformer, reactor, apparatus
3	3.6	42/50
6	7.2	57/70
10	12	75/90
15	17.5	100/120
20	24	120/150
35	40.5	185/230
110	126	460/570

We calculate the voltage on the transformer case when a lightning strikes a lightning rod located on the transformer portal. The transformer case is connected to the grid of the grounding device, which is made of steel bar of circular cross section with a diameter of $d = 2r = 12$ mm, the depth of $h_g = 0.7$ m. Let the soil resistivity is $\rho = 100 \Omega \cdot m$, and the amplitude of the lightning current pulse is $I_l = 20$ kA with the duration of its front $\tau_f = 2 \mu s$. The length of the beam l of the GD varies from 3 to 21 m. The height of the lightning arrester is $h_r = 19.35$ m.

Perform the calculations for three cases:

- 1) the current release of the lightning arrester is connected to two oppositely directed beams of the grid;
- 2) the current release of the lightning arrester is connected to the three beams of the grid directed at an angle of 90° (with the use of GDs in the system (shielding) $\eta_p = 0.8$);
- 3) the current release of the lightning arrester is connected to the four beams of the grid (with $\eta_p = 0.65$).

The results of the calculations are given in Table 2-4.

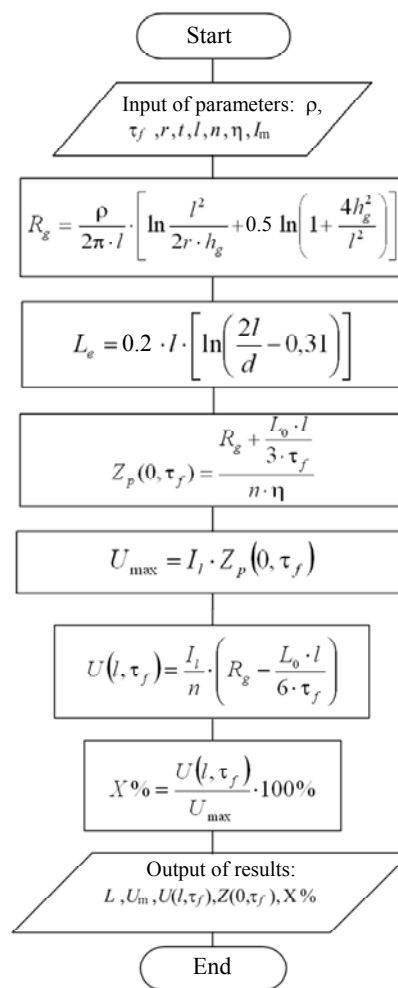


Fig. 1. Block diagram of the algorithm for calculating dependencies of the voltage on the transformer case on the distance of the grounding point of the current release of the lightning release

Table 2

Calculation results for the case of double-beam grounding

L, m	U_l, kV	U_{max}, kV	Z_p, Ω	$X, \%$
3	351.492	360.408	18.02	97.526
6	187.853	206.909	10.345	90.79
9	129.254	159.676	7.984	80.948
12	95.783	138.082	6.904	69.367
15	73.031	127.59	6.379	57.239
18	55.878	123	6.15	45.429
21	42.027	121.967	6.098	34.458

Table 3

Calculation results for the case of three-beam grounding

L, m	U_l, kV	U_{max}, kV	Z_p, Ω	$X, \%$
3	234.328	300.34	15.017	78.021
6	125.235	172.424	8.621	72.632
9	68.17	133.063	6.653	64.758
12	63.855	115.069	5.753	55.493
15	48.687	106.325	5.316	45.791
18	37.252	102.5	5.125	36.343
21	28.018	101.639	5.082	27.566

The obtained results show the following. For the first case, when the transformer case is connected to the grid at a distance of 15 m along the grounding line from the current release (portal) connection point to two beams, the atmospheric overvoltage on the case is 73 kV, i.e. exceeds 70 kV. In this case, the connection of the case to the GD must be performed at a distance of 15.5 m or more.

Table 4
Calculation results for the case of four-beam grounding

L, m	U_i, kV	U_{max}, kV	Z_p, Ω	$X, \%$
3	175.746	277.237	13.862	63.392
6	93.926	159.161	7.958	59.013
9	64.627	122.828	6.141	52.616
12	47.892	106.217	5.311	45.088
15	36.515	98.146	4.907	37.205
18	27.939	94.616	4.731	29.529
21	21.014	93.82	4.691	22.398

For the second case, when the current release of the lightning arrester is connected to the three beams of the grid, and at a distance of 11.03 m along the grounding line there is a grounding point of the transformer case, the atmospheric overvoltage on the case is 70.026 kV, i.e. practically does not exceed 70 kV.

For the third case, when the current release of the lightning arrester is connected to the four beams of the grid, and at a distance of 9 m along the grounding line there is a ground point of the transformer case, the atmospheric overvoltage on the case is about 64.63 kV, i.e. does not exceed 70 kV.

As you can see, at the same lightning current at the point of entry into the GD of the SS with increasing number of beams at $\rho = 100 \Omega \cdot m$, the GD resistance to the pulsed current decreases. In addition, with increasing ρ from $50 \Omega \cdot m$ to $500 \Omega \cdot m$ with the number of beams $n = 4$ and lightning current $I_l = 20 \text{ kA}$, the indicated resistance also increases. Similar results were obtained for other currents, too, for example $I_l = 60 \text{ kA}$.

Figure 2 shows the dependencies of the voltage at the GD point under consideration on the distance L to the point of current input.

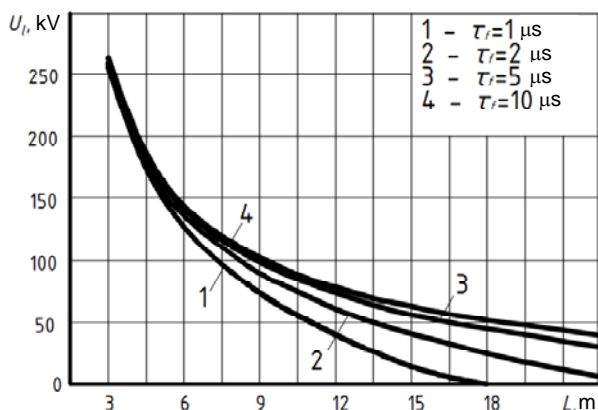


Fig. 2. Dependence of the voltage at the considered GD point at distance L from the point of input of the lightning current $I = 20 \text{ kA}$ for different values of its front length

Figure 3 shows the dependencies of the voltage at the considered GD point on the distance L to the point of input of the lightning current for different values of its amplitude, but with a constant current front length $\tau_r = 2 \mu s$.

As follows from Fig. 2, 3, as the distance (L, m) from the point of input of the lightning current into the GD along the beam of the grounding conductor line is removed, the potential U_i decreases in all the considered cases. In this case, the rate of descent depends both on the amplitude of the lightning current and on the steepness of its front.

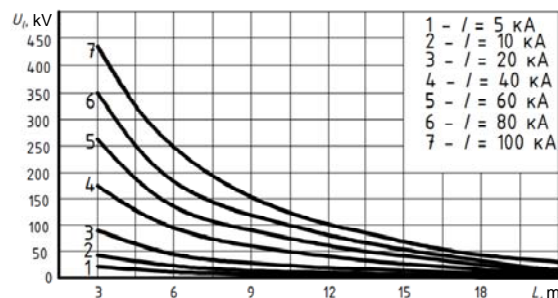


Fig. 3. Dependencies $U_i = f(L)$

Figure 4 shows the dependencies of the resistance of the GD of the SS to the pulsed current at the input point (4 beams) of the lightning current on radius of its spreading along lines (length of beams L) and the length of the front of the lightning current.

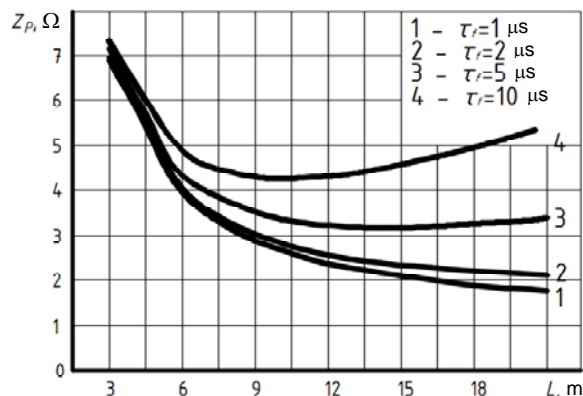


Fig. 4. Dependencies $Z_p = f(L)$

Analysis of the results presented in Fig. 4, shows that the resistance Z_p of the GD of the lightning arrester of the SS to the pulsed current depends complexly on the size of the spreading zone of the lightning current at the time of its maximum at different values of the front length. For example, at $\tau_r > 2 \mu s$, the resistance Z_p decreases with increasing size L of the zone. At the lightning current of 60 kA and the ground resistivity $\rho = 50 \Omega \cdot m$, the curves $Z_p = f(L)$ monotonously decrease, and as $\tau_r (\leq 2 \mu s)$ decreases, the resistance Z_p first decreases and then begins to increase, while the minimum Z_p value shifts towards lower values of L .

Figure 5 presents the dependence $L = f(n)$, which shows a decrease in the zone of spreading the lightning current with an increase in the number of beams of the GD. In this case, the voltage at the boundary of the zone is maintained at the level of the permissible 70 kV.

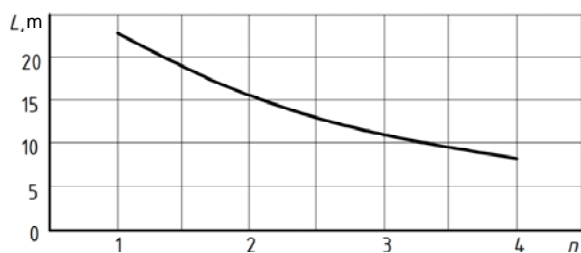


Fig. 5. Dependence of the radius (L) of the lightning current spreading zone along lines of the GD of the SS on the number of beams n at the point of current input

Let us calculate the number of years of operation of the transformer without strike, during which the voltage on its case, caused by atmospheric overvoltage, does not exceed the permissible 70 kV:

$$N = \frac{1}{N_{ls} \cdot P_{I_l}}, \quad (15)$$

where $N_{ls} = \pi(3,5 \cdot h_{lr})^2 \cdot 10^{-6} \cdot \sigma \cdot N_{th}$ is the number of lightning strikes in the lightning arrester of the SS; h_{lr} is the height of the lightning arrester, m; $\sigma = 0,067$ 1/(km)²·lighting hours; $N_{th} = 60$ lighting hours;

$$N_{ls} = 3,14 \cdot (3,5 \cdot 19,35)^2 \cdot 10^{-6} \cdot 0,067 \cdot 60 = 0,058.$$

The probability that the amplitude of the lightning current exceeds the value of I_l is calculated by the formula

$$P_{I_l} = 10^{-I_l/60}.$$

For the lightning current $I_l = 60$ kA we obtain

$$P_{I_l} = 10^{-60/60} = 0,1.$$

Thus, substituting the values obtained above into formula (15), we obtain the number of years of operation of the transformer without strike:

$$N = \frac{1}{0,058 \cdot 0,1} = 172,634 \text{ year.}$$

If the amplitude of the lightning current exceeds 60 kA, the overvoltage will be more than 70 kV. To avoid this, protective devices (surge arresters or surge suppressors) are used.

The calculations performed using this algorithm are shown in Fig. 6. The curve of the dependence of the number of years during which the value of the lightning current may be greater than the specified one, as follows from Fig. 6, increases nonlinearly.

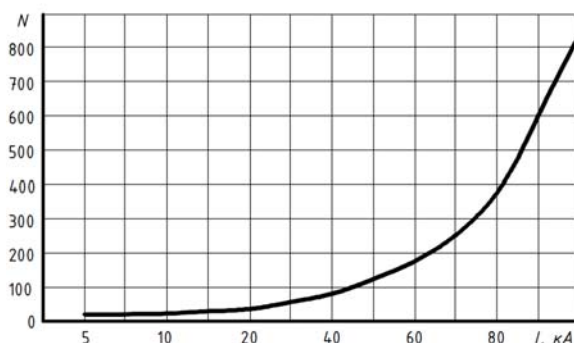


Fig. 6. Dependence $N = f(I_l)$

Calculation of the length of the permissible gap in the ground. For a free-standing lightning arrester, the

shortest distance in the ground between the GD of the lightning arrester and the nearest to it point of the protected device in the ground must be not less than the permissible value.

Assuming that in the ground voltage $E_e \cdot l_e$ is applied to the shortest gap of length l_e , where E_e is the electric field strength permitted in the ground, we write this condition as

$$l_e \cdot E_e \geq I_l \cdot R_p, \quad (16)$$

where l_e is the shortest distance in the ground between the GD of the lightning arrester and the nearest to it point of the protected device in the ground; E_e ($E_{b,g}$) is the pulsed electric strength of the soil (breakdown electric field strength).

From condition (16) we determine the minimum permissible value of l_e :

$$l_e \geq \frac{I_l \cdot R_p}{E_{b,g}}. \quad (17)$$

The results of the experimental determination of the pulsed electric strength of the soil at NTU «KhPI» showed [11] that this quantity is non-linear, i.e.

$$E_{b,g} = f(S) = A + \frac{B}{S}.$$

For large gaps, measured in tens of centimeters, and even more in meters, the value of $E_{b,g}$ tends to numerical values (100-150) kV m, depending on the characteristics of the soil.

Substituting in the expression (17) the value $E_{b,g} = 150$ kV/m and $I_l = 60$ kA, we obtain the condition

$$l_e \geq 0,4 \cdot R_p, \quad (18)$$

which allows to determine the minimum permissible distance in the ground between the grounding conductor of the lightning arrester and the nearest to it point of the protected device.

Conclusions.

An engineering methodology has been developed for calculating the allowable voltage on the transformer case at a lightning strike in the lightning rod of the transformer portal and the allowable number of years of operation of the transformer during which the voltage on its case caused by atmospheric overvoltage does not exceed the allowable value.

An engineering calculation of lightning overvoltage was performed on the equipment of the substation during a lightning strike to its lightning arrester. The conditions of safe for the equipment of the SS of the passage of lightning current through the lightning arrester are formulated. The performed studies showed that the used value of the pulsed breakdown electric field strength of air of 500 kV/m leads to an inaccurate determination of the allowable length l_a of the air discharge gap (with an error of up to 5 %). With an increase in the length l_a of this gap, the pulsed breakdown electric field strength of air nonlinearly decreases and, as a result, the permissible minimum length of the specified interval increases.

Accounting of the nonlinear pulsed electric strength of the soil allowed to obtain a refined minimum allowable distance l_e in the ground between the grounding conductor of the lightning arrester and the nearest to it point of the grounded device.

REFERENCES

1. Bazutkin V.V., Larionov V.P., Pinal' Y.S. *Tekhnika vysokikh napryazheniy: Izolyatsiya i perenapryazheniya v elektricheskikh sistemakh* [High voltage technique. Insulation and surge in electrical systems]. Moscow, Energoatomizdat Publ., 1986. 464 p. (Rus).
2. Gul' V.I., Nizhevskiy V.I., Khomenko I.V. *Koordinatsiya izolyatsii i perenapryazheniya v elektricheskikh vysokovol'tnykh setyakh* [Coordination of insulation and overvoltage in high-voltage electrical networks]. Kharkiv, EDENA Publ., 2009. 270 p. (Rus).
3. Kuchinskii G.S., Kizevetter V.E., Pinal' Iu.S. *Izoliatsiia ustanovok vysokogo napriazheniia* [Isolation of installations of high tension]. Moscow, Energoatomizdat Publ., 1987. 368 p. (Rus).
4. Kuklin D.V., Yefimov B.V. Calculation of hazardous parameters curves at high grounding resistance of power line poles. *Electricity*, 2016, no.6, pp. 16-21. (Rus).
5. Pigni A., Rizzi G., Garbagnati E., Porrino A., Baldo G., Pesavento G. Performance of large air gaps under lightning overvoltages: experimental study and analysis of accuracy predetermination methods. *IEEE Transactions on Power Delivery*, 1989, vol.4, no.2, pp. 1379-1392. doi: **10.1109/61.25625**.
6. Caldwell R., Darveniza M. Experimental and Analytical Studies of the Effect of Non-Standard Waveshapes on the Impulse Strength of External Insulation. *IEEE Transactions on Power Apparatus and Systems*, 1973, vol. PAS-92, no.4, pp. 1420-1428. doi: **10.1109/tpas.1973.293550**.
7. Chisholm W. New challenges in lightning impulse flashover modeling of air gaps and insulators. *IEEE Electrical Insulation Magazine*, 2010, vol.26, no.2, pp. 14-25. doi: **10.1109/mei.2010.5482551**.
8. Burgsdorf V.V., Yakobs A.I. *Zazemlyayushchie ustroystva elektroustanovok* [Grounding device of electrical installations]. Moscow, Energoatomizdat Publ., 1987. 400 p. (Rus).
9. Ryabkova E.Y. *Zazemleniya v ustanovkakh vysokogo napryazheniya* [Grounding installations high voltage]. Moscow, Energy Publ., 1978. 224 p. (Rus).
10. Kalantarov P.L., Tseytlin L.A. *Raschet induktivnostey* [Inductance calculations]. Leningrad, Energoatomizdat Publ., 1986. 488 p. (Rus).
11. Nizhevskiy V.I., Gul' V.I. Dielectric strength of limited soil volumes. *Bulletin of the Kharkov Polytechnic Institute*, 1984, no.213, Series «Electric power industry and automation of power plants», no.12, pp. 3-6. (Rus).

Received 27.12.2018

*I.V. Nizhevskiy*¹, *Candidate of Technical Science*,
*V.I. Nizhevskiy*¹, *Candidate of Technical Science, Associate Professor*,

¹National Technical University «Kharkiv Polytechnic Institute»,
2, Kyrpychova Str., Kharkiv, 61002, Ukraine,
phone +380 57 7076977, e-mail: victornizhevski@gmail.com

How to cite this article:

Nizhevskiy I.V., Nizhevskiy V.I. Calculation estimation of overvoltage on insulation of the equipment of a substation at the lightning strike in its lightning arrester. *Electrical engineering & electromechanics*, 2019, no.3, pp. 67-73. doi: **10.20998/2074-272X.2019.3.11**.

Матеріали приймаються за адресою:

Кафедра "Електричні апарати", НТУ "ХПИ", вул. Кирпичова, 21, м. Харків, 61002, Україна

Електронні варіанти матеріалів по e-mail: a.m.grechko@gmail.com

Довідки за телефонами: +38 050 653 49 82 Клименко Борис Володимирович

+38 067 359 46 96 Гречко Олександр Михайлович

Передплатний індекс: 01216

SET MENU + - ENT

TEST MENU SET IN
CT RATED CUR 1000
RATED CUR 1000
00001

LOCK IN OFF
LOCK
DO NOT USE TO LOCK
ACTS POSITIVE TO
BE NOTED
KEY

ISOLATED TEST CONN

CAUTION